February 11, 2000 CLNS 00/1662

PARTICLE ACCELERATION IN MICROSTRUCTURES EXCITED BY LASER RADIATION

BASIC PRINCIPLES

A.A. Mikhailichenko

Wilson Laboratory, Cornell University, Ithaca, NY 14853*

Based on a talk given at Accelerator Physics Seminar
Wilson Laboratory Large Conference Room
May 28, 1:30-3:00, 1999

---

* Phone: (607) 255-3785, Fax: (607) 255-8062, e-mail: mikhail@lns62.lns.cornell.edu
Supported by NSF.

ABSTRACT

A device for charged particles acceleration described here, uses multi-cell microstructures aligned along the straight beam path. Each cell of these microstructures has an opening from the side. Focused laser radiation with appropriate wavelength excites the cells through these openings. This excitation is going locally in accordance with instant position of accelerated micro-bunch of particles in the structure. For this purpose special devices controllably sweep focused laser spot along the openings. This arrangement, what was called Travelling Laser Focus (TLF), reduces the instant power required from the laser source and reduces the illuminating time for the every point on the structure's surface. The power reduction and the shortening of illumination time equate to the *number of resolved spots* associated with the sweeping device. On practice, the number of resolved spots could reach 10-100 depending on the wavelength. Sweeping along the accelerating structure could be made about 3 *cm* long. Thus, the linac is sectioned with 3-*cm* long modules.

For a wavelength $\lambda_{ac} \cong 10\mu m$ a laser with energy 0.3*J/m* in 100*ps* pulse duration gives the gradient about 3 *GeV/m*. For example, a single flash with 300*J*, could provide the final energy of 3 *TeV* on 1 *km* with the TLF method described. Utilization of a laser radiation with $\lambda_{ac} \cong 1\mu m$ requires about hundred times smaller emittances, but ten times less particles and with the same laser power and accelerating length the final energy could reach ~30 *TeV*. Amplifiers distributed periodically along the linac could deliver this total power required as well. For repetition rate ~160 *Hz* the luminosity associated with colliding beams could reach $L \approx 10^{33} cm^{-2} s^{-1}$ per bunch with population ~10^6. Multi-bunch operation mode together with an increase of repetition rate up to *kHz* scale gives a reasonable value for the luminosity upgrade. Polarization is another important tool, which could be implemented here. Wall plug power required for operation of this linear collider could be as low as ~ *2 MW* for the parameters indicated above.

For 0.5×0.5*TeV* collider, the wall plug power required is ~330 *kW* and the length of collider is 2×170 *m* for $\lambda_{ac} \cong 10\mu m$. For $\lambda_{ac} \cong 1\mu m$ the length shrinks to 2×17 *m*. All components of this laser driven linac, including the source of low emittance beam are within present day technology.

Possible implementation for $\mu\mu$, $\pi\pi$, *pp* and *ion-ion* collisions mentioned also.

1. INTRODUCTION

Laser is a natural source of power for application in accelerator physics. Really, the flux of power P running through the area A

$$\vec{P}\left[\frac{Power}{Area}\right] = \vec{E}\times\vec{H} = \vec{n}\frac{E^2}{377}\ [W/m^2] \tag{1.1}$$

defines the electric field strength as $E \cong \sqrt{377\frac{P}{A}}\,[V/m]$ (see [1.1,1.2] for example). The last could be estimated for the power 1 W running through the area A=1cm^2 as $E \cong \sqrt{377\cdot 10^4} \approx 2$ [kV/m] what is not much. If however, the same radiation is focused onto the spot with area, say, $A \approx 4\mu m^2$ ($\lambda_{ac} \cong 1\mu m$*), then $E \cong \sqrt{377\cdot\frac{10^{12}}{4}} \approx 10^7\ [V/m]$. One can easily scale the last numbers to GW and even TW levels of laser power.

Natural limit for the field strength emerges from requirement that the work done by electric field to the particle on the distance of Compton wavelength $\lambda\!\!\!^{-}_C = \hbar/mc$ is equal to the rest energy of electron-positron pair as $eE^{\infty}\lambda\!\!\!^{-}_C \cong 2mc^2$. The last gives the break down limit for a vacuum**

$$E^{\infty} \cong \frac{2mc^2/e}{\lambda\!\!\!^{-}_C}\ , \tag{1.2}$$

what is $E^{\infty} \cong 1MV/3.86\cdot 10^{-13}m \cong 2.6\cdot 10^{18}\ V/m$. Of cause, the breakdown limit in media is much lower.

The laser radiation is not able to accelerate particles in a vacuum. Without any restriction to the common case, this could be demonstrated with TM field. This type of field could be defined by equations

$$\vec{\nabla}\times\vec{E}\Big|_S = \frac{\partial E_y}{\partial x} - \frac{\partial E_x}{\partial y} = -\frac{\partial B_s}{\partial t} = 0 \tag{1.3}$$

The components of electromagnetic field could be represented as the following

$$\overline{E} = E_x - iE_y = \frac{\partial W}{\partial z} + \frac{\partial W}{\partial \overline{z}},\quad E_S = \int\left(\frac{\partial^2}{\partial s^2} - \frac{1}{c^2}\frac{\partial^2}{\partial t^2}\right)W(z,\overline{z},s,t)ds$$

$$B_S \equiv 0,\qquad \overline{B} = B_x - B_y = i\varepsilon_0\frac{\partial}{\partial t}\int\overline{E}(z,\overline{z},s,t)ds\,, \tag{1.4}$$

where $z = x+iy, \overline{z} = x-iy$, $i^2 \equiv -1$, s - is a longitudinal coordinate,

$$\frac{\partial}{\partial z} \equiv \frac{1}{2}\left(\frac{\partial}{\partial x} - i\frac{\partial}{\partial y}\right), \frac{\partial}{\partial \overline{z}} \equiv \frac{1}{2}\left(\frac{\partial}{\partial x} + i\frac{\partial}{\partial y}\right). \tag{1.5}$$

---

* λ_{ac} –is the wavelength of accelerating laser radiation.

** So called Schwinger field.

With definition (1.5) Laplasian could be expressed as the following

$$\nabla^2 \equiv \frac{\partial^2}{\partial x^2} + \frac{\partial^2}{\partial y^2} + \frac{\partial^2}{\partial s^2} = 4\frac{\partial^2}{\partial z \partial \bar{z}} + \frac{\partial^2}{\partial s^2} . \qquad (1.6)$$

Complex potential $W(x, y, s, t) \equiv W(z, \bar{z}, s, t)$ satisfies the equation

$$4\frac{\partial^2 W}{\partial z \partial \bar{z}} + \left(\frac{\partial^2}{\partial s^2} - \frac{1}{c^2}\frac{\partial^2}{\partial t^2} \right) W(z, \bar{z}, s, t) = 0 . \qquad (1.7)$$

Electromagnetic field accelerates the particle if it provides the energy change

$$\Delta \mathrm{E} = \int_{-\infty}^{+\infty} (\vec{F} \cdot \vec{v}) dt = \int_{-\infty}^{+\infty} \{ (F_S \cdot v_S) + (\vec{F}_\perp \vec{v}_\perp) \} dt = ec \int_{-\infty}^{+\infty} E_S \cdot dt \bigg|_{s = ct} + e \operatorname{Re} \int_{-\infty}^{+\infty} (\overline{E} \cdot v) ds , \qquad (1.8)$$

where $(\vec{F} \cdot \vec{v})$ –is an instant power, $\vec{F}$ –is the force, $\vec{v}$ –is the velocity, $\overline{E}$ defined by equations (1.4) and $v = v_x + i v_y$. Integrals are taken along the trajectory of the (relativistic) particle. Let us introduce complex potential U, so that $W(z, \bar{z}, s, t) = \partial U / \partial s$. One can see that this is basically a *s*-component of Hertz's vector [1.2]. This potential satisfies the same equation (1.7) and introduced here for simplification of expressions. With this potential longitudinal component of electrical field becomes

$$E_S = \left(\frac{\partial^2}{\partial s^2} - \frac{1}{c^2}\frac{\partial^2}{\partial t^2} \right) U(z, \bar{z}, s, t) = -4\frac{\partial^2 U}{\partial z \partial \bar{z}} . \qquad (1.9)$$

From last expression one can see that any *plane* electromagnetic wave in *s*-direction, $U = U(s - ct)$, does not have longitudinal components, and, hence, does not accelerate particles moving along straight line. In some sense this is a kind of tautology. As one can see from (1.9) plane wave has no transverse structure, $\partial^2 U / \partial z \partial \bar{z} = 0$. So the source of longitudinal component associated with nonzero derivative $\partial / \partial \bar{z} \neq 0$. This nonzero derivative in its turn associated with nonzero longitudinal derivative, i.e. potential must vary in longitudinal direction. Condition (1.8) that the field of some particular configuration *accelerates* the particles (with the first term in (1.8)) could be expressed now as the following

$$c \int_{-\infty}^{+\infty} E_S dt = \int \left(\frac{\partial^2}{\partial s^2} - \frac{1}{c^2}\frac{\partial^2}{\partial t^2} \right) U(z, \bar{z}, s, s/c) ds = 4\frac{\partial^2}{\partial z \partial \bar{z}} \int U(z, \bar{z}, s, s/c) ds \neq 0 . \qquad (1.10)$$

One can see from the last expression that for nonzero acceleration condition potential derivation $\partial U / \partial \bar{z} \neq 0$. This means, formally, that the potential as a function of complex variable is an analytical function[♣] only at the axis, $|z| = 0$. Some accelerating methods proposed, which suppose to accelerate the particles in a focal waist of laser

---

♣ Function $U(z, \bar{z})$ is analytical if $\partial U / \partial \bar{z} = 0$ –is the Cauchi-Rieman condition.

beam summarized in [1.3]. One can see that this is an attempt to arrange acceleration on the basis of (1.9).

Other attempt to accelerate the particles in free space connected with (1.8), second term. Now the particle and the wave must have an angle, arranged with additional external field or by initial condition. Typically this is a wiggler system. If this wiggling field is a periodic one with period λ_u there is a possibility to have a long-term interaction on the full length of the wiggler. For this some requirements need to be satisfied. Let us consider the electromagnetic wave propagating in s direction, $\vec{E} = E_\perp \cos(\omega t \mp ks + \varphi)$, where $k = \omega / v_p$, v_p –is the phase velocity of the wave, in vacuum $v_p = c$. Energy variation, what could be treated as *induced absorption*, could be expressed as the integral along particle trajectory

$$\Delta E = \int_0^T P dt = e\int \left(\vec{v}_\perp \vec{E}_\perp\right) dt = e\beta_\perp c E_\perp \int Cos\Omega t \cdot Cos\left(\omega t \mp k v_\| \, t + \varphi\right) dt =$$
$$= \frac{eKcE_\perp}{\gamma}\int Cos\Omega t \cdot Cos\left(\omega t\left(1 \mp \frac{v}{v_p}\left(1 - \frac{\beta_{\perp x}^2}{2} - \frac{\beta_{\perp y}^2}{2}\right)\right) + \varphi\right) dt = \frac{eKL_w E_\perp}{2\gamma} Cos\varphi \tag{1.11}$$

where $v_\| \cong \sqrt{v^2 - v_\perp^2} \cong v\left(1 - \frac{v_\perp^2}{2v^2}\right) \cong v\left(1 - \frac{\beta_{\perp x}^2 + \beta_{\perp y}^2}{2}\right)$, deflection parameter K (undulatority factor) defined as $K = \beta_\perp \gamma$, L_w is the length of the wiggler. In case if transverse velocity arranged with the help of dipole magnetic wiggler, the last factor could be expressed as $K = eH_\perp \lambda_u / 2\pi mc^2 \cong 93.4 \cdot H_\perp [Tesla] \lambda_u [m]$. The resonance condition was used here

$$\Omega \cong \omega\left(1 \mp \frac{v}{v_p}\left(1 - \frac{\beta_{\perp x}^2 + \beta_{\perp y}^2}{2}\right)\right), \tag{1.12}$$

In case of *co-directional* movement of the wave and the particle, the resonant frequency is

$$\Omega \cong \omega\left(1 - \frac{v}{v_p}\left(1 - \frac{\beta_{\perp x}^2 + \beta_{\perp y}^2}{2}\right)\right) = \omega\left(1 - \frac{v}{v_p} + \frac{v}{v_p}\frac{\beta_{\perp x}^2 + \beta_{\perp y}^2}{2}\right) \cong$$
$$\cong \omega\left(\frac{\left(1 - v/v_p\right)\left(1 + v/v_p\right)}{2} + \frac{\beta_{\perp x}^2 + \beta_{\perp y}^2}{2}\right) = \omega\left(\frac{1}{2\gamma^2} + \frac{\beta_{\perp x}^2 + \beta_{\perp y}^2}{2}\right) = \frac{\omega}{2\gamma^2}\left(1 + K^2\right)$$
$$\lambda \cong \lambda_u \cdot (1 + K^2)/(2\gamma^2). \tag{1.13}$$

As one can see this is the same as the frequency of *spontantenous* radiation ω defined as a Doppler shifted frequency of transverse oscillations

$$\omega = \frac{\Omega}{1-\vec{\beta}\vec{n}} \cong \frac{\Omega}{1-\beta_{\parallel}\, Cos\,\vartheta} \cong \frac{\Omega}{1-\beta_{\parallel}\cdot(1-\frac{\vartheta^2}{2})} \cong \frac{\Omega}{1-\beta\sqrt{1-\frac{\beta_{\perp}}{\beta^2}}\cdot(1-\frac{\vartheta^2}{2})}$$

$$\cong \frac{\Omega}{1-\beta\cdot\left[1-\frac{\vartheta^2}{2}-\frac{\beta_{\perp}^2}{2}\right]} \cong \frac{2\Omega\gamma^2}{1+K^2+\gamma^2\vartheta^2} = \frac{\omega_{\max}}{1+\frac{\gamma^2\vartheta^2}{1+K^2}} \qquad (1.14)$$

ϑ –is the observation angle, calculated from the forward direction, $\omega_{\max} = 2\Omega\gamma^2/(1+K^2)$ corresponds to the *forward* direction (we suggested $\vartheta = 0$ in (1.11). However this method is not really working in practice as for acceleration the beam must have a longitudinal structure what must be a fraction of the laser wavelength, see (1.11), so in this case *coherent spontantenous* radiation becomes significant. To compensate the last one, the laser power becomes out of real limits.

To finish this review with acceleration in a wiggler, we would like to say that more realistic look acceleration of the bunch, interacting with oppositely moving (incoming) wave in the wiggler [1.4]. Really from (1.12) yields that incoming wave must have a period what is *two* times the period of the wiggler. As this wave now becomes a radio frequency band, the vacuum chamber need to be made bi-connected so the wave could propagate in a strip line inside the chamber placed in a wiggler field. In this case there is no microbunching with the frequency of spontantenous forward radiation. This method however looks less effective than direct acceleration with cavities. Only one advantage what may be used with this method- less impedance in some cases, as the strip lines loaded at the ends are ideal matched system. It gives even a decrement if installed properly [1.5].

So the only way to accelerate with electromagnetic wave – to use any additional agent as accelerating structure. This is also important as all power lasers are working, evidently, in pulse mode. Accelerating structure of any kind scaled for laser wavelengths could not be excited in series due to enormous losses in material of the structure. Desire to have acceleration as high as possible brings the laser power close to the destruction limit for the materials an accelerator structure made on. In this case proper arrangement of excitation of accelerating structure of any kind becomes a ***first*** crucial moment of all acceleration strategy.

So if we accept that an accelerating structure is absolutely necessary, we accept naturally, that the structure must have *tiny dimensions*, corresponding to the laser wavelength. Tiny dimensions of accelerating structure in its turn require extremely small beam emittances. It is clear, that the pass holes must have dimensions as a fraction of accelerating wavelength. The size of passing holes δ need to be made with a fraction of this value, say 20%, $\delta \cong 0.2\cdot\lambda_{ac}$, where λ_{ac} is an accelerating wavelength. Taking into account that this must have a safety margins as big as ten sigma of the beam, one can estimate $\sigma \cong \sqrt{(\gamma\varepsilon)\cdot\beta/\gamma/\pi} \cong 0.1\cdot 0.2\cdot\lambda_{ac}$. So emittance required must be $\gamma\varepsilon \cong 4\pi\cdot 10^{-4}\lambda_{ac}^2\cdot\gamma/\beta$. From this expression emerges desire to have injection energy as high as possible keeping the size of the beam the same. If the focusing elements distributed along trajectory of the beam with period, say 3*cm*, then the envelope function

could be lowered down β~12*cm*. For $\gamma \cong 2 \cdot 10^3$(1*GeV*), $\lambda_{ac} \cong 10\mu m$, maximal allowable value for invariant emittance given by last formula is $\gamma\varepsilon \cong \pi 6 \cdot 10^{-8} cm \cdot rad$. Some reduction of the envelope function in the accelerating structures by the sectioning with 1 *cm* is possible here and this emittance probably could be considered as a conservative value.
With *RF focusing*, for *E*=2 *GeV* the effective focusing parameter could reach $k \cong 2 \cdot 10^6 \cdot Sin\varphi [m^{-2}]$ for the phase deflection φ, see Chapter 7. If this phase deflection applied along some part of the structure *l*, the envelope functions could be about $\beta \cong 1/kl$. Substitute here for estimation *l*~0.1*mm* (or about 100 cells), one can obtain $\beta \cong 1/(2 \cdot 10^6 \cdot 10^{-4}) = 5mm$ could be expected here. Together with increased energy ~2*GeV* all this yields $\gamma\varepsilon \cong 3.2\pi \cdot 10^{-6} cm \cdot rad$. Emittance of $\gamma\varepsilon \cong \pi 10^{-5} cm \cdot rad$ is probably maximal allowed emittance value for $\lambda_{ac} \cong 10\mu m$. For $\lambda_{ac} \cong 1\mu m$ emittance $\gamma\varepsilon \cong \pi 10^{-7} cm \cdot rad$ required. An attempt to have such a small emittance makes considerations about possible limitations for emittance arising from the quantum mechanical phenomena actual.
So the source of particles emerges as a ***second*** crucial element of any scheme.

2. THE TLF METHOD

Now we came to the illumination problems. It is naturally not to apply a laser power to the places of the structure, where there are no particles. This is evident. This brings us to a desire to have the laser radiation structure as represented in Fig.2.1 below.

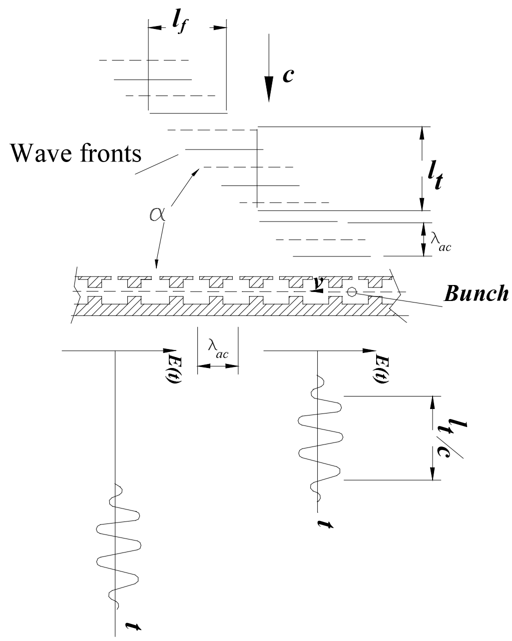

FIGURE 2.1: The concept of illumination. The time dependence of the field at two different locations along the structure is represented on the graphs at the bottom. Beam has a speed $\vec{v}$ to the left.

It is evident, that the $\tan\alpha = c/v$, where c is the speed of light, and v is the speed of the bunch. The time duration of the radiation at each point on the structure lasts for a l_t / c, where l_t is the instant height of the sloped laser bunch along the perpendicular to the plane of the structure, see Fig. 2.1. The number of the cells excited instantly defined by l_f / λ_{ac}.

Due to this arrangement, all pulsed laser power is acting for generation of accelerating field at the instant particle's location only. By this way the total power, required from the laser becomes reduced. The illuminating time for any point on the structure is lowered also.

Basically the problem now how to create the laser structure like it is shown in Fig.2.1. The goals here are the lowering the power from laser. Evidently, that for the fixed *energy* located in the laser bunch, the instant *power* defined by this energy divided by the time in which this power delivered there.

Traveling Laser Focus (TLF) method [2.1-2.5] deals with a laser radiation focused onto a spot with minimal area. This spot *sweeped* in longitudinal direction as a function of time, following the particle in its motion along the accelerating structure. As the motion of the focused laser spot along the structure is going with the speed of particle, this yields the picture, shown in Fig.2.1, see Fig.2.2.

In [2.6] one can find a picture with sloped laser bunch, created by a *short* laser bunch reflected by the grating. In this proposal the angular distribution, what the short laser bunch will have after reflection from the grating and the wave fronts directions at each point –are the crucial moments. But even without these evident questions, one can conclude, that the *power* required from the laser source in the sweeping method, is less by the ratio of length of the laser bunch to its transverse size, that is $\sim L/l_f \cong c\tau / l_f \cong 100$*. Also, a good quality grating is less damage resistant, than the mirror.

With the TLF method, the power reduction and shortening of illuminating time is equal numerically to the *number of resolved spots* (*pixels*), associated with the sweeping device. The elements, playing important role in acceleration process are the laser-sweeping device itself, accelerating structure, focusing elements, injector and the final focusing elements.

We would like to stress here once again that TLF method does not exclude the problems, associated with breakdown limit of the structure, but *it allows drastically reduce the laser impulse power, required for excitation the structure* to this level. This method also cuts down the illumination time for every point of the structure. The last brings hope that the break down limit will be increased due to shortening of illuminating time.

Fig. 2.2 describes the idea of the sweeping. The pulse of laser radiation lasts for a time τ, so it has the length $\approx c\tau$, pos. 1 in Fig.2.2. The deflecting device 4 is positioned at the distance R from the open structure 6. 1, 2 and 3 numbers beam of particles 5 is going inside this structure with velocity $\vec{v}$. The laser bunch positions in three different times.

* Even so, the arrangement [2.6] still covered by our author's certificate [2.1].

The structure 6 has a length L in longitudinal direction. Device 4 is driven by electrical pulse. Device 4 directs the head of the laser bunch to the entrance of accelerating structure and the tail of the laser bunch to the exit of the structure 6. By this way it *sweeps* the laser beam in longitudinal direction synchronously with the particle’s passage. Full angle of deflection is $\Theta \cong L/R$. As the sweeping lasts for the time τ *also*, the angular speed of the laser spot on the surface of the grating is $\Omega \cong L/(R\tau) \approx V/R$, where V –is the speed of particle*. At the moment, when the laser bunch arrives at the grating, it has an angle α with respect to the particle’s trajectory. The condition of synchronism is now the following [2.1]

$$\Theta \cdot \tan\alpha = \frac{cL}{VR}. \qquad (2.1)$$

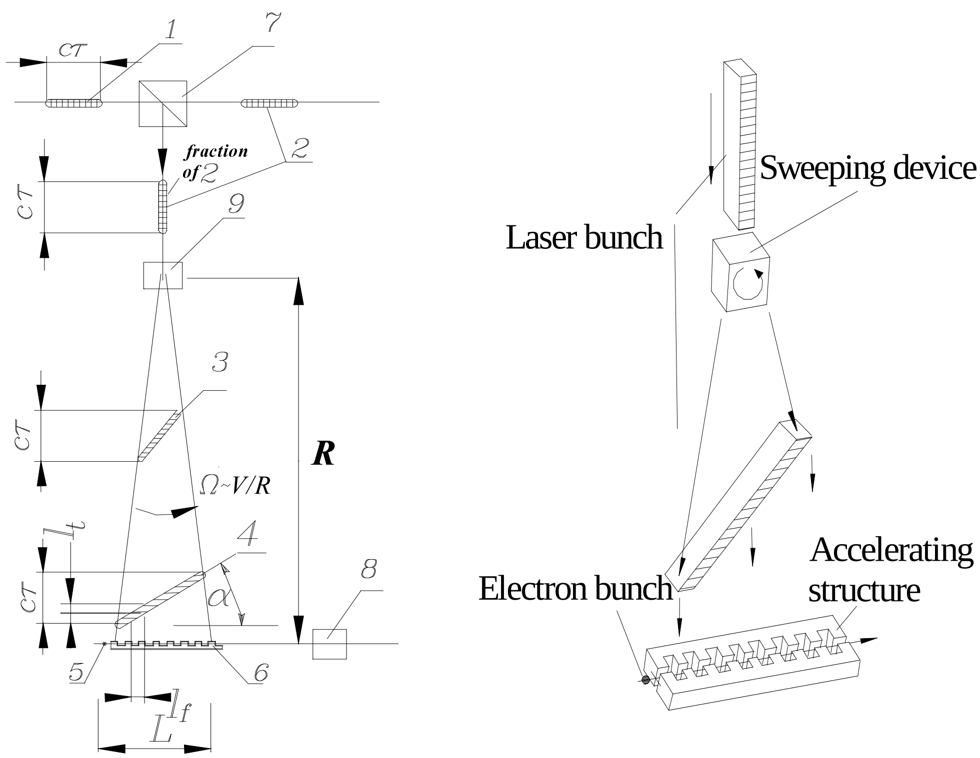

FIGURE 2.2: The TLF principle. At the right an isometric view is represented. The numbers 1, 2, 3 and 4 are numbering the laser bunch positions in four different moments of time. The length of the laser bunch is $c\tau$. This projection of the laser length to the radius vector always remains $c\tau$. 5 –is the particles’ beam, what is going through the accelerating structure 6. 7–is a splitting device, 8–is a focusing element, 9–is a sweeping device. The lines across laser bunch show the wavefronts. This is a single accelerating module. l_f and l_t –are the cross-sections of the bunch in longitudinal and transverse directions respectively, see Fig.2.1. Each point on the structure illuminated during the time $\approx l_t / c$.

* In principle the speed of the spot could be higher, than the speed of light. This does not create a problem, as this is a phase speed. In this case the radiation of the places illuminated will follow usual laws of electrodynamics.

For electrons or positrons, velocity *V* is close to the speed of light, so $\alpha \cong \pi / 4$.
Electric field in each point of the laser beam (pos. 2, 3) polarized rectangularly to the line, connecting this point with the center of the sweeping device 4. With the other words- the wavefronts have common center of curvature coincident with effective center of the sweeping device. The laser bunch projection to the radius vector hence is always $c\tau$. The field in the wave zone can be represented as integral over aperture *S* of the deflecting device [1.2, 2.7]

$$\vec{H}(\vec{r},t) = -\frac{ike^{i\omega t+\psi}}{4\pi}\left[\vec{n}_R \times \vec{F} - \vec{n}_R \times (\vec{n}_R \times \vec{F}')\right], \qquad (2.2a)$$

$$\vec{E}(\vec{r},t) = \frac{ike^{i\omega t+\psi}}{4\pi}\left[\vec{n}_R \times (\vec{n}_R \times \vec{F}') + \vec{n}_R \times \vec{F}'\right], \qquad (2.2b)$$

where

$$\vec{F}(\vec{r},t) = \int_S \frac{(\vec{H}(x,y,t)\times \vec{n}_R))e^{i\vec{k}\vec{r}}}{r} d\sigma, \quad \vec{F}'(\vec{r},t) = -\int_S \frac{(\vec{E}'(x,y,t)\times \vec{n}_R))e^{i\vec{k}\vec{r}}}{r} d\sigma$$

and $\vec{H}(x,y)$, $\vec{E}(x,y)$ –are the magnetic and electric field distribution at the output surface of the device, $\vec{r}$ –is the radius vector from the point (*x* ,*y*) to the point of observation, ψ –is a phase, ω –is a frequency of the laser source and $\vec{k}$ –is a wave vector, $\vec{n}_R$ is the unit vector in $\vec{R}$ direction. Integration is going over the output surface. Of cause in reality the laser cross-section is moving across the aperture, see Fig.3.8, but this effect will be not taken into account here.

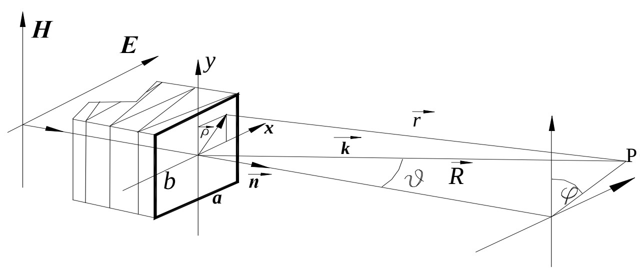

FIGURE 2.3: The system of coordinate in integration over output plane of the sweeping device.

Let us suggest that the laser radiation have the *y* component only. Representing radius vector $\vec{r} = \vec{R} - \vec{\rho}$, where $\vec{\rho}$ –is a vector in the plane of output surface (plane *x, y*) $\vec{R}$ –is a vector from the center of the sweeping device to the point of observation, Fig.2.3, we can rewrite the formula for magnetic field

$$H_y(t) = -\frac{ik}{2\pi}\frac{\exp(ikR)}{R}\int_{-b/2}^{+b/2}\int_{-a/2}^{a/2} H_y(x,y)e^{ikSin\,\vartheta(xCos\,\varphi + ySin\,\varphi)}e^{-i\chi(x,y)}dxdy \quad , \quad (2.3)$$

where $a \times b$ is the aperture of the sweeping device, ϑ is an angle in the sweeping plane, φ is an angle in the plane (*x*, *y*), $\chi\,(x,y)$ –is a phase distribution across aperture.

As we are interesting here the sweeping only in one plane, we can put φ = 0. Substitute $2x/a=\xi$, $\frac{1}{2}kaSin\vartheta=\alpha_1$ and representing $\chi(x,y)=\delta(t)\cdot x$, i.e. suggesting that the phase across the aperture of the sweeping device variation is linear, we can obtain for uniform distribution $H_y(x,y)=H_0$ = const*,

$$H(t)=-\frac{ikH_0}{2\pi}\frac{\exp(ikR)ab}{2R}e^{i\omega t+\psi}\int_{-1}^{+1}e^{i(\alpha_1-\delta)\xi}d\xi=-\frac{ikH_0}{2\pi}\frac{\exp(ikR)ab}{R}e^{i\omega t+\psi}\frac{Sin(\alpha_1-\delta)}{\alpha_1-\delta}.\quad(2.4)$$

The maximum of this expression corresponds $\alpha_1=\delta$, or $ka/2Sin\vartheta\cong ka\vartheta/2=\delta$. The last yields $\vartheta_{\max}\cong 2\delta(t)/ka$. In our case $\delta=\delta(t)\propto\Delta t$, this means that the maximum of the field distribution in direction to the grating also moves $\vartheta\propto\Delta t/ka$. Angular speed of the maximum motion is $\dot{\vartheta}\propto\Delta/ka$, what must be equal to *c*/*R*. This defines the slope of the phase across the aperture $\Delta\propto cka/R=\omega a/R$.

The surface of constant phase defined by the eikonal $k\Gamma=\omega R/c\pm\Omega t-\omega t+\psi=const$. As far as the direction of the wavefronts at the surface of the sweeping device, the eikonal, according to (2.4) is $k\Gamma=2(\alpha_1-\delta)x/a$. To obtain the direction, one needs to take a derivative $\partial k\Gamma/\partial x=2(\alpha_1-\delta)/a$. The last expression yields, that the direction is moving proportionally to $\delta(t)$. Globally, the laser bunch looks like a part of opening spiral, which has a center at the sweeping device. The points of the spiral are running from the sweeping center with the speed of light.

For the focusing and deflecting the radiation at the same time, the phase variation across the aperture of the deflecting device must be as the following: $\chi(x,y)=\delta\cdot x+\kappa x^2$. The ordinary optical lens gives the necessary parabolic phase distribution. In this case the integral (2.4) transforms into

$$H(t)=-\frac{ikH_0}{2\pi}\frac{\exp(ikR)ab}{2R}e^{i\omega t+\psi}\int_{-1}^{+1}e^{i(\alpha_1-\delta)\xi-i\kappa a^2\xi^2/4}d\xi\,.\quad(2.5)$$

Introducing abbreviations $\alpha_1-\delta=A$, $\kappa a^2/4=B$ and introducing a variable

$$\varsigma=\xi\sqrt{B}-A/2\sqrt{B}\,,\quad(2.6)$$

one can transform (2.5) into

$$H(t)=-\frac{ikH_0}{2\pi}\frac{\exp(ikR)ab}{2R}\frac{e^{i\omega t+\psi-iA^2/2B}}{\sqrt{B}}\int_{-u}^{v}e^{-i\varsigma^2}d\varsigma\,,\quad(2.7)$$

where $u=(A+B)/2\sqrt{B}$, $v=(B-A)/2\sqrt{B}$. The last integral could be expressed as a sum of two Fresnel integrals** as the following

$$\int_{-u}^{v}e^{-i\varsigma^2}d\varsigma=-\int_{0}^{u}e^{-i\varsigma^2}d\varsigma+\int_{0}^{v}e^{-i\varsigma^2}d\varsigma=\sqrt{\frac{\pi}{2}}[C(u)+C(v)-iS(u)-iS(v)]\,.$$

---

* Used here for simplicity.

** $C(x)-iS(x)=\frac{2}{\sqrt{2\pi}}\int_0^x e^{-it^2}dt$ [2.8]

Formal analyses of this expression show, that the focal distance of the spot on the focal surface is in the center of curvature of the wave front at the sweeping aperture. Intensity of the magnetic field defined by $[C(u)+C(v)]^2+[S(u)+S(v)]^2$. Argument o this expression could be represented as

$$u=\frac{\frac{1}{2}\cdot kaSin\vartheta-\delta(t)+\kappa a^2/4}{a\sqrt{\kappa}}, \quad v=\frac{-\frac{1}{2}\cdot kaSin\vartheta+\delta(t)+\kappa a^2/4}{a\sqrt{\kappa}}. \tag{2.7}$$

In (2.7) the angle ϑ represents polar angle to the observation point, Fig.2.3.
Instead of focusing lens, which is always a source of chromatic aberrations, the mirrors 1,2 in Fig.5.3 can be used for the focusing as well.
In Fig. 2.4 an assembly of such accelerating modules is shown. Here the laser bunch 1 passed trough the splitting devices 7 generated the secondary bunches 2-4. Sweeping device marked by 9, 8 are the particle's beam focusing elements. The last elements are the same as in Fig.2.1. All deflecting elements are synchronized so that the bunch 5 has continuous acceleration in all sections. Distance *R* and elementary length *L* defined by technical properties of deflecting device 7 to sweep the laser beam. As the secondary bunches are generated by the same primary laser bunch (1 in Fig. 2.3), the longitudinal position for each module does not influence to the accelerating process. In Fig. 2.1 and Fig.2.3 some optical elements necessary for focusing the laser radiation are not shown for simplicity, see lower.

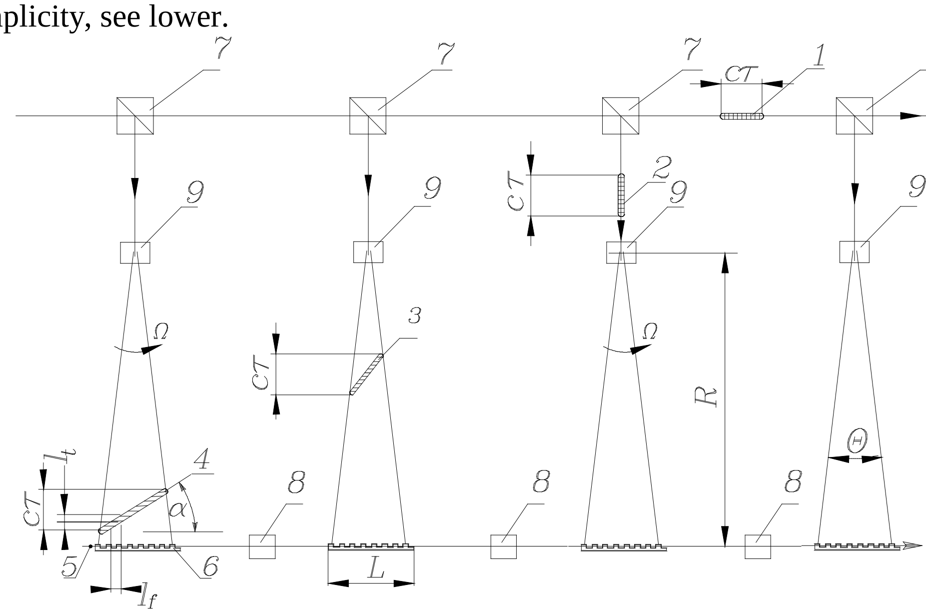

FIGURE 2.4: Accelerating complex scheme. 1–4–are the instant laser bunch positions; 1–is a primary laser bunch which is moving from the left side on the picture to the right. 5– is the beam of accelerated particles. 6–is the accelerating structure. 7–are the optical splitters. 8–are the particles' beam focusing elements (in additional to RF focusing). 9–are the sweeping devices. The distances between the structures are increased for better view.

So one can conclude, that parameters of deflecting device are crucial for TLF method.
Below we start with description of possible realizations for such devices.

3. SWEEPING DEVICE

Here we begin consideration of methods concerning generation of the laser bunch with the properties shown in Fig.2.1 with the help of a sweeping device. Each sweeping device uses controllable deflection of the laser radiation in time. The device could be characterized by a deflection angle ϑ and the angle of natural diffraction $\vartheta_d \cong \lambda / a$, where a —is the aperture of the sweeping device. The ratio of deflection angle to diffraction angle, is a fundamental measure of the quality for any deflecting device. This ratio defines the *number of resolved spots (pixels)* on the surface of the structure, $N_R = \vartheta / \vartheta_d$. The deflection angle could be increased by appropriate optics, but the number of resolved spots N_R is *an invariant* under such transformations. As we mentioned above, N_R value gives the number for the lowering the laser power required for gradient desired and, also, the number for the duty time reduction. The last is important for the structure heating reduction. So it is desirable to have this number as big as possible.

Electro-optical devices [3.1-3.9, 3.11-3.12] use controllable dependence of refractive index on electrical field strength and direction applied to some crystals. The refractive index in active media has a dependence like

$$1/n_i^2 = 1/n_{0i}^2 + \sum_j r_{ij} \cdot E^j \, , \tag{3.1}$$

where r_{ij} –are 6×3 tensor. Index i runs from 1 to 6. 1 stands for *xx*, 2–for *yy*, 3– *ss*, 4–for *ys*, 5–for *xs*, 6– for *xy*, *s*-longitudinal coordinate. Indicatrix allows to determinate the refraction index n components for monochromatic plane waves as a function of their polarization. For Cartesian coordinate system with the principal axes of a crystal, the indicatrix can be represented as

$$\left(\frac{1}{n^2}\right)_1 x^2 + \left(\frac{1}{n^2}\right)_2 y^2 + \left(\frac{1}{n^2}\right)_3 s^2 + 2\cdot\left(\frac{1}{n^2}\right)_4 ys + 2\cdot\left(\frac{1}{n^2}\right)_5 xs + 2\cdot\left(\frac{1}{n^2}\right)_6 xy = 1 . \tag{3.2}$$

The change of reflecting index is equal to $\Delta n_i \cong (\partial n_i / \partial E_j) E^j(t)$. The (3.1) yields $\partial n_i / \partial E_j = -n_{0i}^3 r_{ij} / 2$ and the net change of refractive index becomes

$$\Delta n_i \cong (\partial n_i / \partial E_j) E^j(t) \cong -n_{0j}^3 r_{ij} E^j / 2 \tag{3.3}$$

For electro-optic effect, an electric field applied changes each of coefficients in (A2.1) so that they linearly dependent on electrical field applied as (2). With abbreviation $\Delta(1/n)_i = 1/n_i - 1/n_{0i}$ this could be rewritten as the following [3.9]

$$\begin{pmatrix} \Delta(1/n^2)_1 \\ \Delta(1/n^2)_2 \\ \Delta(1/n^2)_3 \\ \Delta(1/n^2)_4 \\ \Delta(1/n^2)_5 \\ \Delta(1/n^2)_6 \end{pmatrix} = \begin{pmatrix} r_{11} & r_{12} & r_{13} \\ r_{21} & r_{22} & r_{23} \\ r_{31} & r_{32} & r_{33} \\ r_{41} & r_{42} & r_{43} \\ r_{51} & r_{52} & r_{53} \\ r_{61} & r_{62} & r_{63} \end{pmatrix} \times \begin{pmatrix} E_x \\ E_y \\ E_s \end{pmatrix}, \tag{3.4}$$

where the vector $\vec{E} = \{E_x, E_y, E_s\}$ describes the electrical driving field applied. So if original axes are the principal ones, the indicatrix becomes

$$\left[\frac{1}{n_x^2}+\Delta\left(\frac{1}{n^2}\right)_1\right]x^2+\left[\frac{1}{n_y^2}+\Delta\left(\frac{1}{n^2}\right)_2\right]y^2+\left[\frac{1}{n_s^2}+\Delta\left(\frac{1}{n^2}\right)_3\right]s^2+2\cdot\Delta\left(\frac{1}{n^2}\right)_4 ys+2\cdot\Delta\left(\frac{1}{n^2}\right)_5 xs+2\cdot\Delta\left(\frac{1}{n^2}\right)_6 xy=1. \tag{3.5}$$

For the parameters under discussion at the deflecting device, see Fig.3.1, the power density of the laser radiation as $10mJ/(w\cdot d)^2 \cong 10mJ/cm^2$ with $\tau \cong 100\ ps$ duration, yields the laser electrical field strength of the order 1% of the driving electrical field. If any of components $r_{i3} = 0$, then laser field does not influence to the deflection at all.

Typical values of the r_{ij} are of the order $\cong 10^{-12} m/V$. For example, for *GaAs (ZnSe, CdTe)* cubic structure and for *KDP (ADP*, *CdGeAs$_2$)* tetragonal structure we have correspondingly

$$(r)_{ij} = \begin{pmatrix} 0 & 0 & 0 \\ 0 & 0 & 0 \\ 0 & 0 & 0 \\ 1.5 & 0 & 0 \\ 0 & 1.5 & 0 \\ 0 & 0 & 1.5 \end{pmatrix} \times 10^{-12}[m/V], \qquad (r)_{ij} = \begin{pmatrix} 0 & 0 & 0 \\ 0 & 0 & 0 \\ 0 & 0 & 0 \\ 8.8 & 0 & 0 \\ 0 & 8.8 & 0 \\ 0 & 0 & 10.5 \end{pmatrix} \times 10^{-12}[m/V] \tag{3.6}$$

With the driving field applied in *x*-direction, E_x (normal to direction of acceleration), the indicatrix according to (3.2) and (3.5) becomes

$$\frac{x^2}{n_0^2}+\frac{y^2}{n_0^2}+\frac{s^2}{n_e^2}+2\cdot r_{41}E_x\cdot ys \cong 1 \tag{3.7}$$

So one can see that the principal axes have a new direction. The new principal axes of ellipsoid (3.7) have an angle $\cong r_{41}E_x/n_e^2$ to the previous one. Accelerating field has a component parallel to *s*, E_s^a. Component of accelerating field in *y* direction at the face of deflection device is $E_y^a \cong E_s^a \cdot \Delta\vartheta$. So the cut could be made so that the prisms have their orthogonal edges parallel to old principal axes.

For a ***prism-based device***, Fig.3.1, deflecting angle is defined by the phase delay across the laser beam front arising from differences in the path lengths in material of the prism having a refractive index *n*.

$$\vartheta \cong n\frac{(L_a - L_b)}{w},$$

Here *w* –is the width of incident laser beam, L_a and L_b –are the distances through which the edges of the laser beam traverse the prism, Fig.3.1. A change in refractive index value yields a deflection angle change. To arrange such a change in refraction index, the basements of the prism are covered by metallization. When a voltage $V(t)$ applied to the metallization, the refractive index changes $\Delta n = \Delta n(V(t))$ according to (3.2), what yields the change (3.8) in deflection angle as

$$\Delta\vartheta \cong \Delta n \frac{(L_a - L_b)}{w}. \tag{3.8}$$

For such a sweeping device, a lot of electro-optical crystals can be used, see Table 1 below. For example, a crystal *KDP* (KH_2PO_4) is transparent for a radiation with the wavelength $\lambda \cong 0.2 \div 1\,\mu m$. Some other crystals, such as a *CdTe*, *CuCl*, *GaAs*, *ZnTe*, *ZnS* are transparent in the region of wavelengths around $\lambda \approx 10\,\mu m$. The last group of materials have rather high refractive indexes n_0~(2-4) what compensate smaller electro-optical coefficient.

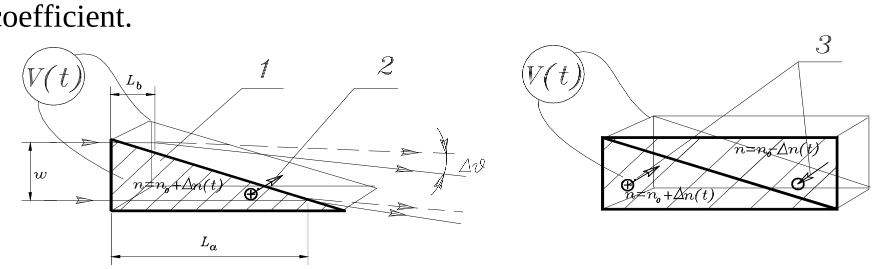

FIGURE 3.1: The prism deflection device concept. At the left side, the electro-optical crystal prism has metallization 1 (hatched) on both basements of the prism. Direction of optical axis had shown by 2. Time dependent voltage applied to metallization. At the right side *two* prisms have oppositely oriented optical axes 3 with the same polarity of electrical field applied.

The number of resolvable sports for this device N_R can be found now as

$$N_R \cong \frac{\Delta\vartheta}{\lambda / a} = \frac{\Delta n \cdot (L_a - L_b) \cdot a}{\lambda w} \cong \Delta n \frac{l}{\lambda}, \tag{3.9}$$

where $l = L_a - L_b$ stands for the prism base length and $a / w = 1$ in our case. Substitute for example the numbers for *ZnTe* (transparent for CO_2 laser radiation) which has $n_o \approx 2.9$, $r_{41} \cong 4.4 \cdot 10^{-12} m / V$, $E \cong 10 kV / cm \equiv 10^6 V / m$ one can obtain $\Delta n \cong 10^{-4}$. For *KTN* (*Potassium Tantalate Niobat*) crystal $\Delta n \cong 7 \cdot 10^{-3}$ for $\lambda \cong 0.63 \mu m$ is possible [3.11]. Anyway, the shorter wavelength is preferable from this point of view.

One can see from (3.8) and (3.9) that with the increase in optic path difference both the deflection angle and the number of resolved spots increase also.
To increase the last numbers (N_R, $\Delta\vartheta$), *multiple-prism* deflectors were developed, see Fig.3.2. We added a *traveling wave* regime here to be able to sweep the short laser bunches. The plates are wider in transverse direction, than the prisms. This has done for uniform field generation in the volume of crystals. Some electrostatic optimization could be done easily.
Here neighboring prismatic crystals have oppositely oriented optical axes. These crystals positioned between the strip–line electrodes. To be able to sweep short laser bunches, the voltage pulse $V(t)$ is propagating along this strip-line as a *traveling wave* together with

the laser bunch to be swept, as it was proposed in [2.4]. This gives the necessary voltage profile along the laser pulse at *cm* distances, what corresponds to the pulse duration $c\tau$.

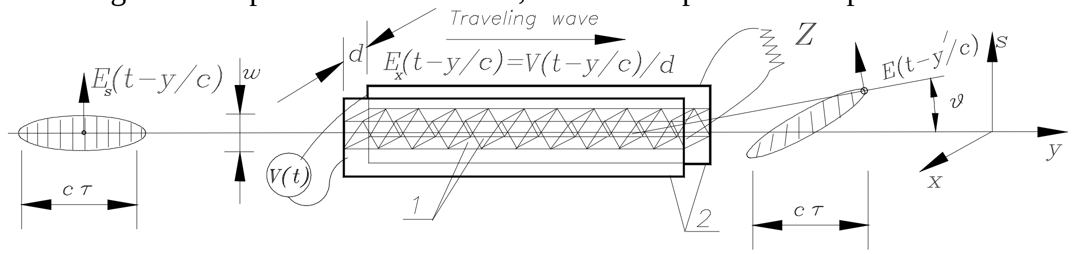

FIGURE 3.2: Prisms 1 with *oppositely directed optical axes* installed in series between two parallel strip–line electrodes 2, *d*–is the distance between them. *Z*– is matching impedance. Lines across the laser bunch schematically show the wave fronts. $E_x(t-y/c)$–is a driving electrical field.

As we mentioned, the radiuses of curvature of wavefronts in the swept beam have a common center in the deflecting device. Necessary correction of this effect could be easily done, for example, by variation of the thickness of cylindrical lens 7 in Fig.5.1[♣], see chapter 5. This systematic variation is of the order of $\pm 80\mu m$. The deflection angle and the number of resolved spots become now

$$|\Delta\vartheta| \cong \Delta n \frac{2L_d}{w} \cong \frac{L_d}{w \cdot d} n_0^3 \cdot r_{ij} \cdot V , \qquad N_R \cong \Delta n \frac{2L_d}{\lambda} \tag{3.10}$$

Where L_d stands for full length of deflecting device, *w*–is the laser beam width (along direction of deflection). For L=50*cm*, one can expect for $w \cong 1cm$, that deflection angle is $\Delta\vartheta \cong 10^{-2}$ and $N_R \cong 10$ for $\lambda \cong 10\mu m$ and, correspondingly $\Delta\vartheta \cong 10^{-2}$ and $N_R \cong 100$ for $\lambda \cong 1\mu m$.

We estimated the field applied to the crystals as 10 *kV/cm*. This is really a field strength *variation* along the laser bunch. This *variation is traveling together with the laser beam* along the sweeping device, Fig. 3.2. This strip line sweeping device could be sectioned (sliced) for the voltage reduction. For example, utilization of hundred slices in direction orthogonal to $w \cong 1$ *cm* will reduce the voltage to 0.1 *kV* per slice. If we suggest that electrical impedance of the strip-line be of the order $Z \cong 100\,\Omega$, the impulse power required to generate this voltage becomes $P \cong 100\,W$ per slice, while average one remains on the level $P_{av} \cong P \cdot f \cdot \tau \cong 16\ mW$ for repetition rate $f \cong 160\,Hz$. Special devices with avalanche diodes could be used here.

The thickness of the package is defined by the level of the damage to the material of electro–optical crystal. We will see, that the laser flash energy passing through the single crystal is 10*mJ* . In our example we estimated the area cowered by the laser beam as $S \cong w \cdot d$, what is about 1*cm*^{2}. This yields the energy density 10 *mJ/ cm*^{2} only. One can

[♣] This lens can be made with a mandrel for additional focusing directly to the orifice of each individual cell of the structure, see Fig.5.2.

decrease the area at least 10 (up to 100) times. Reduction of orthogonal dimension will further reduce the power required for deflection. Some optimization is possible here.
Example of technical realization of this traveling wave deflector is represented in Fig. 3.3 below. Here, basically, a strip-line electrodes 2 have a triangle crystals with opposite optical axes orientation (see Figs.3.1, 3.2) in between. A para-phase impulse, applied to one end of strip-line trough connectors 3, propagates to the other end and further connected to the matching impedance. So only half of full voltage is applied trough each connector. Matching dielectric 6 adjusts the speed of deflecting wave to the speed of laser radiation, propagating in crystals.

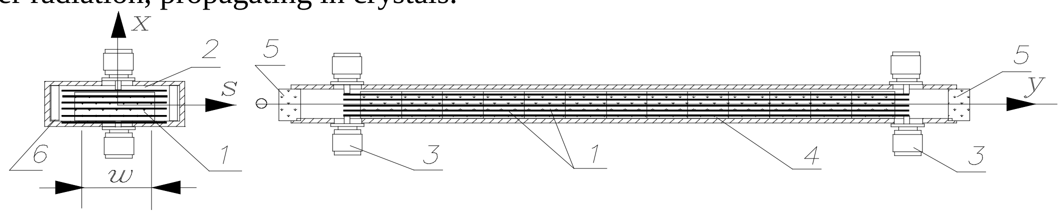

FIGURE 3.3: Example of technical realization of multi-prism traveling wave sweeping device. Electro-optical crystals 1 are positioned between strip-lines 2, attached at the end to the connectors 3. 4–is a cabinet with optical windows 5 from both sides. 6–is a matching dielectric.

The broad band traveling wave deflector could be obtained also if the same crystals located in the middle of a waveguide shortened from both sides. In this case it is possible to arrange a standing wave in a waveguide what requires a relatively small power, taking into account that the losses in crystals are small. As the standing wave can be represented as a superposition of two traveling waves in opposite directions, one can conclude, that the only co-directional wave will deflect the laser beam. Despite the materials transparent for longer wavelengths have lower value of r_{ij}–components, they have higher values of refracting index, so the variation of refractive index becomes about the same, (3.7) (see Table 1, below).
The broad band traveling wave deflector could be obtained also if the same crystals located in the middle of a waveguide see Fig.3.4. There is no difference in principle between these two deflectors. The last one has a bandwidth of a waveguide. Group velocity of electrical wave-pulse must be adjusted to the velocity of the laser radiation in the prisms. Widening of the waveguide helps to reach this goal.

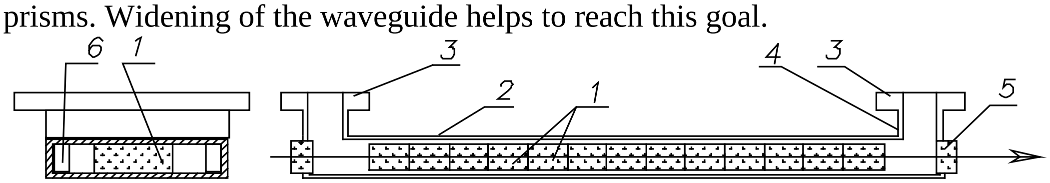

FIGURE 3.4: Multi-prism traveling wave sweeping device in a waveguide. 1–is electro-optical crystals, positioned in a waveguide 2, having bends 4 with flanges 3. 5–is an optical window. 6 –is a matching dielectric.

A lot of slowly operating devices is routinely in use, see [3.7, 3.9]. In [3.8] for example, the voltage applied about $V = \pm 5kV$ provided the deflection angle $\theta = \pm 10^{-3} rad$ in *KDP* device. The device has 10 *KDP* crystals with total 20c*m* length and about 1cm^2 of input aperture.

As we mentioned, from (3.10) emerges, that with lowering the cross-section of the laser beam *w*, the deflection angle could be increased. However, *w* must be chosen so, that the power density kept below the damage level for this crystal.

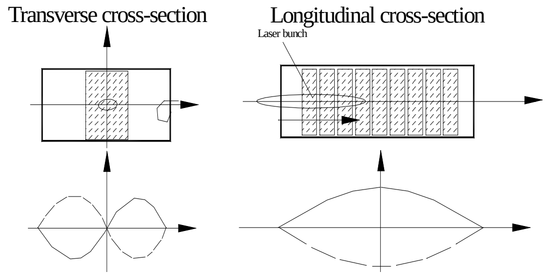

FIGURE 3.5: The concept of transverse feeding for electro-optical device.

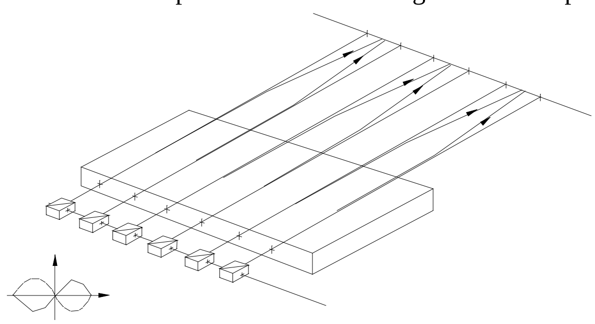

FIGURE 3.6: The array of transversely feeding electro-optical devices. From this instant view it is clear, that the neighboring rays have opposite deflecting angles due to a half wavelength separation of the splitting devices.

Other possible electro-optical sweeping device for deflecting of short laser pulses is the ***transverse feeding*** of electro-optical device, Fig.3.5. Here a standing wave excited in a metallic box. The wave has two variations in scanning direction and basically one in direction of the laser beam propagation. In terms of the wavelength it has first size around a wavelength in a transverse direction. In some kind it is another way to arrange a gradient of electrical field and, hence, a variation of refraction index across the laser front. The wavelength of driving voltage is close to the laser bunch length and effective length of the crystal in longitudinal direction is shorter, than the laser bunch length. In this case the optical gradient across the laser front will deflect a laser bunch in transverse direction. In Table 3.1 we summarized general parameters of electro optical deflectors.

TABLE 3.1. Electro-optical materials for deflector

Wavelength	Materials	ϑ , *rad*	N_R
$\lambda \cong 10\mu m$	*GaAs, ZnTe, ZnS, CdS, CdTe, CuCl*	0.01-0.02	10
$\lambda \cong 5\mu m$	$LiNbO_3$, $LiTaO_3$, *CuCl*	0.01-0.02	20
$\lambda \cong 1\mu m$	*KDP, DKDP, ADP, KDA*, $LiNbO_3$	0.01-0.02	100

Some materials for $\lambda \cong 10\mu m$ have limited transparency about 70% (*ZnS*) what need to be taken into account. In this sense the $\lambda_{ac} \cong 1\mu m$ and even optical wavelengths are preferable.

Optimization.

To optimize the deflecting device for the maximal number of resolved spots, one need to specify the deflection per unit length *K*. Then the angle inside deflecting device will be $\vartheta(z) \cong \vartheta_i + K \cdot dz$, where ϑ_i is an incoming angle. This angle needs to be compared with the angle of divergence $\cong \lambda / w$ what yields $dN \cong w(z)Kdz/\lambda$, where it was suggested, that the optical beam width *w(z)* -is a function of distance due to the focusing.

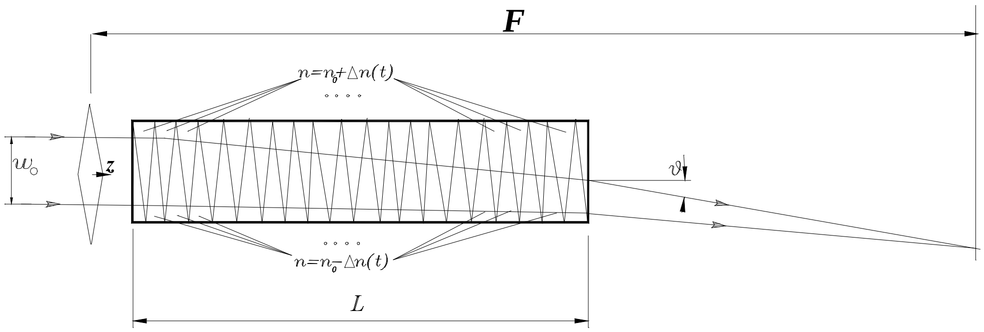

FIGURE 3.7: Dimensions used in optimization procedure.

Let us suggest also that the plane, where the accelerator structure is located, is a focal one, i.e. $w(z) = w_0 \cdot (F - z)/F$, where F -is the distance from the *input* plane to the focal plane and w_0 is the width on input plane, see Fig.3.9. Substitute the last expression into expression for *dN*, one can obtain $dN \cong \dfrac{w_0(F-z)}{\lambda F} K \cdot dz$. Integrating the last equation, and substitute $L = w_0 / KF$, one can obtain, that the optimal number of resolved spots is $N_{\max} \cong \dfrac{w_0}{\lambda} \cdot \sqrt{32Kw_0/27}$ and optimal length of deflecting device is $L_{opt} \cong w_0 \cdot \sqrt{\dfrac{2}{3Kw_0}} \approx \dfrac{2}{3}F$ [3.3]. These formulas are valid for any distributed deflection system with the focusing lens installed in front of deflecting device.

Mechanical deflection system.

Angular frequency of sweeping required is equal $\Omega \cong V / R$, and the spot sweeped along the structure, so $\Theta \cong \Omega\tau \cong c\tau / R \cong L/R$, Fig.2.2, Fig.2.4. Estimating $R \cong 1m$, we obtain $\Omega \cong 3 \cdot 10^8$ *rad/sec* for $V = c$. The corresponding frequency $f_m \cong \Omega / 2\pi \approx 47\, MHz$. In principle, a *mechanical* deflection system with a piezoelectric (a quartz for example) can be used for this purposes♣. For obtaining the deflection angle of $\vartheta \cong L/R \cong 10^{-2}$ at high frequency, the quartz plates must be arranged as a tandem assembly. The sweeping angle delivered by a single mirror is $\vartheta_1 \cong \Theta / M = L/RM$, where M –is the number of stages in a system. So the frequency of mechanical oscillation of the mirrors must be $f_m / M \cong 5MHz$ in ten-stage tandem.

♣ Quartz plates, sealed in vacuumed bulbs and operating at 50 *MHz* are commercially available. At low frequency~45 *kHz*, single mirror could give 2^o deflection, see [3.10] .

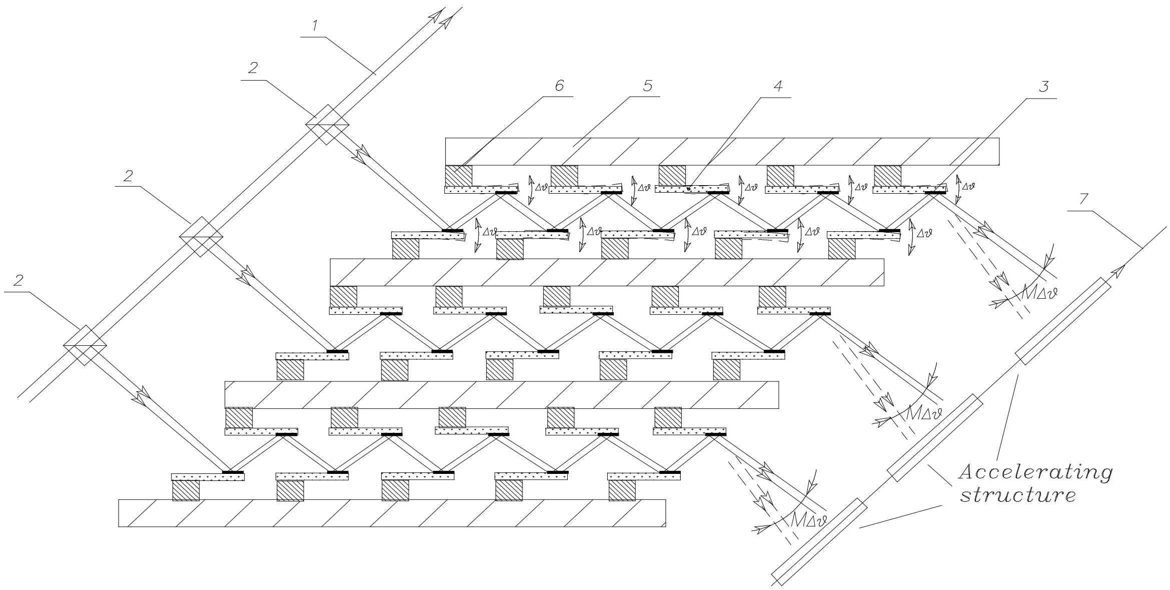

FIGURE 3.8: A ten stage mechanical deflecting array of three sweeping devices. *M* mirrors marked by 3 (*M* = 10 here) installed on the quartz crystals 4. 1–is a primary laser beam, 7 –is a trajectory of a particle's beam. Crystal's oscillations phased for a maximal deflecting angle. Resulting deflecting angle is *M* times bigger than with a single mirror. The system shown could feed three accelerating structures.

For operation with this high frequency the quartz plates must be placed in a vacuum and must be thin to reduce the power dissipation in a crystal. Example of such array is represented in Fig.3.8. Here the laser radiation propagates along the line 1. A fraction of a power scratched with help of splitters 2. Mirrors 3 made on the surface of quartz plates 4. Beryllium mirrors are used for these purposes commonly. The quartz plates made on two metallized slices glued together and feed in opposite phase. Here we supposed that the cut made along the Y axes of the quarts crystal. For a sheak-cut the quartz plates need to be attached to the housing by one side of the plate and the mirror to rectangular one, see Fig. 3.9.

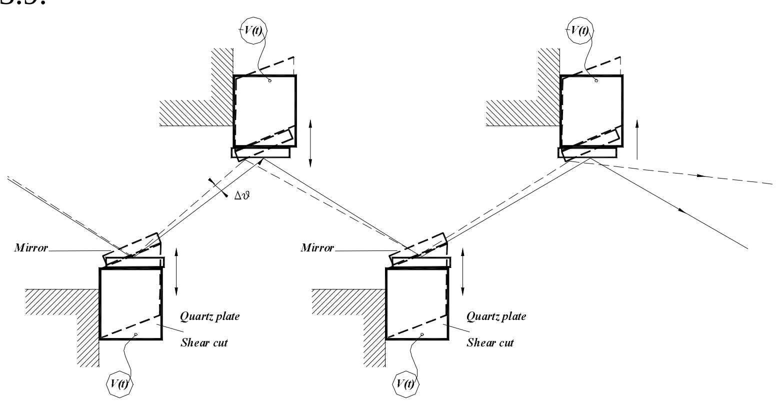

FIGURE 3.9: Deflection arrangements with quartz plate shear cut [3.3]. This cut done with angle~55^{o} to the Y- axis of the quartz crystal. Metallization applied to the front and opposite sides of the crystal. Tilt angle shown is not in scale (unfortunately).

The quartz plates attached to the grounded basement 5 through intermediate supports 6. 7 –is the particle's beam line direction. So, parameters for mechanical sweeping device are about the same as shown in Table 1.

For a *single* mirror attached to a piezoelectric, peak-to-peak angular motion with frequency around 5 *MHz* $\Delta\vartheta \cong 8.7\cdot 10^{-4}\,rad$ is possible. Ten mirrors will give $\Delta\vartheta \cong 8.7\cdot 10^{-3}\,rad$, what is acceptable. $N_{\max} \cong \frac{\sqrt{\Delta\vartheta}}{\lambda_{ac}/w} \cong \frac{1}{10^{-3}}\cdot\sqrt{8.7\cdot 10^{-4}} \cong 30$ for $\lambda_{ac} \cong 10\mu m$ and $w \cong 1cm$. For $\lambda_{ac} \cong 1\mu m$, the number of resolved spots will achieve $N_{\max} \cong 300$. Cooling of the quartz plates helps to reach higher repetition rates. So this is probably mostly effective sweeping device.

However, like for any mechanical device, the lifetime will be strongly limited probably. It definitely could be used at the proof of principle stage.

Acousto-optical deflector [3.1, 3.2, 3.13, 3.14].

Another possibility to deflect a laser beam is an acousto-optical. Basically this is a kind of diffraction grating method. Acoustic wave, induced in a media with piezo-optic effect, provides a cyclic change in the index of refraction with a space period Λ, comparable with the wavelength of radiation. This radiation, having width *w*, crosses the media and gets an angle, defined by the Bragg condition, given by $\vartheta \cong \lambda/\Lambda$. If v stands for acoustic velocity, then $\Lambda f \cong v$, where f -is a frequency. Effectively changing acoustic wavelength by changing the *f* during the laser radiation pass through the crystal, one can provide the changing in direction of the radiation, passed through this device as

$$\Delta\vartheta \cong \frac{\lambda}{v}\Delta f \cong \frac{\lambda}{w}\tau\cdot\Delta f\ , \tag{3.11}$$

where we recalled the time required for the wave to pass trough the laser beam width *w* as $\tau = w/v$ and Δf stands for the range of frequency change.

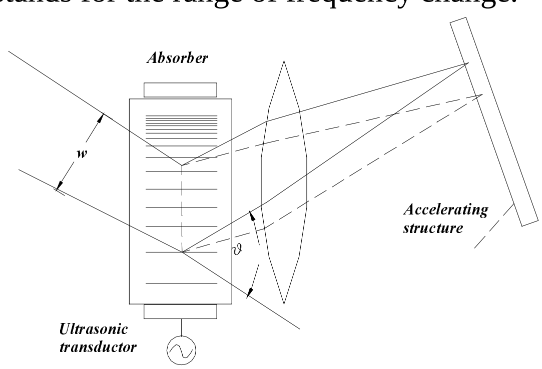

FIGURE 3.10: Acousto-optical deflection.

Therefore for the number of resolved sports we obtain

$$N_R \cong \frac{\Delta\vartheta}{\lambda/w} \cong \tau\cdot\Delta f\ , \tag{3.12}$$

so the product of bandwidth and crossing time is crucial for this method. For example, for typical velocity $v \cong 0.6mm/\mu s$, $w \cong 5mm$ the time will be about $\tau \cong w/v = 5/0.6 \cong 8\mu s$. To obtain a reasonable number $N_R \approx 20$, one needs to have $\Delta f \cong N_R/\tau \cong 20/8 = 2.4MHz$. For increasing the speed of deflection, some sectioning for sound wave excitation need to be done to reduce the effective passing time τ.

Important item here is suppression of radiation in other, than general, maximums.

Short laser bunch.

We suggested, that the laser bunch is long enough, so the $l_b \cong c\tau \equiv L > 2w/\tan\vartheta$, see Fig. 3.10. If the bunch is short, the picture of the laser bunch passed through diffraction grating will have the shape as it is shown in Fig. 3.11 below. The distances *a1* and *a2* defined basically the slope of the laser bunch. If we suggest that the width of the incoming laser bunch *w=L*, $\tan\alpha \cong (a1+a2)/w$. In it's turn $a1+a2 \cong \dfrac{2w}{\tan[(\pi-\vartheta)/2]}$, so the relation between the angles becomes

$$\tan\alpha \cong 2/\tan[(\pi-\vartheta)/2] \ . \qquad (3.13)$$

So the way like the laser bunch looks after diffraction formally satisfy the requirements expressed in Fig.2.1. The width of the laser bunch must be $w \cong L$. The length of the spot on the accelerating structure is $\sim l_b$.

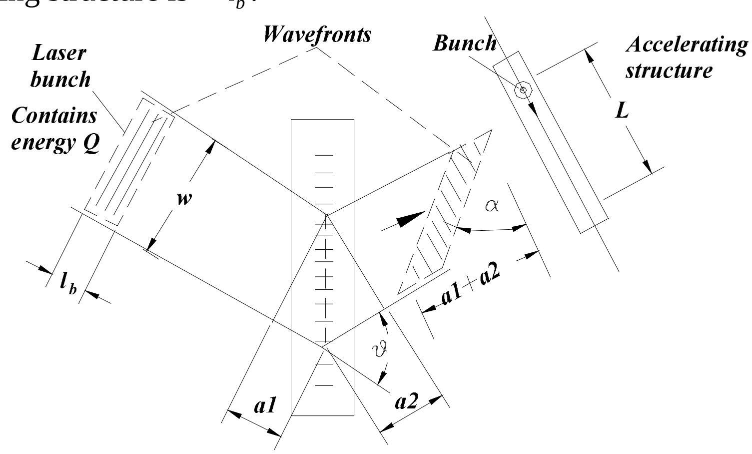

FIGURE 3.11: A short laser bunch diffraction with arrangements from Fig.3.10. Angle α here and in the Figs.2.1, 2.2, 2.4 has the same meaning.

The disadvantage of this way, as we mentioned in association with proposal [2.6], is the following. The energy *Q* delivered by the laser source contained in the laser bunch, see Fig.3.11, must be delivered in this method by the time l_b/c or the power required $\cong Qc/l_b$. Meanwhile in TLF method the same energy *Q* must be delivered in time $\tau \cong L/c$. So the ratio in power is $L/l_b \cong w/l_b$ in favor of TLF. In it's turn, this is around $L/(L/N_R) = N_R$. Distribution of diffracted radiation among the other maximums is another difficulty with the grating.

One interesting possibility emerges here. If we take a laser bunch, sweep it and direct further to the grating (from right to left in Fig.3.12), the bunch at the out of the grating (left side in Fig.3.12) will be compressed. This method of compression may have some sense in connection with preparation of short powerful laser pulses. A laser amplifier positioned after sweeping device will have a wide aperture, so this reduces the problems with saturation of active media in amplifier.

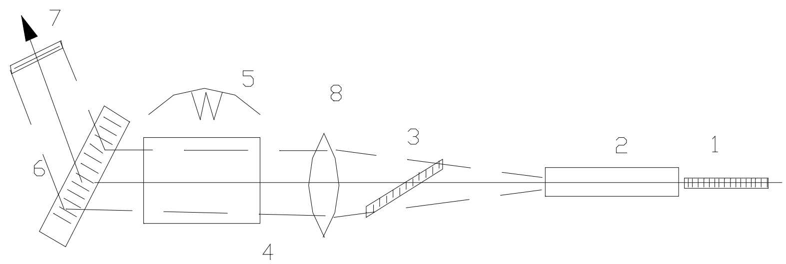

FIGURE 3.12: A laser bunch amplification and compression. 1 –is a primary laser bunch. 2–is a sweeping device. 3–is a laser bunch after sweeping. 4–is amplifier with the pumping system 5. 6–is the grating. 7–is the laser bunch at the output, 8 –is a correction lens.

The size of deflecting system in longitudinal (to the accelerating electron beam) direction is limited by sum of the length of accelerating structure and the length of focusing elements. For practical reason the ratio R/a could be $R/a \approx 100$. So the diffraction size of the spot in longitudinal direction could reach $l_f \cong 100\lambda_{ac}$ for $\lambda_{ac} = 10\mu m$. For $\lambda_{ac} = 1\mu m$ $l_f \cong 30\lambda_{ac}$. These figures reflect the maximal possible number of the bunches in the train. The optics can reduce the spot size on the structure or increase the angle of deflection. The number of resolved spots will be the same, however. The value of l_f gives the maximal possible value for *Q -factor* of the one cell of accelerating structure (see lower).

General conclusion for this Chapter is that the laser beam deflectors are available with parameters necessary for successful sweeping. Shorter wavelengths are preferable from the point of maximization of the number of resolved spots. Shorter wavelengths, however, are limited by the emittances for the particle's beam available (beam must pass through the structure), see lower.

4. ACCELERATING STRUCTURE

Accelerating structure is a vital component of any accelerator. It serves as a housing for accelerating field. The mostly important role of the structure is, however, in proper *positioning* of accelerating field in space. Many projects on laser acceleration suffer from sensitivity to fluctuations in laser homogeneity. This is especially so in some schemes used splitted lasers beam and combined further to obtain symmetrically crossed wave fronts. In its turn precise location defined by accuracy of fabrication, accuracy of positioning, how far from equilibrium the fields are and by physical limitations. Example of last kind gives atomic nature of material, what limits the accuracy of fabrication to the atomic distance. From this point a monocrystallic materials is desirable. The coupled electrons having frequencies much higher, than the laser one, define the effective boundaries of the structure for nonconductive materials. Accuracy due to electron plasma in a metal is $\sim r_D/\lambda$, where Debye radius r_D defined as

$r_D = \frac{v_p}{\omega_p} \cong \frac{\sqrt{k_B T/m}}{\omega_p} = \sqrt{\frac{k_B T}{4\pi n e^2}}$, where $k_B \cong 1.38 \cdot 10^{-23}$ J/^{o}K –is Boltzmann's constant, T –is electron temperature, n –is an electron density in a metal, r_0 –is a classical electron radius. Formally, as $\omega_p \cong 10^{16} 1/s$, $v_p \cong 10^8 cm/s$, $r_D \cong 10^{-8} cm$ and the ratio $r_D/\lambda \cong 10^{-4}$. In diluted plasma with density $\sim 10^{-6}$ of density in metal, the last ratio becomes $r_D/\lambda \cong 10^{-1}$ only. In general, the plasma methods must experience problems with fluctuations of the number of electrons in Debye sphere $\Delta n \cong \sqrt{N_D}$. The last number is $N_D \cong \frac{4}{3} n r_D^3 \cong \frac{1}{\sqrt{n}} \left(\frac{k_B T}{4\pi e^2} \right)^{3/2}$ so $\Delta n \sim 1/\sqrt[4]{n}$. Namely this makes stable acceleration in plasma problematic on the physical background.

As far as ***electromagnetic properties of metals*** at high frequencies, corresponding to infrared radiation $\lambda_{ac} \approx 1-10\mu m$, they are well described theoretically in [4.1]. General output of these considerations is the following. When the frequency of incoming radiation increases and comes to infrared region, the minimal among three dimensions: skin depth δ, free electron path in metal l_{free} and v_F/ω, where v_F –is the electron velocity at the Fermi surface, the last one becomes the smallest one. The mean free path of electrons at room temperature is ~10^{-4}*cm*. The time between collisions, hence $l_{free}/v_F \cong 10^{-12} s$. With decreasing temperature the last time drops ~$1/T^2$.

This is natural sequence of dependence $\delta\omega \sim \omega^{2/3}$ for anomalous region. What is important, that the energy of incoming laser radiation still lower than the Fermi energy E_F. Under these conditions the conductivity of the metal becomes imaginary

$$\sigma \cong \frac{i}{4\pi} \frac{\omega_p^2}{\omega} \quad . \tag{4.1}$$

In definition of the plasma frequency here the only electrons of conductivity are taken into account. If the frequency becomes higher (optical), then the atom's electrons participate in the propagation of radiation and in definition of plasma frequency it is necessary to take all electrons. Formula (4.1) means, that equation of diffusion of electric field in the metal $E'' = -\frac{4\pi i \omega \sigma}{c^2} E$ becomes $E'' - (\omega_p^2/c^2)E = 0$ so $E \cong E_0 \exp(-\omega_p x/c)$ * and the penetration depth is not a function of the frequency. The surface impedance $E/H \cong -i\omega/\omega_p$ is *fully imaginary*. This means that reflection of the laser wave from the surface is going *without dissipation*. This is a natural sequence of the assumption made: the electrons do not collide during the period of incoming radiation. Hence there is no dissipation. Decreasing the temperature of the metal helps to reduce the dissipation as the *phonon* density decreases with temperature, as the time between electron phonon collisions drop ~$1/T$. At lower temperatures the electron scattering on crystals defects became dominant. For Copper at low temperatures the time

---

* For typical metals $c/\omega_p \cong 10^{-5}$ *cm*.

corresponding to electron-imperfection collisions goes to ~$10^{-8}s$ [5.2]. Some electrons could collide under these conditions in few oscillations, however. This is the sequence of equations of motion in oscillating field formally. For some starting phase, electrons have constant term in acceleration. This formally similar behavior of electrons in oscillating field is well known to RF engineers dealing with multipactor phenomena: for some starting phases, electrons have small constant acceleration in oscillating field, $x \cong -eE_m \cdot t \cdot Cos\varphi / m\omega$. It is possible nevertheless to consider in first approximation the metallic structure in infrared region of laser frequencies practically as having no dissipation. This statement is valid for pure metals without any oxide film on the surface. We will continue discussion on this subject in Chapter 8.

The concept of the structure.

For the loss reduction, the structure is excited from the side. There are proposals for accelerating structures what could be scaled down to match the wavelength of laser radiation [4.2-4.4]. *Any of these* could be used with TLF method, as the TLF method is more, than any particular accelerating structure. We took the foxhole-type structure described in [4.3] as a basis, Fig. 4.1.

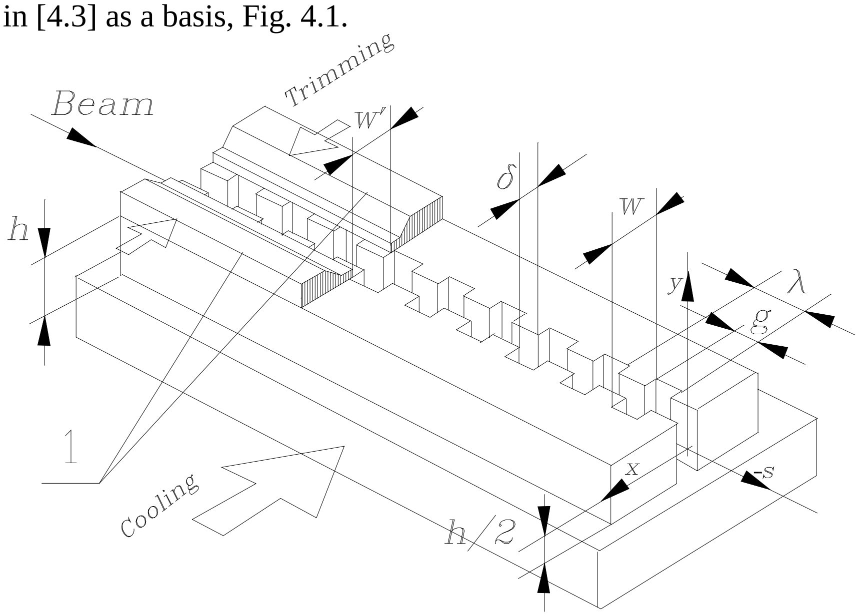

FIGURE 4.1: The foxhole type accelerating structure. Height h is $h \cong \lambda_W / 2$, where λ_W –is a wavelength of laser radiation inside the cell. $g / \lambda \cong 1/2$, $W \cong 0.7\lambda$, $\delta \cong 0.2\lambda$. 1–are the masks along the structure. $W' \leq W$. The masks are used for trimming the inductive coupling (Q_{RF}–factor).

This structure has advantages in pumping, alignment and cooling. It is mechanically strong and could be easily fabricated with nanolithography. The mostly important feature, however, is that this structure gives a good 3D positioning for electrical field map. This is very important property. For *cm* wavelength accelerating structures, it is natural, that the walls of the structure properly locate the electrical field and this even not mentioned♣. This proper location of electric (and magnetic) field map reduces sensitivity

♣ Structure [4.2] does not locate the field in transverse direction, so it is not possible to use it for acceleration. This structure also has difficulties in thermal stability and pumping.

to fluctuations in laser beam homogeneity. Structure also gives a good basis for further improvements. We will consider here for a moment the simplest among these types, Fig. 4.1. Structures once used at Cornell some years ago [4.5] and using in [4.4] are very close to this type.

We made however, some change which looks not drastic, but it is very important. Namely we reduced the height of the cell closer to the half wavelength in cell's grove. In Fig. 4.1 the covers 1 adjust the coupling between the cell and outer space. With these covers the height *h* is about $h \cong \lambda_W / 2$ and the cells have *inductive* coupling with outer space. The *x*-axes directed across the structure, which has a groove of the width *W* in this direction (see Fig. 4.1) and *x* has a zero in the middle of the slot. The *y* directed to the depth of the groove and has a zero at the distance *h*/2 from the bottom. The channels for the passing of the beam have a size $\delta \le 0.2\lambda$. This accelerating structure with open slots in narrow place can accept the field with polarization perpendicular to direction of motion. This yields a systematic modulation of transverse motion. To prevent this one can locate polarization filters on the lens 7, on Fig. 5.1. Other possibility- to extend the masks over narrowest places marked by dimension δ. More complicated mask profile with *horn-type extensions* around each opening could be made for accepting the radiation from larger area for re-direction the power captured into each individual cell.

For obtaining necessary magnetic coupling of the structure with outer space, the masks 1 (Fig.4.1) are used here. The last defines a quality factor Q_{RF} of the structure.

It is clear from the boundary conditions considerations, that as the electrical field on the bottom, *y*=- *h*/2 is zero, then the variation of electrical field along the *y* direction must come to zero again. Evidently this happens at the distance $y \cong h/2 \cong \lambda_W / 4$, where λ_W is a corresponding wavelength of radiation in the grove, $\lambda_W \approx \lambda / \sqrt{1-(\lambda/2W)^2}$. The last formula is more exact, if $\delta \to 0$. If the width *W*, *g* and δ are chosen, the depth of the structure *h* must be adjusted around $h \cong \lambda_W / 2$.

So electrical field, required from boundary condition at the bottom, yields electrical field at orifice also zero, what makes the boundary condition at orifice for incoming radiation looks like for metal, $Z_s \cong E_s / H_s \approx 0$. This reduces the field strength at orifice down to the value, defined by dissipation of energy in the cell only. Analytically the field inside the cell could be described in first approximation simply as in a box

$$E_s \cong E_m Cos\frac{\pi x}{W} Cos\frac{\pi y}{h} Cos\omega t \,,\; H_x \cong \frac{E_m \lambda}{2hc} Cos\frac{\pi x}{W} Sin\frac{\pi y}{h} Sin\omega t \,,\; H_y \cong \frac{-E_m \lambda}{2Wc} Sin\frac{\pi x}{W} Cos\frac{\pi y}{h} Sin\omega t \,.$$

These equations are exact if the cell is closed. Analytical consideration of fields in similar structure [4.4] one can find in [4.7]. The difference between our structure and the structure [4.4] is that there is no propagating wave from cell to cell in our structure.

Original foxhole structure [4.2] has $h \cong 3\lambda_W / 4$. In this case electrical field reaches the maximum at the orifice and the coupling between the cell and outer space is *capacitive* with high input impedance $Z_s \cong E_s / H_s \to \infty$. We found this unacceptable. First, additional height $\cong \lambda_W / 2$ stores the energy what is not in use. Second, one can see that in the structure with such height electric field at lest *doubled* at orifice and this may increase the problems with damage threshold. Third, infinite impedance at the orifice breaks a continuity of surface impedance. That is because the impedance of material at the transit slit is close to zero, as it is valid for metal. That is why to correct all these disadvantages the structure with the height $\cong \lambda_w / 2$ was chosen.

Exact dimensions define the balance between the power going in the cell and back. Higher value of Q_{RF} reduces the power required from laser to reach the gradient desirable. But *mostly important role* this plays in establishment of equilibrium distribution of the field in the structure, preventing a traveling wave regime along *y* direction. This traveling wave regime occurs in transition period, when the cell is under filling with laser radiation. The Q_{RF} factor of the order 5-10 could be expected here.

We would like to stress here, that for strong electrical field generation, even $Q_{RF} \cong 1$ is enough. Cell with Q_{RF} >1 provides a *few oscillations* of the field in the cell before it reaches the maximum, thereby reducing influence of fluctuations in positioning the electrical field map inside the cell.

Despite the group velocity for this structure formally equals to zero, there is a strong coupling between neighboring cells trough orifices.

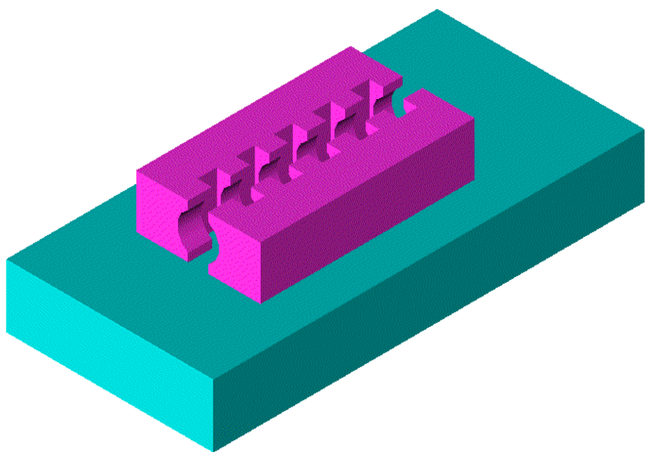

FIGURE 4.2 (color)**:** An example of the structure with round passing holes. Dimensions are the same as on Fig.4.1. Covers (masks) are not shown. Five cells are shown.

Mostly calculations for this type of structure done with of **GdfidL** code [4.6]. There were investigated different shapes of cell and transit slit between the cells. Example of a structure with round passing holes and smoothed passing holes are represented in Figs.4.2, 4.3. The final shape is a trade between technology and optimal filling properties.

Ideally the structure must look like a series of individual cells connected by round holes. Each cell is open from the side. From opposite side there must be some extraction for compensation the asymmetry from input orifice. Diamond coating will help to increase the damage threshold, see lower.

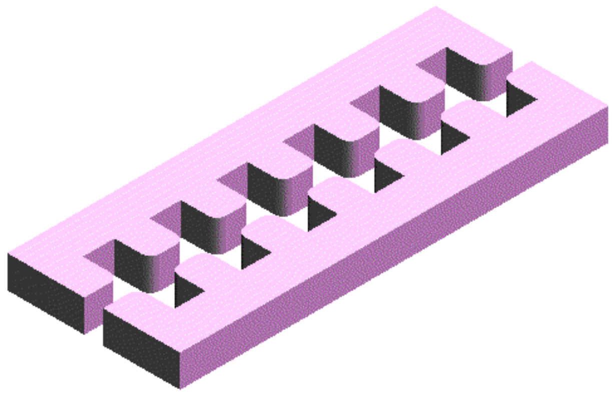

FIGURE 4.3 (color): An example of the structure with smoothed passing holes. Covers and base are not shown. For better visibility the height shown is reduced also.

The following numbers give an idea of parameters. Typical longitudinal and transverse wakes *normalized to one cell* are $W_{\|} \cong -7\,kV/pC$ and $W_{\perp} \cong 2.2 \cdot 10^{2}\,V/pC/\mu m$ correspondingly for the accelerating structure with $\lambda \cong 10\mu m$, $\delta = 2\mu\,m$, $W = 7\,\mu\,m$ (see Fig. 4.1) and the bunch with the longitudinal length $\sigma_{l} \cong 1\,\mu\,m$ and bunch population $N \cong 10^{6}$. So total charge is $eN \cong 1.6 \cdot 10^{-13}C$ or 0.16*pC*. An example of wake calculated for some modification of the structure is represented in Fig. 4.4. The charge in the bunch here is 0.2 pC. One can see that the wake is slightly inductive. On Fig. 4.5 there is represented an example of the field in a structure, obtained with GdfidL code.

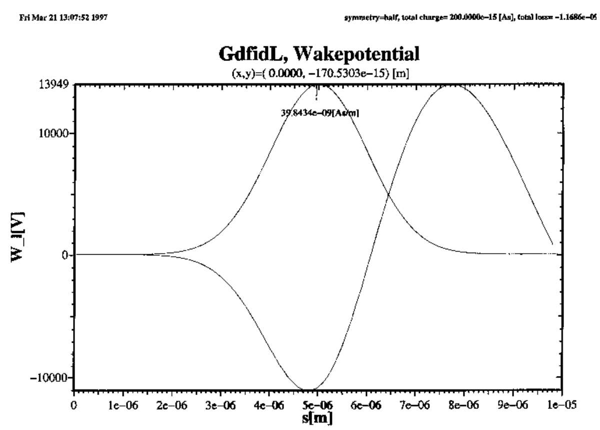

FIGURE 4.4: Example of the wake for 5 cells. Wake in the center of the bunch is about -10 *kV*. Charge in the bunch is ~0.2 *pC*.

So one can see compare the wake energy drop $\approx 7kV/pC \times 0.16\,pC \cong 1.12kV$ with the energy gain in one cell as ~30 *kV*, (see Section 8). So the accelerating voltage drop is about ~1.12/30 ≅ 3.7%. The energy, carried out of the cell is, hence ~7.4%.

To reduce the wakes it is necessary to increase the length of the bunch. As this wake is sitting on the top of the accelerating sin-like voltage, there is a possibility even to reduce

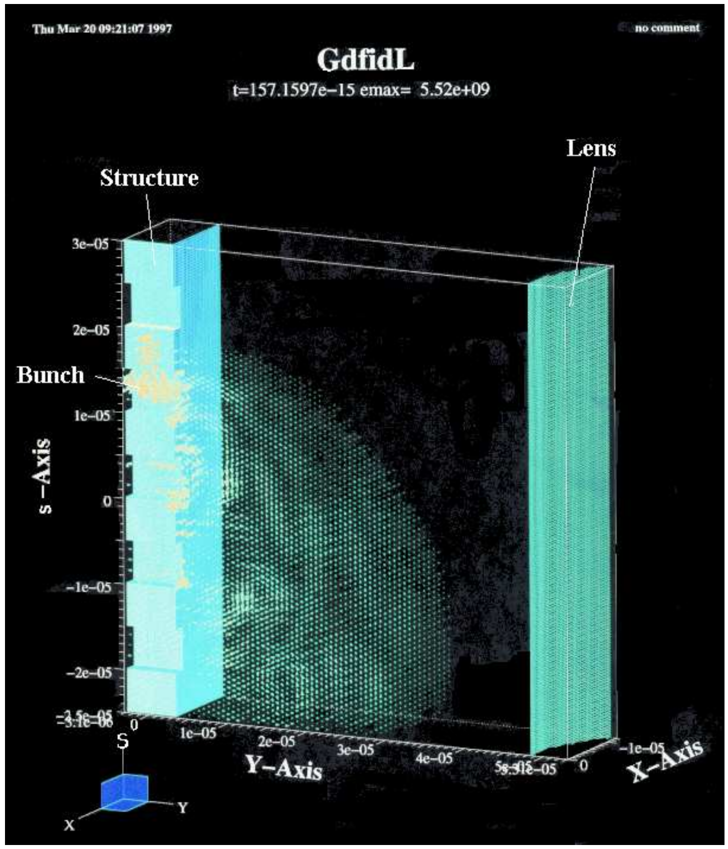

FIGURE 4.5 (color)**:** The bunch in the structure. A half of full picture is represented. The bunch is running through the structure on the left. A cylindrical lens (pos. 7 in Fig.5.1 is on the right side of the picture; ¼ of the geometry is shown).

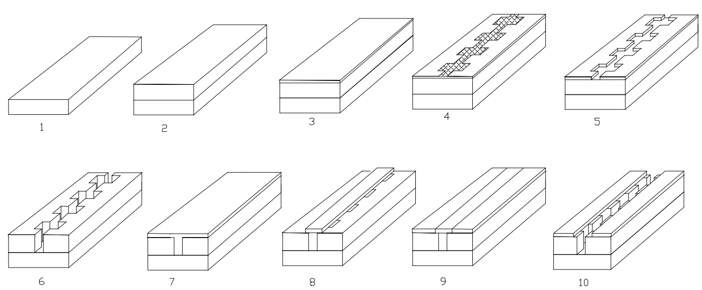

FIGURE 4.6: Fabrication of the structure. 1– is a base. 2–material of the structure is placed on the base. 3–a photoresist is placed at the top. 4–the photoresist is exposed. 5–some of photoresist is removed. 6–material of the structure etched. 7–a new cover of photoresist is placed. 8–extra resist is removed. 9–material of the structure is added. 10–structure etched again.

the energy spread along the bunch. This is a result of combination of accelerating field and wake as this combination can provide a flat top. That was proposed to use in conventional linear collider [9.2]. In more details this subject considered in Chapter 9.
The technological possibilities in lithography are advanced far beyond the requirements associated with this structure scaled down to $\lambda_{ac} \cong 1\mu m$. In Fig. 4.6 the process of manufacturing is shown schematically. The latest technologies use much more advanced

tools than was used even few years ago. One can expect that these technologies will go hand in hand with microchip technology development. Even now mostly impressive technologies allow placing and positioning of *individual atoms* on the surface. More complicated and more advanced structure will be made to compensate the influence of the orifice of the cell, which basically shifts the center of the field if vertical direction. For this purpose, similar to what is done for microwave structures, some symmetrical extractions could be made in the bottom of each cell.

Each structure is installed on a micro-table moved by a piezoelectric with appropriate orientation of the crystal axes, Fig. 5.5. This allows aligning the structures for minimization the wakes. Structures are cooled down to keep the mechanical tolerances within the margins allowed.

A broad variety of materials could be used for the structure. For beginning it is possible to consider gold as mostly stable one. The final conclusion could be made after experimental work in this field. Silicon of different types of conductivity is possible here.

General conclusion is that there is a structure, acceptable for particle acceleration with wavelengths $\lambda_{ac} \cong 1-10\mu m$.

5. SOME TECHNICAL DETAILS OF THE SCHEME

In Fig. 5.1 there is represented an isometric view from Fig.2.2, fulfilled with more or less realistic components, required by TLF method.

Laser radiation generated at central station travels through splitters 1 aligned in longitudinal direction. Each of secondary beams 2 after passing long focusing lenses 3 goes through deflecting devices 4, described in previous section. Polarization of radiation in beams 2 directed along the structure. Further on the way there is a lens 5 for focusing the laser beam in longitudinal direction. After deflection, the laser beam 6 goes through a short focusing cylindrical lens 7. This lens focuses the laser beam on the structure 8 in transverse direction into a spot 9 with a transverse size of a few laser wavelengths.

The lenses 3,5 and 7 produce a small focal point on the structure. In this particular moment, the accelerated particles are located there. The beam is moving along the trajectory 10 and is focused by quadrupoles 11. Each part of the lens 7 is shortly illuminated, so for successful focusing the material with *appropriate* dispersion must be chosen[♣].

Deflecting voltage must be synchronized with the appearance of the particle's beam in the structure. The focal point 9 is following the beam, *in average*. Some mismatches yield a loss in energy gain only, as the *phase* of the laser radiation is synchronized once with the particle's beam motion. As the driven radiation has the same primary source, all modules remain synchronized. The laser focus sweep is limited to the distance about 3*cm* for practical reasons (see above), so the accelerating device looks like a sequence of 3 *cm* long accelerating structures with the focusing elements between them. A short focusing cylindrical lens appeared first probably in [5.1].

[♣] Utilization of mirrors instead of lens could help in this problem.

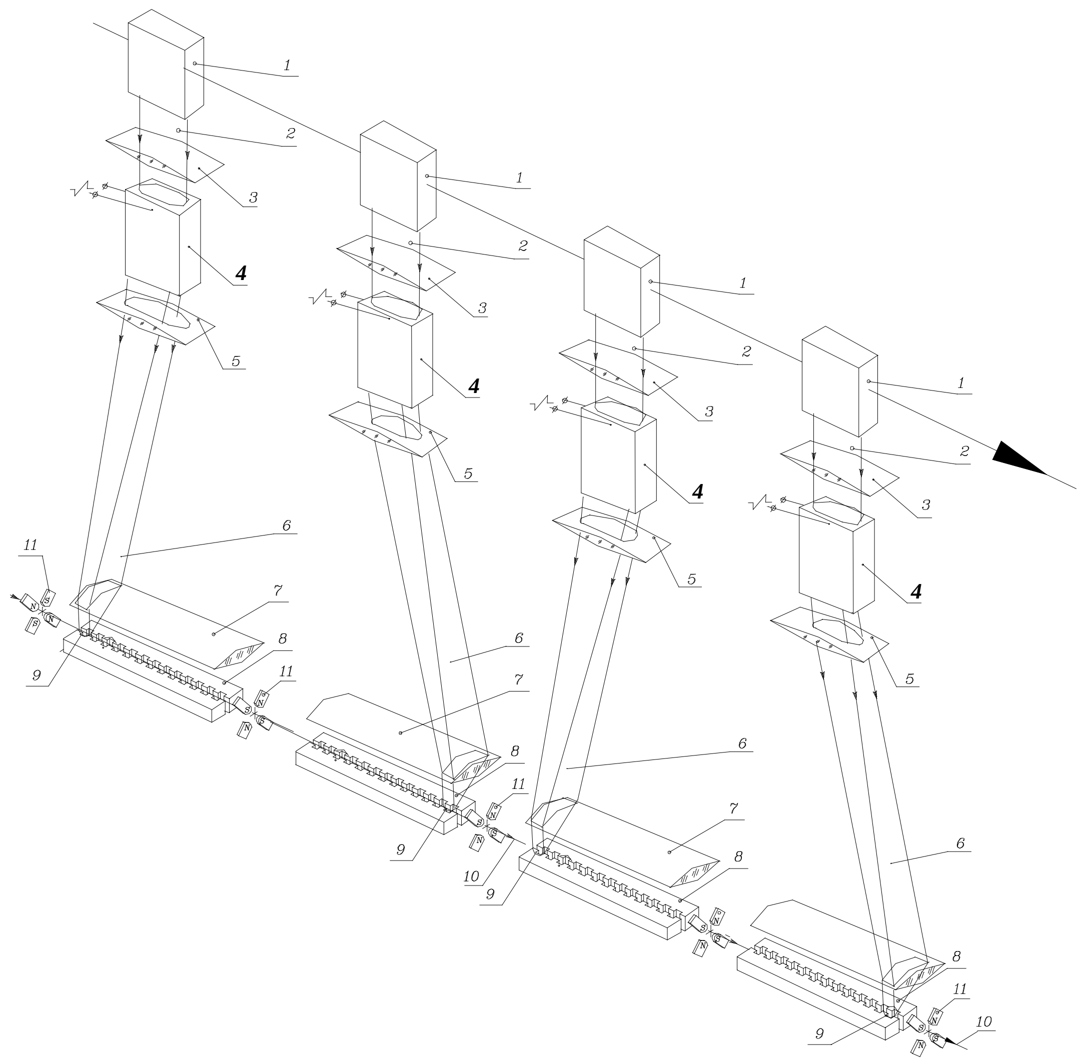

FIGURE 5.1: The Accelerating assembly. This is an isometric view from Fig.2.4. Some elements were added. 1–are the splitting devices. 2–is the laser bunch envelope. 3 and 5–are the lenses for longitudinal focusing. 4–is the sweeping devices. 6–is the instant directions of the laser bunch deflected. 7–is a cylindrical lens for transverse focusing of the laser beam. 8–are the accelerating structures. 9–is the focused laser spot. 10–is the electron beam trajectory. 11–are the focusing quadrupoles.

Different distances to the sweeping device between central and edge parts of the structure yield a systematic phase shift, what can be easily compensated, however, by variation of the thickness of lens 7 in Fig. 5.1. Really for the point on the grating, having a longitudinal coordinate *s*, calculated from the center of the grating, the distance *r* between this point and the sweeping device center can be evaluated as

$$r = \sqrt{R^2 + s^2} \cong R + s^2 / 2R \equiv R + r\delta , \qquad (5.1)$$

what rise a phase variation $\delta\varphi \cong 2\pi\delta r/\lambda = 2\pi s^2/\lambda R$. From the other hand, an extra thickness $\Delta(s)$ of the lens provides a phase shift $\delta\varphi \cong 2\pi\Delta(s)\cdot(n-1)/\lambda$, where n –is refractive index of material of the lens. So, if the thickness variation following the law

$$\Delta(s) = \frac{s^2}{R\cdot(n-1)} \qquad (5.2)$$

(not depends on λ), then the phase variation will be compensated. Estimation of this value for the end distance $s \approx 1.5cm$, $R \cong 3m$, $n-1 \cong 0.5$, will give $\Delta \cong 2.3/150cm = 0.15mm \equiv 150\mu m$ only. Basically this reflects the requirement that the focal point for this lens located at the output plane of the sweeping device. Some controllable phase variation can be arranged by variation of the lens thickness in longitudinal direction. This required by alternative phase focusing method (APF), see lower. The correlation between the laser *phase* and position of the particles yields a transverse force acting to the particle (and what used for effective focusing, see lower). A shot focusing cylindrical lens 7 reduces *the transverse size* of the spot to a minimal one due to its position close to the accelerating structure. Here the ratio $r/w \approx 1$, where r is the distance between the lens 7 and the structure 8. The cross section of the laser beam could be described as $w(y) \cong w(0)\cdot\sqrt{1+(y/Z_R)^2}$, where $w(0)$ is the waist of the beam at orifice of the grove, y calculated out from the surface of the structure, Fig.4.1, $Z_R = \pi\, w^2(0)/\lambda$ is the Relay length. Strictly speaking this formula is valid for stationary positioned laser beam, but the properties in transverse direction (what we are interesting in) could be described by these conditions as well. We are interesting in regimes, when $w(y) \cong w(0)\cdot(y/Z_R) \approx y\cdot\lambda/\pi\, w(0)$. In extreme case $w(0) \sim \lambda$, we have $w(y) \approx y/\pi$, so the width of the lens 7 is about the distance between the lens and the structure.

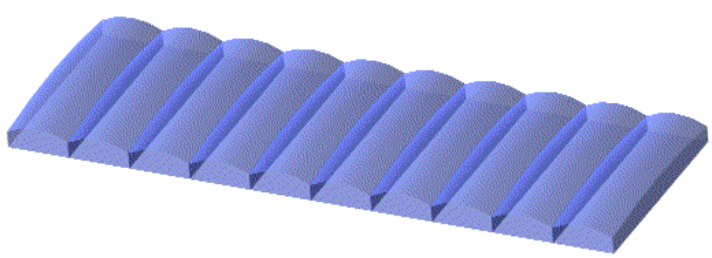

FIGURE 5.2(color**):** An isometric view of short focusing cylindrical lens, 7 in Fig.5.1. Each of the pieces focuses the incoming laser radiation to individual opening of the structure. Basically the surface of each element of this lens is a part of sphere. Picture is not in scale. Period equals to the period of the structure, what is the wavelength of the laser radiation. This also could be treated as diffraction pattern.

As this device looks like a grating, the question may be asked about the possibility to use a grating instead of the solid state lens at all. As this device must focus in transverse direction only, the pattern looks like long lines along the direction of sweeping. These lines have varying width symmetrically to the central line. This might have sense, as the cost of such type of Fresnel lens could be cheap.

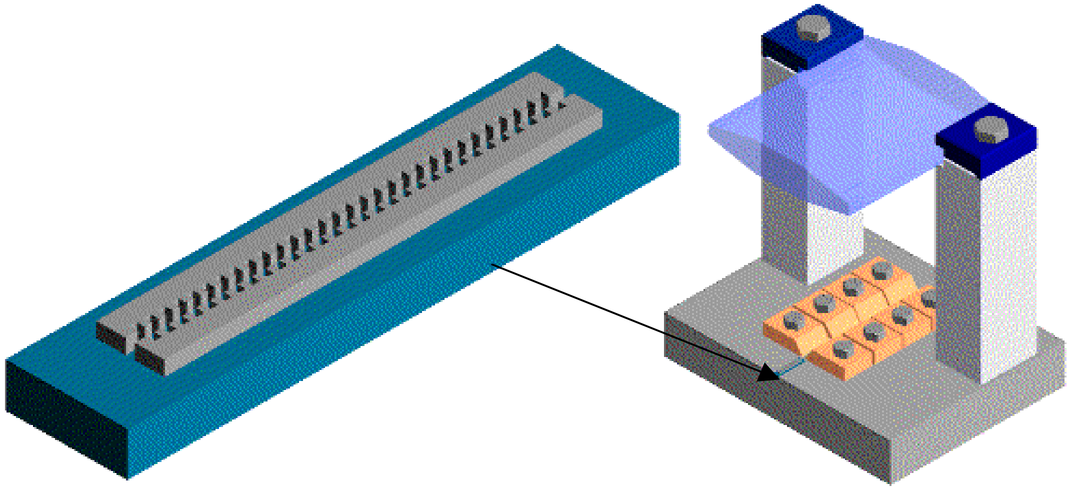

FIGURE 5.3 (color)**:** An isometric view of accelerating structure and cylindrical lens. Structure on the left is scaled. Covers on accelerating structure are not shown. The short focusing lens is shown simplified also.

This short focusing lens might be fabricated with curved in longitudinal direction surface to arrange some short focusing longitudinal focusing, see Fig. 5.2. Basically, the surface of each element of the lens is a part of spherical surface, having the focal point at the orifice of the accelerating cell. A natural way to increase the deflecting length with the same deflecting angle –is to increase the distance between deflecting device and the accelerating structure. Example of such arrangement is represented in Fig.5.4. These arrangements could be very useful for acceleration with laser wavelength $\lambda \cong 1\mu m$, where the number of resolved spots is about 100. This can reduce the total number of deflecting devices (increase *L* in Fig.2.1, 2.2).

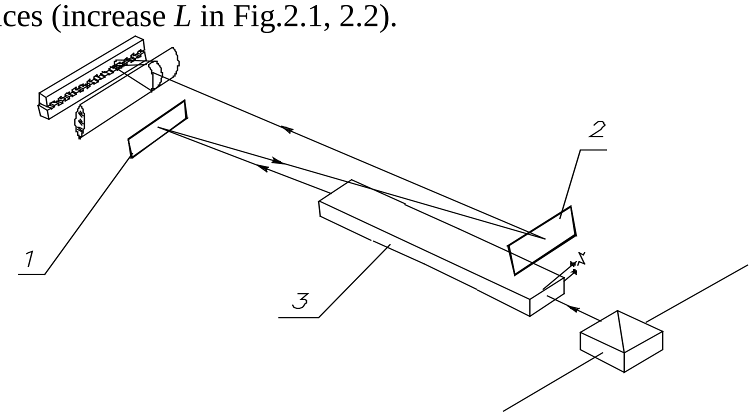

FIGURE 5.4: The way to increase the distance between deflecting device and accelerating structure. 1,2 –are the mirrors, 3–is the deflecting device. Mirrors might be slightly curved to obtain some focusing properties.

Other way stands for utilization of *telescopic optics* between the sweeping device and the structure. N_R is an invariant, as the telescopic optics increases both angles λ / a and $\Delta\vartheta$ in the same proportion.

For movement of the structure two quartz plates having different cuts could be used here,

Fig. 5.5. The plate with shear and x cuts uses for horizontal and vertical motion respectively.

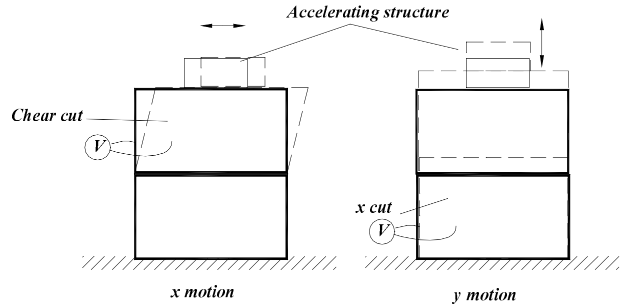

FIGURE 5.5: The concept of transverse movers for accelerating structure. Two piezoelectric plates have different types of cuts with respect to the crystallographic axes.

In some places, where fast reaction is not required Barium Titanate and other crystals with much bigger piezoelectric properties could be used.

So, using a combination of focusing lenses 3, 5, 7 and the sweeping device 4 in Fig. 5.1, it is possible to focus *all* radiation onto a small spot on the structure and to move this focal point along the structure in synchronism with instant particle's beam position♣.

After one module passed the particles go to next module and so on.

As it was mentioned, the laser amplifier could be sectioned, Fig.5.6.

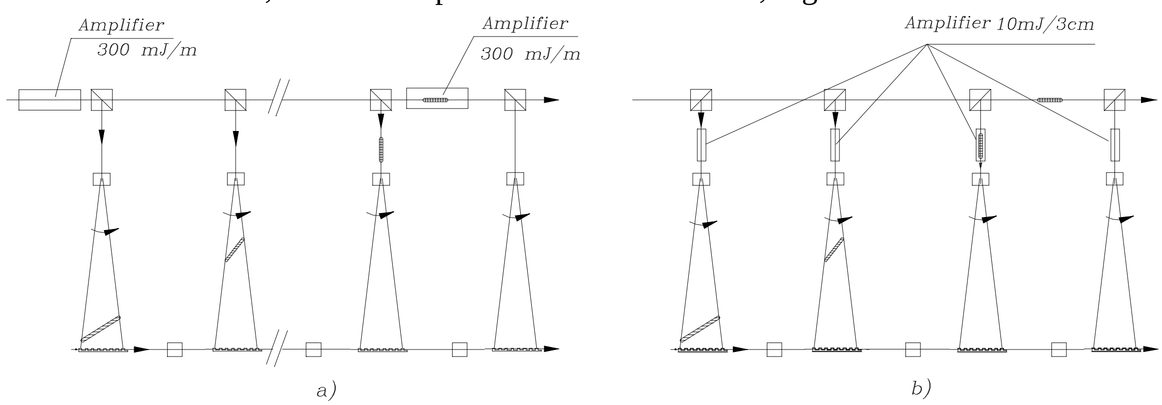

FIGURE 5.6: Possible installations of amplifiers. a) –Sectioning with few structures. b) –Each 3*cm* section has it's own amplifier.

Each part of the grating structure is illuminated by duration, which is defined by longitudinal size l_t, Fig.2.1. For example, if we consider $l_t \cong 100\lambda$, $\lambda = 1\mu m$, then $l_t / c \cong 3 \cdot 10^{-13} sec$. For $\lambda = 10\,\mu m$ this value is ten times more. This time is less than the time between electron-electron collisions $\tau \approx l_{free} / v_F \cong 10^{-12}\, sec$, where l_{free} is the free path length, v_F is the electron velocity at Fermi surface [5.2]. The time of illumination still, however longer, than the time, corresponding to reaction of electron plasma in metal $\tau \cong 2\pi / \omega_p = 2\pi / \sqrt{4\pi n r_0 c^2} \approx 3 \cdot 10^{-16} sec$, where n is the electron density in a metal.

♣ Longitudinal length of the particle's beam is a fraction of accelerating wavelength.

6. INJECTION SOURCE

We will consider here how to prepare the beams with emittances required, see Chapter 1. First of all, there is well developed way with a dedicated damping ring technique*. Second way – is a direct extraction of electrons from nanoprotrusions on single-crystal tip. The last one could be used for electrons and ions. Positrons supposed to be prepared through conversion of photons, generated by high-energy beam in a wiggler/undulator or from electrons, converted in a heavy target. So the positron production requires a damping ring in any case.

Damping rings for generation of low emittance electrons and positrons bunches.

This way to prepare electron or positron beams with low emittance (temperature) was developed in framework of Linear Collider activity [6.1]. This way uses a damping ring as a cooler. A lot of damping-rings were considered for the Linear Collider schemes. Typically, they have invariant emittances as low as $(\gamma\,\varepsilon_x) \approx 3\cdot 10^{-4}\,cm\cdot rad$ – radial and $(\gamma\varepsilon_y) \approx 3\cdot 10^{-6}\,cm\cdot rad$ –vertical. Energy spread about $\sigma_\varepsilon \cong 10^{-3}$ and the bunch length $\sigma_z \cong 5\,mm$. The length of the bunch after one stage compression is of the order 500 μm and the number of the particles is about $N \approx 10^{10}$. The second stage compresses the bunch typically to 100 μm at 10 *GeV*. So if we need only $N \approx 10^6$, we can loose four orders of magnitude in intensity by *scrapping* the extra particles ejected from appropriate damping ring, thereby coming to the figures in emittance $(\gamma\varepsilon_{x,y}) \approx 10^{-10}\,cm\cdot rad$. For pre-bunching the FEL mechanism can be used here as well, see below.

Some type of coolers able to reach extreme emittances considered in [6.2]. It was shown here for the first time, that there exists a strong quantum limitation for the lowest emittances in the beam like

$$(\gamma\varepsilon_x)(\gamma\varepsilon_y)(\gamma\varepsilon_s) = (\gamma\varepsilon_x)(\gamma\varepsilon_y)(\gamma l_b(\Delta p / p_0)) \geq \tfrac{1}{2}(2\pi\lambda\!\!\!^{-}_C)^3 N\,, \qquad (6.1)$$

where $\lambda\!\!\!^{-}_C = r_0/\alpha$ –is a Compton wavelength, $r_0 = e^2/mc^2$–is a classical electron radius, $\alpha = e^2/\hbar c$–is a fine structure constant, $\gamma = E/mc^2$, N–is a bunch population, l_b–is a bunch length, $\Delta p/p_0$–is a relative momentum spread in the bunch, $(\gamma\,\varepsilon_s) = \gamma l_b(\Delta p/p_0)$– is an invariant longitudinal emittance. There was pointed out that some among cooling systems could provide emittance not drastically bigger, than this fundamental physical limit [6.4].

Linear damping system (LDS)–[6.5] is a sequence of wigglers and accelerating structures, installed along a straight line. The rate of losses in the wigglers is the same as the rate of energy gain given by the accelerating structures. So the particles are moving with practically constant energy. To keep so high losses high energy required. A Kayak-Paddle Cooler (KPC) [6.6], Fig. 6.1, is a racetrack, which made as a sequence of wigglers and accelerating structures, installed along straight line and having the bends at the end.

* First proposed in [6.19].

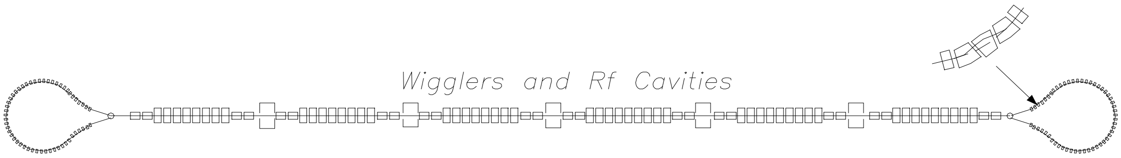

FIGURE 6.1: A Kayak-paddle cooler. The length of straight section might be a few hundred meters. Bends made with many short period divisions to prevent emittance dilution. In first approximation it could be considered as a *very* short-period *planar* wiggler with lot of bending elements. Each element of this bend could be considered as an achromatic three-magnet bend with the focusing quads in between. One of the three-magnet bending elements is represented in scale at the right top. It has three magnets and two quads.

The straight sections squeezed together for a compact size, so the back and forward trajectories might be congruent. The longer the straight section is–the smaller fraction the bends give to the cooling process. The bends itself could be made to give a small input into cooling dynamics. We used separate short quadrupoles for transverse focusing. These quadrupoles are positioned in between three-magnet achromatic bend. If the focusing implemented in the poles of the wiggler (Steffen's ring) this yields a radiation heating, what is not the case with quadrupoles.

In this cooler a particle needs to re-radiate its full energy few times, like in ordinary damping ring. The rate of energy losses is given by

$$d\gamma / ds \cong -\frac{2}{3} r_0 \frac{K^2}{\lambda\!\!\!^{-2}} \gamma^2 , \tag{6.2}$$

where $K = eH_\perp \lambda\!\!\!^{-} / mc^2$, $H_\perp$–is a magnetic field value in the wiggler, $2\pi\lambda\!\!\!^{-}$–is the wiggler period. We would like to mention here, that $d\gamma / ds$ *is not a function of the wiggler period*. The γ – factor on right side of (6.2) needs to be considered as a constant. Substituting here for estimation $\gamma \cong 2 \cdot 10^3$(*1 GeV*), $K \approx 5$ ($H_\perp \cong 0.17T$, $\lambda\!\!\!^{-} \cong 5cm$), one can obtain $\frac{d\gamma}{ds} \cong -\frac{2}{3} 2.8 \cdot 10^{-13} \cdot 10 \cdot 4 \cdot 10^6 \cong 7.5 \cdot 10^{-6}$ [*1/cm*] or 0.00075 [*1/m*]. For so called characteristic-damping length one can obtain

$$l_s = -\frac{\gamma}{d\gamma / ds} = \frac{3}{2} \frac{\lambda\!\!\!^{-2}}{r_0 K^2 \gamma} . \tag{6.3}$$

One can see that $1/l_s$ has *linear* dependence on energy. For parameters under discussion $l_s = -\frac{\gamma}{d\gamma / ds} \cong \frac{2 \cdot 10^3}{7.5 \cdot 10^{-4}} \cong 2.6 \cdot 10^6 m$. This means that after passing such a length, the energy re–radiated by the particle will be the same as it's initial one. The cooling time associated with this length is

$$\tau_{cool} \cong l_s / c = -\frac{\gamma}{c d\gamma / ds} = \frac{3}{2} \frac{\lambda\!\!\!^{-2}}{c r_0 K^2 \gamma} \tag{6.4}$$

One can see from here, that the cooling (damping) time *does not depend on the wiggler period*. From (6.4) one can obtain the estimation $\tau_{cool} \cong 2.6 \cdot 10^6 / 3 \cdot 10^8 \cong 8.6 \cdot 10^{-3} s$, or 8.6 *ms*. This cooling time obviously does not depend on the length of the straight section, as the influence of the bends was neglected –shorter the length, faster the revolution.

Emittance dynamics defined by equations (averaging over the period)

$$\frac{d\varepsilon_x}{ds} \cong \left\langle \left(H_x + \frac{\beta_x}{\gamma^2} \right) \frac{d(\Delta E / E)^2_{tot}}{ds} \right\rangle - 2\alpha_x \varepsilon_x , \tag{6.5}$$

with similar equation for vertical motion, where defined

$$H_{x,y} = \frac{1}{\beta_{x,y}} \left(\eta^2_{x,y} + (\beta_{x,y}\eta'_{x,y} - \frac{1}{2}\beta'_{x,y}\eta_{x,y})^2 \right), \tag{6.6}$$

$\eta_{x,y}$ –are dispersion functions. We omitted here some terms $\sim \beta'^2\eta/\gamma + \beta\eta'/\gamma$. They are negligible for *x* motion and for *y* motion also, as $\eta_y, \eta'_y \cong 0$. Derivatives are taken over longitudinal direction, which is *s*, see Fig. 16 below. In Fig. 6.2 there is represented the relationship between coordinate systems used here and in Chapter 4. One can suggest another orientation of the wiggler field polarization and accelerating structure. This orientation, however, gives the direction of largest emittance along the narrow side of the slit.

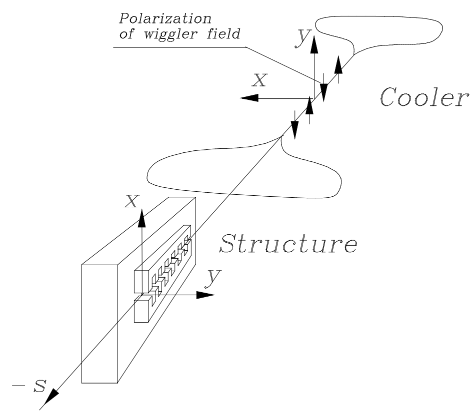

FIGURE 6.2: Relation between coordinates of the cooler and the structure. Polarization of the wiggler field is vertical; the bends of cooler are going in horizontal plane. If polarization of the wiggler field is horizontal, the x coordinates might be the same, and the cooler plane and the plane of the structure may coincide.

Partial decrements $\alpha_{x,y,s}$ are defined as $\alpha_i = \frac{J_i}{2\, l_s}$, where $J_x \cong 1, J_y = 1, J_s \cong 2,\ J_x + J_s = 3.$

Partial decrement for energy spread is the same as for emittance. The source of energy spread has two components arising from synchrotron radiation and IBS,

$$\frac{d(\Delta E/E)^2_{tot}}{ds} = \frac{d(\Delta E/E)^2_{IBS}}{ds} + \frac{d(\Delta E/E)^2_{QE}}{ds} - \alpha_s \left(\frac{\Delta E}{E} \right)^2 , \tag{6.7}$$

$$\frac{d(\Delta E/E)^2_{QE}}{ds} \cong \frac{55}{48\sqrt{3}} \frac{r_0^2 \cdot \gamma^5}{\alpha|\rho|^3}, \qquad \frac{d(\Delta E/E)^2_{IBS}}{ds} \cong \frac{N r_0^2 \ln_C}{\gamma^3 \varepsilon_x \sqrt{\varepsilon_y \beta_y} l_b}, \qquad (6.7a,b)$$

where $\ln_C = \ln(\rho_{\max}/\rho_{\min}) = \ln\sqrt{(v'/c)^6/4\pi \cdot r_0^3 n_e'}$ – is Coulomb's logarithm, v'–is a transverse velocity, n_e'–is density of particles in it's rest frame, l_b – is the bunch length.

We would like to stress here, that despite similarity, the term β_y/γ^2 in (6.5) has a different physical nature for QE and IBS. For IBS it reflects that transverse momentum is invariant under Lorentz transformation, while for QE is reflects the opening angle of radiation $\approx 1/\gamma$.

For a dipole wiggler, with vertical polarization of magnetic field, the periodic solution for η_x can be expressed as[♣]

$$\eta_x = \frac{K_x \lambdabar}{\gamma} Sin\frac{s}{\lambdabar} = \frac{\lambdabar^2}{\rho_x} Sin\frac{s}{\lambdabar}, \tag{6.8}$$

where $\rho_x = \lambdabar\gamma / K_x$ is the bending radius in magnetic field of the wiggler[♣♣]. The length of formation of radiation is $\rho_x/\gamma = \lambdabar/K_x$.

For the function H_x we can estimate $H_x \cong \beta_x \eta_x'^2$. As the $\eta_x' \cong K_x/\gamma \cdot Cos(s/\lambdabar)$ one can obtain

$$H_x \cong \beta_x K_x{}^2/\gamma^2 \cdot Cos^2(s/\lambdabar).$$

So formula (6.5) becomes

$$\frac{d\varepsilon_x}{ds} = \left\langle \left(1 + K_x^2 Cos^2(s/\lambdabar)\right)\frac{\beta_x}{\gamma^2}\frac{d(\Delta E/E)^2_{tot}}{ds}\right\rangle - 2\alpha_x \varepsilon_x \tag{6.9}$$

For vertical emittance $K_x = 0$ (and the wiggler field has no horizontal polarization). Equilibrium emittances defined by condition $d\varepsilon_{x,y}/ds = 0$. For quantum excitation the source (6.7a) does not depend on emittance. Combining (6.2), (6.7), (6.9) for quantum excitation *only* we obtain

$$(\gamma\varepsilon_x) \cong \tfrac{1}{2}\cdot\lambdabar_C \overline{\beta}_x (1 + K_x^2/2)\gamma/\rho_x \cong \tfrac{1}{2}\cdot\lambdabar_C \overline{\beta}_x (1 + K_x^2/2) K_x/\lambdabar \tag{6.10}$$

$$(\gamma\varepsilon_y) \cong \tfrac{1}{2}\cdot\lambdabar_C \overline{\beta}_y \gamma/\rho_x \cong \tfrac{1}{2}\cdot\lambdabar_C \overline{\beta}_y K_x/\lambdabar, \tag{6.11}$$

where $\overline{\beta}_{x,y}$ – are averaged envelope functions in the wiggler. The last formulas together with (6.4), $\tau_{cool} \cong \frac{3}{2}\cdot(\lambdabar^2/r_0 c K^2 \gamma)$, define the cooling dynamics under SR. One can see that equilibrium invariant emittances *do not depend on energy*. In addition, quantum equilibrium *vertical emittance* and the cooling time do not depend on the wiggler period at all. According to (6.10), (6.11), and the ratio $(\gamma\varepsilon_x)/(\gamma\varepsilon_y) \cong (1 + K_x^2/2)\overline{\beta}_x/\overline{\beta}_y$.

Substitute for estimation $\overline{\beta}_{x,y} \approx 1m$, $\lambdabar \cong 5\,cm$, $K \cong 5$, one can obtain for *quantum emittances* the following estimations

$$(\gamma\varepsilon_x) \cong 2.5\cdot 10^{-8}\ cm \cdot rad, \tag{6.10a}$$

[♣] The wiggler must have the ending field in poles relation as ¼, -¾, 1, n(-1,1), - ¾ , ¼ . n=0,1,... This will give ~zero averaged displacement of trajectory [6.3].

[♣♣] For simplicity we supposed that the transition region between wiggler poles is much less, than the pole width itself, so the *absolute* value of radius is a constant.

$$(\gamma\varepsilon_y) \cong 9.5 \cdot 10^{-10} cm \cdot rad\ . \tag{6.11a}$$

On expense of damping time these last values could be reduced by the factor 5, putting $K \cong 1$. In this case one need to increase the number of the bunches in the damping ring to satisfy the repetition rate. One can suggest also installing *additional* damping ring before the Kayak Paddle cooler. This ring could have short damping time and *not* small equilibrium emittance. It's task to make preliminary cooling only. These ideas broadly discussed in [6.1]. Additional decrease of emittance could be obtained by reducing $\overline{\beta}_{x,y}$. So a decrease of the order of 10 for each emittance could be expected here.

Let us compare the emittances from (6.10), (6.11) with the fundamental one (6.1). Combining (6.10), (6.11), one can obtain

$$(\gamma\varepsilon_x)(\gamma\varepsilon_y)(\gamma l_b(\Delta p/p_0) \cong \tfrac{1}{4}\cdot(\lambda\!\!\!^{-}_C)^2 \cdot (1+K_x^2/2)K_x^2(\overline{\beta}_x\overline{\beta}_y/\lambda\!\!\!^{-}{}^2)(\gamma l_b(\Delta p/p_0)\,. \tag{6.12}$$

To reach a quantum limit, one need to have

$$(1+K_x^2/2)K_x^2(\overline{\beta}_x\overline{\beta}_y/\lambda\!\!\!^{-}{}^2)(\gamma\, l_b(\Delta\, p/p_0)) \approx \lambda\!\!\!^{-}_C N \cdot (2\pi)^3\,. \tag{6.13}$$

Substitute here in extreme case $(\overline{\beta}_x\overline{\beta}_y/\lambda\!\!\!^{-}{}^2) \approx 1$, $\frac{1}{2}(1+K_x^2/2)K_x^2 \approx (2\pi)^3$ one need to have

$$\gamma\, l_b(\Delta\, p/p_0) \approx \lambda\!\!\!^{-}_C N\ . \tag{6.14}$$

As $\delta' = \gamma\, l_b / N$ –is an average distance between particles in the rest frame, (6.14) has a clear physical meaning like individual phase space cell must be of the order of Compton length, $\delta' \cdot (\Delta\, p/p_0) \approx \lambda\!\!\!^{-}_C$. Substitute for estimation, $l_b \cong 1cm$, $\gamma \cong 2\cdot 10^3$, $N \cong 10^9$, one need to have the energy spread like $(\Delta\, p/p_0) \approx 2\cdot 10^{-5}$, what is not drastically far from really available. For IBS scattering we have from (6.2), (6.7b), (6.9)

$$\left(1+K_x^2/2\right)\frac{\beta_x}{\gamma^2}\frac{N\cdot r_0^2 \ln_C}{\gamma^3\varepsilon_x l_b\sqrt{\varepsilon_y\beta_y}} = \frac{\varepsilon_x K^2\gamma}{(3\!/\!2)\lambda\!\!\!^{-}{}^2} \tag{6.15}$$

$$\frac{\beta_y}{\gamma^2}\frac{N\cdot r_0^2 \ln_C}{\gamma^3\varepsilon_x l_b\sqrt{\varepsilon_y\beta_y}} = \frac{\varepsilon_y K^2\gamma}{(3\!/\!2)\lambda\!\!\!^{-}{}^2} \tag{6.16}$$

Even in absence of artificial coupling, using (6.15), (6.16), we are coming to conclusion, that there is a coupling between horizontal and vertical degrees of freedom like[*]

$$\left(1+K_x^2/2\right)\frac{\varepsilon_y}{\beta_y} = \frac{\varepsilon_x}{\beta_x}\,. \tag{6.17}$$

This ratio of emittances is the same as for quantum excitation[**], but here we have *a real* coupling. Substitute (6.17) into (6.15), (6.16) we obtain

[*] In [6.3] the condition was fond for the coupling, arising from IBS in an ordinary damping ring as $(\gamma\varepsilon_y)/(\gamma\varepsilon_y) \cong <\sqrt{\beta_y}>/(\gamma^2 < H_x/\sqrt{\beta_y}> \approx R/(\gamma\, l)$, where R -is an average radius of the ring, l- is the length of period. So these expressions are the same in the wiggler.

[**] As the functions in the angular brackets in formula (6.5) are, formally, the same.

$$\varepsilon_x^{5/2} \cong \frac{3}{2} \cdot \frac{\left(1+K_x^2/2\right)^{3/2}}{K^2} \frac{N}{\gamma^6} \frac{\beta_x^{3/2} \cdot r_0^2 \cdot \lambda\!\!\!^{-2} \ln_C}{l_b \beta_y^2} \; . \tag{6.18}$$

One can see that there is a strong dependence on the beam energy $\varepsilon_x \sim \gamma^{-12/5}$.

For $N \cong 10^9$, $\gamma \cong 4 \cdot 10^3$, $l_b \cong 1cm$, $\overline{\beta}_{x,y} \approx 1m$, $\lambda\!\!\!^{-} \cong 5cm$, $K \cong 5$, we obtain for *IBS emittances*

$$\gamma\varepsilon_x \cong 4 \cdot 10^{-6} cm \cdot rad \, ,$$
$$\gamma\varepsilon_y \cong 3 \cdot 10^{-7} cm \cdot rad \, .$$

So the only way to come to emittances as required compared with ones defined by quantum process only– is increasing the energy of the beam and following *scrapping* the extra particles. For example raising energy up to, say 10 *GeV* will drop emittance about three orders of magnitude. For successful operation of Laser Linear Collider the only $N \approx 10^6$ particles are required [2.5], see Chapter 11.

In [6.7] there was considered the conditions required under which the system comes to equilibrium. General output is that the system must have *positive* longitudinal mass, $m_s = m\gamma^3/(1-\eta\gamma^2)$ i.e. *negative* momentum compaction factor η. KPC satisfies this requirement, having $\eta \cong -0.0001$.

Optical Stochastic Cooling method.

This method could be used in a damping ring. From previous part we could see, that the only source of damping is the classical synchrotron radiation. Namely this radiation is responsible for damping time like (6.4). If some other source of damping is present in the system, then resulting damping time τ_{res} will be described

$$\frac{1}{\tau_{res}} \cong \frac{1}{\tau_{cool}} + \frac{1}{\tau_{osc}} \cong \frac{c}{l_s} + \frac{1}{\tau_{osc}} = \frac{2}{3} \frac{c r_0 K^2 \gamma}{\lambda\!\!\!^{-2}} + \frac{1}{\tau_{osc}} \, , \tag{6.19}$$

where τ_{osc}– is effective damping time associated with this additional cooling process. This additional cooling process might be Optical Stochastic Cooling (OSC) method [6.8]. This is basically a stochastic cooling with the bandwidth extended to optical one. The cooling time in this method is associated with the number of the particles in the bandwidth as the following

$$\tau_{cool} \cong N_u \cdot T \, , \tag{6.20}$$

where N_u– is the number of the particles in the bandwidth, *T*–is period of revolution.

$$N_u \cong \frac{f}{\Delta f} N \frac{\lambda_u}{l_b} \cong \frac{f}{\Delta f} N \frac{2\pi\lambda\!\!\!^{-}}{l_b \gamma^2} \, , \tag{6.21}$$

where $2\pi\lambda\!\!\!^{-}$– is the wiggler period, λ_u– is the central wavelength of radiation amplified. Amplification coefficient κ of optical amplifier can be expressed as following [6.8]

$$\kappa \cong \frac{(\gamma\varepsilon_s)}{r_0 N} \frac{\Delta f}{f} \, , \tag{6.22}$$

where $(\gamma\varepsilon_s)$–is an invariant longitudinal emittance, see (6.1), $\Delta f\ /\ f$–is a relative bandwidth, N –is the number of the particles. One can see the only phase density in longitudinal direction $\rho_\varepsilon = (\gamma\varepsilon_s)\ /\ N$ is important for the level of amplification.
The decrease of emittance is equal to

$$\frac{\varepsilon_f}{\varepsilon_0} \cong \frac{1}{\alpha N_u}. \tag{6.23}$$

For $N \cong 10^{10}$, $\lambda_u \cong 10^{-4}\ cm = 1\ \mu m$, $l_b \cong 1 cm$, $(\Delta f\ /\ f) \cong 20\%$ one can expect $N_u \cong 5 \cdot 10^{10} \cdot 10^{-4} \cong 5 \cdot 10^6$ and $\varepsilon_f / \varepsilon_0 \cong 2.7 \cdot 10^{-5}$. This is of course the maximal possible value of cooling.
If this cooling system is forced to work with electron/positron gas close to generation, one can see from (1) that amplification coefficient (6.22) becomes

$$\kappa \cong \frac{(\gamma\varepsilon_s)}{N}\frac{1}{r_0}\frac{\Delta f}{f} \cong \frac{1}{2}\frac{(2\pi ƛ_C)^3}{(\gamma\varepsilon_x)(\gamma\varepsilon_y)}\frac{1}{r_0}\frac{\Delta f}{f} = 2\alpha\pi^2\frac{ƛ_C^2}{(\gamma\varepsilon_x)(\gamma\varepsilon_y)}\frac{\Delta f}{f} << \alpha\frac{\Delta f}{f}, \tag{6.24}$$

what is less than unity–attenuation for such a cold beam. That means that the level of cooling is much higher– not lower than energy of quanta in moving system of reference.
Simultaneous cooling of transverse and longitudinal emittances yields some threshold value in the invariant emittance level as

$$(\gamma\varepsilon_x)_x^{th} \cong \lambda_u\gamma \cdot (\Delta E\ /\ E) = (\lambda_u\ /\ l_b) \cdot l_b\gamma \cdot (\Delta E\ /\ E), \tag{6.25}$$

The above value is of the order $\gamma\varepsilon_x^{th} \cong 3 \div 5 \cdot 10^{-4}\ cm \cdot rad$ for $\lambda_u \cong 1\mu m$, what does not affect our case.
One can also arrange the cooling system so that it is able to cool only the particles with lower derivatives of trajectory that satisfy the condition (6.25). For example one can screen the radiation from some parts of the beam to avoid heating the core by peripheral parts of emittance. One positive property of quadrupole wiggler as a pick up, is that the central parts of the beam, what have higher values of slope x_0' are moving *closer* to the center of the lens and, hence, radiate less. One can see also, that the particles with higher slope x_0' in the pick up (and having maximal lengthening), will be at the center in *the quadrupole wiggler used as a kicker* if transformation matrix ***-I*** (or for cosine trajectory $C(s \to kick) = -1$). That will reduce the heating from interaction with radiation amplified.
Formulas (6.22) and (6.24) give an idea about amplification required and the power contained in the laser flash. Two examples considered below use these formulas.
Example 1.
For $N \cong 10^{10}$, $l_B \cong 15 cm$, $M = 5$, $(\Delta E\ /\ E) \cong 10^{-3}$, $\gamma \cong 10^3$ (500 *MeV*), $\lambda \cong 1\mu\ m$, optical amplifier must be able to have amplification about $\kappa \approx 300$, peak power about 5 *kW*, average power about 25 *W* with repetition rate *f* of the order of 10 *MHz*. Number of the particles in the bandwidth $N_S \cong 3 \cdot 10^5$ defines the number of the turns and the damping time $\tau_C \cong N_S\ /\ f \cong 30 ms$. Emittance reduction $\varepsilon_f / \varepsilon_0 \cong 1/\alpha N_S \cong 10^{-3}$.
Example 2.

For $N \cong 10^8$, $l_B \cong 5cm$, $M = 5$, $(\Delta E / E) \cong 10^{-4}$, $\gamma \cong 10^3$ (500 *MeV*), $\lambda \cong 1\mu\, m$, optical amplifier must be able to have amplification about $\kappa \approx 100$, peak power about 225 *W*, average power about 0.075 *W* with repetition rate of 2 *MHz*[♣]. Number of the particles in the bandwidth $N_S \cong 2 \cdot 10^3$ defines the number of the turns and the damping time $\tau_C \cong N_S / f \cong 1ms$. Emittance reduction $\varepsilon_f / \varepsilon_0 \cong 1/\alpha N_S \cong 7 \cdot 10^{-2}$.

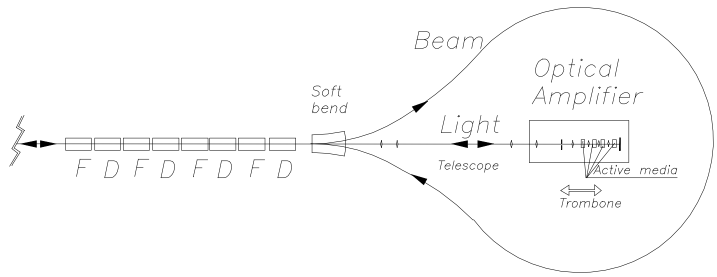

FIGURE 6.3: Example of installation of OSC system in a Kayak-paddle cooler.

The parameters described above look as realistic from the energetic. Optical amplifier needs to be done with lowest phase distortion and minimal time delay.

An example of installation of OSC system for electron/positron cooler is represented in the Fig. 6.3.

TABLE 6.1. Parameters of amplifiers.

Amplifier	**Dye**	**Ti:Al$_2$O$_3$**
Wavelength	$\lambda \approx 340 \div 540$ *nm*	
Life time	$\tau_L \cong 5$ *ns*	$\tau_L \cong 3.5\,\mu s$
Absorption cross section	$\sigma_{01} \cong 2 \cdot 10^{-16} \div 4 \cdot 10^{-16}$ cm^2	$\sigma_{01}(490nm) \cong 10^{-19}\ cm^2$
Emission cross section	$\sigma_{10} \cong 2 \cdot 10^{-16} \div 4 \cdot 10^{-16}$	$\sigma_{10}(790nm) \cong 3 \cdot 10^{-19}\ cm^2$
Density	$n_0 \approx 10^{17}\ cm^{-3}$	$n_0 \approx 10^{20}\ cm^{-3}$
Absorption length, $l_{ab} \cong 1/n_0\sigma_{01}$	$0.05 \div 0.1\ cm$	0.1 *cm*
Pumping area, $S_{pump} \cong \lambda \cdot l_{ab}$	$5 \cdot 10^{-6} cm^2$	$7 \cdot 10^{-6} cm^2$
Saturation power density, $P_{sat} \cong \hbar\omega\ n_0 l_{ab} / \tau_L$	$\leq 100\ kW / cm^2$	$\leq 1\ MW / cm^2$
Pumping power, $I = P_{sat} \cdot S_{pump}$ /stage	0.5 *W/stage*	7 *W/stage*
Pumping time, $\tau_{pump} \cong \hbar\omega S_{pump} n_0 l_{ab} / I$	0.15 *ns*	
Amplification$^{*)}$, $\kappa \cong \exp[\sigma_{10}(\lambda) \cdot n_1 \cdot l]$	≈ 7	20
Pumping	Nitrogen laser, $\lambda = 308nm$	Argonne laser
Number of stages	3	2

$^{*)}\ l \cong l_{ab}$, $n_1 \approx n_0$.

For parameters we used above, period of the lenses must be $2L \cong 2\gamma^2 \lambda / (1 + K^2)$ what is about 2 *m*. More hard radiation from the dipole wigglers

[♣] Low frequency of revolution is result of the presence of long straight sections in a Kayak-Paddle type cooler.

installed in straight section has *different* wavelength and does not interfere with optical amplifier operating at lower wavelength around $1\,\mu m$. Optical amplifier installed at stabilized platform. For the fine phase adjustments one can use the dual prism system. Initial phase adjustments made by movement the table (trombone). Optical telescopes at both ways used for proper conjunction the radiation from the wiggler and amplifier.

Diluted bunch.

One may expect that the space charge effects can be strong here. From the other hand, the number of the particles required in laser acceleration is about 10^6-10^7 only. This defined by a loading the acceleration structure. So one may hope that space charge effects are not strong enough to destroy the beam emittance.

Average distance between particles in a moving bunch can be defined as l_b/N, where l_b–is the bunch length in Laboratory frame, *N*–is the number of the particles in the bunch.

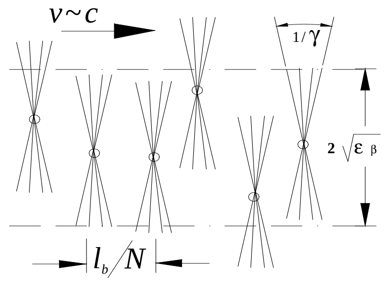

FIGURE 6.4: Diluted bunch.

We called beam *diluted*, if the particles separated in longitudinal direction so, that the pancakes of its individual fields having an opening angle $1/\gamma$, are not overlapped at the cross section $\sqrt{\varepsilon\beta}$ of the bunch,

$$l_b/N \geq \sqrt{\varepsilon\beta}/\gamma\,. \tag{6.26}$$

Fig. 6.4 illustrates the condition (6.26). One can see that this condition is Lorenz-invariant, as the (6.26) could be rewritten as $\gamma l_b/N \geq \sqrt{\varepsilon\beta}$, where $\gamma\, l_b$ –is now a bunch length in its rest frame, and the transverse size $\sqrt{\varepsilon\beta}$ is an invariant under Lorentz transformations. The last means that the closest particle in rest frame located at the distance of the order of the transverse bunch size.

With such small emittances as above the beam size is about $\sqrt{\varepsilon\beta} \cong 1.6\cdot 10^{-6}$ cm, $\gamma \cong 10^4$ and this may give a reason for estimation of the transverse effects as a betatron tune shift and longitudinal effects. The length of the bunch required for laser acceleration is a fraction of the laser wavelength. Even suggesting the bunch compression one can have the bunch length in a cooler about $100\mu m$.

For $N \cong 10^7$, the bunch will be diluted if it has the length $l_b \geq N\sqrt{\varepsilon\beta}/\gamma$, what is

$$l_b \geq 10^7 \cdot 1.6\cdot 10^{-6} \cdot 10^{-4} = 1.6\cdot 10^{-3} cm \cong 16\mu m\,.$$

One can expect that any space charge phenomena can look in diluted beam different from a dense beam. First of all the space charge effects what tolerate to the transverse beam dynamics. The last one includes the betatron tune shift and Intra-Beam Scattering. One can see also that for diluted beam the effects of radiation at IP of collider may look different also. In this publication we consider the transverse space charge effects.

Let us, first, consider the *non-coherent tune shift*. This tune shift exists even when the beam is going exactly in the axis of the round chamber.

So the corresponding tune shift will be

$$\Delta(Q\omega_0)^2_{usual} \cong \frac{e^2}{m}\frac{N}{2l_b(\gamma\varepsilon)\beta_x\gamma^2}\,. \tag{6.27}$$

For the tune shift one can obtain

$$\Delta(Q\omega_0)^2_{diluted} \cong \frac{e^2}{m}\frac{1}{(l_b/N)^3\gamma^5}\,. \tag{6.28}$$

For comparison (6.27) and (6.28) one can make some transformations

$$\frac{\Delta(Q\omega_0)^2_{diluted}}{\Delta(Q\omega_0)^2_{usual}} \cong \frac{l_b(\gamma\varepsilon)\beta_x}{N(l_b/N)^3\gamma^3} \cong \frac{N^2}{l_b{}^2\gamma^2}\frac{(\gamma\varepsilon)\beta_x}{\gamma} \approx 1,$$

where we used condition (6.26). Of cause exact value of *one* is out of accuracy of our calculations. This result however is a reflection of the fact that from the point of view of the observer in the moving frame there is no *qualitative* difference if the beam is diluted or not. In this system magnetic *focusing magnetic* field of the cooler transferred into electrical field as $E'_x = \gamma B_y$. So the electrical focusing field is horizontal now. Magnetic field $B'_y = \gamma B_y$. So the focusing system in the moving frame looks as incoming electromagnetic wave with a period, which now is γ times higher: $\omega' = \gamma 2\pi \cdot c/\lambda_F$, where λ_F –is a longitudinal period of the focusing system.

So one can use usual formulas for betatron tune shift. Taking into account the ratio between electrical and magnetic field one can obtain the change in local focusing parameter

$$k(z) \cong -\frac{1}{pc}\frac{\partial\Delta F}{\partial r} \cong -\frac{2r_0N}{a^2 l_b\gamma^3} \cong -\frac{2r_0N}{\beta_x(s)(\varepsilon\gamma)l_b\gamma^2}\,.$$

This is a defocusing effect. The corresponding *non-coherent* tune shift is

$$\Delta Q_{NC} \cong -\frac{1}{4\pi}\int_0^C \beta_x(s)k(s)ds \cong -\frac{1}{2\pi}\frac{r_0NC}{l_b\varepsilon\gamma\cdot\gamma^2}$$

where C –is the circumference of the cooler, or the length of the transport line. For the cooler $C \cong 2\pi Q\overline{\beta}$. So, the resulting formula for relative betatron tune shift will be

$$\frac{\Delta Q_{NC}}{Q} \cong -\frac{r_0N\overline{\beta}}{l_b(\varepsilon\gamma)\gamma^2}\,. \tag{6.29}$$

Substitute here for estimation $\overline{\beta}_{x,y} \approx 100\ cm$, $\gamma \cong 10^4$, $l_b \cong 100\mu\ m$, one can obtain

$$\Delta Q_{NC}/Q \cong -\frac{2.8\cdot 10^{-13}10^7 100}{10^{-2}2.5\cdot 10^{-8}10^8} = -0.011\ .$$

For vertical relative tune shift one obtains $\Delta Q_{NC}/Q \cong -0.038$. So one can see, that even for such tiny emittances (dimensions) the space charge effects does not look as drastic ones.

Solid-state source of low emittance electron and ion beams.

We describe here one potential way to obtain the low emittance electron beam directly. Unfortunately there is no way to avoid low emittance damping ring as injector, as it requires for positrons. But at least for electrons it could be useful. This source could be useful for compact electron accelerators also. The physics describing these new types of electron source one can found in [6.9]-[6.11]. Basically there are three regimes in emission. First is usual thermionic emission. The slope of external potential in Fig.6.5a is small. The barrier, which electron must jump through is the work function eU_W ~ 4-5*eV*. The Richrdson law $j \cong AT^2 e^{-eU_W/k_B T}$, where A –is a material dependent constant, T –is a temperature of the cathode, describes the emission current density j. Second regime corresponds to higher slope of potential function. In this case potential barrier becomes lower by $\Delta U \cong e\sqrt{eE/4\pi\varepsilon_o}$, $\varepsilon_0 \cong \frac{1}{36\pi}10^{-9} F/m$ –dielectric permeability of vacuum, see Fig. 6.5. This is a Schottky regime. And the last regime happens when the potential slop becomes so high, that the width of the barrier W in Fig. 6.5 becomes comparable with the DeBroigle wavelength of the electron at the Fermi surface, then the tunneling begins. This is so called a field emission regime [6.11]. These regimes are used for emission from the tips for obtaining a high brightness electron beams. Idea is very simple. At the tip the electric field strength could reach V/ρ, where V is a voltage applied and ρ is the radius of the tip. In this case the divergence of electrical lines defined by the height of the tip at distances bigger, than the radius. If, however, the other small height tip with height about its radius attached to the first tip, then the radius of the top tip will define the divergence.

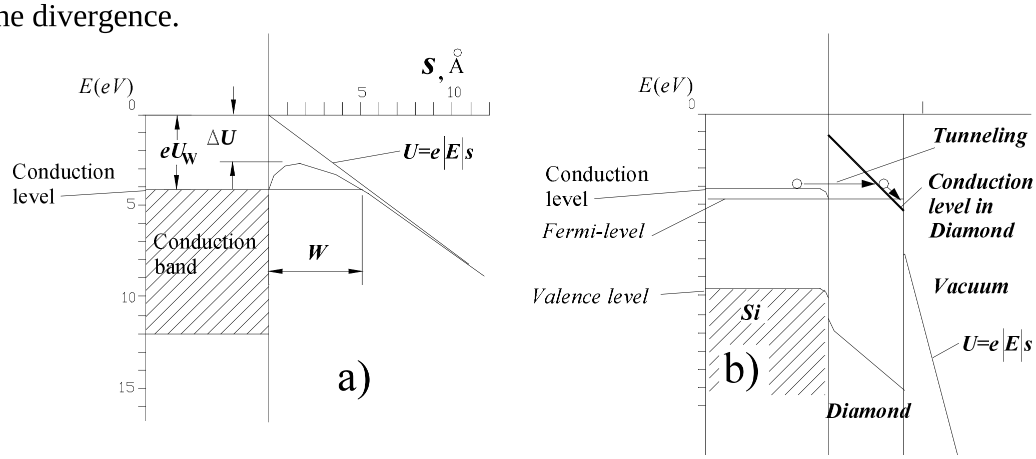

FIGURE 6.5: To the physics of electron source based on cold emission from the tip. At the left the pure W-vacuum surface shown. At the right- Si cover by diamond film. The field strength shown at the left is ~ $4V/5A° = 8\cdot 10^7 V/cm$ as example.

This gives typical divergence about 1/100 *rad*. Basically this is nothing else, but formation of the best potential profile with the help of material. Similar to what is done for macroscopic electron guns. Now it is possible to obtain the tips with nanometer-level radius routinely. So the emittance of the electron beam, one could expect here be

$$\gamma\varepsilon \cong 10^{-7}\,cm\cdot 10^{-2}\,rad = 10^{-9}\,cm\cdot rad\,. \tag{6.30}$$

This is an invariant emittance, as the electrons are nonrelativistic. This is an impressive number. The question is, however, is it possible to get the number of electrons required. The tips described above routinely working with currents ~100 *nA*. The last number gives the total charge ~10^{-7} *Q/s*. In its turn, this corresponds to $N \cong Q/e \cong 6.25\cdot 10^{11}$ electrons per second. The longitudinal emittance defined by the temperature of the tip. In any case the longitudinal energy spread is less, than the work function eU_W.

In [6.10] there was shown that Diamond coating of the Si tip surface could significantly increase the electron yield in the Schottky regime. This was explained by specific location of diamond conduction band with respect to the band of Si, see Fig. 6.5b. With appropriate donor doping conduction level of Si becomes populated. So the electrons from the conduction level tunneling to the conduction level of diamond and after that they simply escaping into vacuum, as the conduction level of diamond is higher, than in vacuum as external field is applied.

If the mechanism described correctly, we may suggest that utilization of Si tips with donor concentrations instead of diamond will also help in electron emission.

There are some proposals to increase the heat capacity of the surface of accelerating structure by coating it by thin diamond film [6.14]. We will discuss the possibility to increase the surface field strength by this way further in Chapter 8.

Emittance (6.30) is tremendously small, so it is necessary to check the ***restrictions arising from the quantum mechanics*** [6.4]. This defines the minimal emittance as a requirement that the beam temperature must be much less, than the Fermi energy. The last is [6.13]

$$E_F = \begin{cases} \left(3\pi^2\right)^{2/3} \dfrac{\hbar^2}{2m}\rho^{2/3}, v << c \\ \left(3\pi^2\right)^{1/3}\hbar c\rho^{1/3}, \; v \approx c \end{cases} \tag{6.31}$$

where $\rho \approx N/V$ –is a density of electrons in metal.

Using (6.31) one can find the condition for degeneration as

$$k_B T \le \begin{cases} \dfrac{(3\pi^2)^{2/3}}{2} mc^2(\lambdabar_C^3\rho)^{2/3} \quad v << c \\ (3\pi^2)^{1/3} mc^2(\lambdabar_C^3\rho)^{1/3}, \quad v \approx c \end{cases}, \tag{6.32}$$

where $k_B \cong 1.38\cdot 10^{-23}$ J/^{o}K –is Boltzmann's constant. The electron gas temperature T in a moving frame can be calculated as the following. The transverse momenta is invariant and the transverse kinetic energy is

$$\frac{p_x^2}{2m} + \frac{p_y^2}{2m} \cong \frac{1}{2m} m^2c^2\gamma^2 \frac{\varepsilon_x}{\beta_x} + \frac{1}{2m} m^2c^2\gamma^2 \frac{\varepsilon_y}{\beta_y}\,. \tag{6.33}$$

Full energy is a sum of kinetic and potential energy of motion in a focusing system. According to the virial theorem for harmonic oscillator the average potential energy equals to the kinetic one. Adding to (6.33) the longitudinal energy, the temperature of the beam could be represented as the following

$$\tfrac{3}{2}Nk_BT \cong N\cdot mc^2\gamma[\gamma\varepsilon_x\big/\beta_x + \gamma\varepsilon_y\big/\beta_y + \beta^2(\Delta p_{\|}\ /p_0)^2/\gamma], \tag{6.34}$$

where $\beta^2 \cong 1-$ is a square of normalized speed in the lab frame.

Let us consider ***one example***. In damping rings developed as injectors for future linear colliders, typical values are $\beta_{x,y} \cong 10m$, $l_b \cong 1cm$, $\Delta p/p \cong 5{\cdot}10^4$, $\gamma\varepsilon_s \cong 3\,\text{cm}$, $\gamma\varepsilon_x \cong 3\cdot10^{-4}\,cm$ *rad*, $\gamma\varepsilon_y \cong 3\cdot10^{-6}\,cm\ rad$. This gives $\tfrac{3}{2}k_BT \cong mc^2\gamma[3\cdot10^{-7} + 3\cdot10^{-9} + 4\cdot10^{-11}]$. One can see that despite the longitudinal emittance is the biggest one, the longitudinal temperature is the lowest one. This yields the possibility for redistribution the temperatures. Combine formula (6.34) and (6.32) one can obtain for relativistic (in the rest frame) electron gas

$$mc^2\gamma\left[\frac{\gamma\varepsilon_x}{\beta_x} + \frac{\gamma\varepsilon_y}{\beta_y} + \frac{1}{\gamma}\left(\frac{\Delta p}{p_0}\right)^2\right] << (3\pi^2)^{1/3}mc^2(\lambda\!\!\!^{-}_C\rho)^{1/3}, \tag{6.35}$$

where $\rho = \rho_0/\gamma$, ρ_0 –is the density in the Laboratory frame. Neglecting the longitudinal temperature and supposing that, $\gamma\varepsilon_x \approx \gamma\varepsilon_y$ one can obtain the condition for degeneration of electron gas with linear density N/l_b

$$(\gamma\varepsilon_x)^4 \le \beta_x^2\lambda\!\!\!^{-}{}_C^3(N/l_b)/\gamma^3. \tag{6.36}$$

The electrons in the bunch could be considered as a gas as the collisions are rare. We suggested that the phase space corresponds to 3D motion in real space. So the particle could reach every point in phase space. Defining the speed of motion in the rest frame as $v \cong \sqrt{3k_BT/m}$, one can find the frequency of collision $f_{x,y}$ with the potential wall as

$$f_{x,y} \cong \frac{v_{x,y}}{a_{x,y}} \cong c\sqrt{\gamma(\gamma\varepsilon_{x,y})/\beta_{x,y}}\Big/\sqrt{(\gamma\varepsilon_{x,y})\beta_{x,y}/\gamma} = \frac{c\gamma}{\beta_{x,y}} \tag{6.37}$$

like it must be if one transforms the frequency into moving frame. This frequency does not depend on emittance. For longitudinal motion one can estimate $f_s \cong v_{\|}\big/\gamma l_b \cong c(\Delta p/p)\big/\gamma l_b$. So one can see that the frequency of longitudinal oscillations is much smaller, than the transverse one. In motion along the focusing channel the longitudinal motion is practically absent at all. The same is in case of tip as a source.

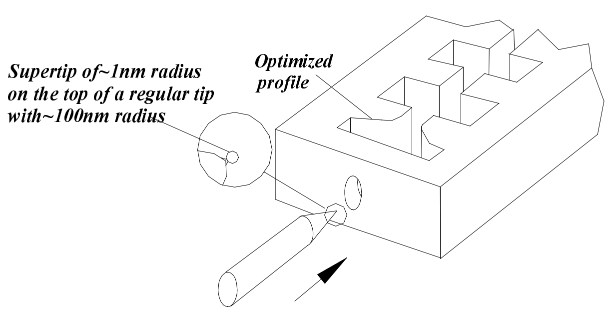

FIGURE 6.6: Schematic view of a tip installed on the holder. All elements illuminated by the same laser source swept. Tip is not shown in scale and shown removed from the cell.

Substitute in (6.36) for estimation $\beta_x \approx l_b \approx 1cm$, $N \approx 10^6$, $\gamma \cong 1$, one can obtain $\gamma\varepsilon_x \le 0.87 \cdot 10^{-7}$ *cm rad*. This is estimation for the *maximal* possible transverse emittance required for degeneration of the bunch with population indicated. So one can conclude, that here we are close to manifestation of quantum effects.
The reason for this is the following. As the electrical field is so high, that electrons are tunneling from conductance level, they might have the same momentum distribution, as inside the metal. As the electrons are degenerated inside the metal, this degeneration might exist on some distance outside the tip.
So the general picture of the electron source might be as it is represented in Fig. 6.6. Basically it is the same accelerating structure, but with insertion of the holder with the tip at the end. The same laser radiation swept along illuminates the cell with the tip. At the accelerating phase the emission occurs. So in this source the electron beam is bunched from the very beginning. The longitudinal phase duration defined by the energy acceptance of the focusing system distributed along the structure. RF focusing is used here also, see Chapter 7.
Ion source is based on the gas ionization close to the tip is the same as electron one, except that now the super tip and all arrangements are working in the gas atmosphere. These gas field ionization sources (GFIS) demonstrated a spectral brightness up to 1 *TA/cm²/srd/eV* [6.9]. So the acceleration structure at injector region must work in gas atmosphere in this method. The necessity of such arrangement conditioned by bunching at the same time as extraction of the ions. One can separate these functions and bunch the ion beam later, after extraction. Design of the optical system for GFIS continuous source one can find in [6.9]. As far as installation the ion source in accelerating structure, Fig.6.6, the condition for synchronism (2.1) must be satisfied. In practice, the distances between the cells could be made changing in accordance with the effective phase velocity established by the phasing of the laser ray.
For the ions on low temperature melting materials, such as Lead for example, the well-developed techniques represented by high temperature needle-type damped by material desired [6.15]. The liquid surface in electric field investigated first in [6.16]. It was shown here, that equilibrium liquid cone in electric field has a semi-angle at the tip of 49.3^0 . On the surface of the cone with this angle the electric field dependent on the distance *r* from the top has the form $\sim r^{-1/2}$. So some electric field there is a balance between electric and capillary pressures. Some of sources are described in [6.17] also.
Bunching
In any way of preparation of low emittance beam, the bunching is useful procedure for redistribution of longitudinal emittance. We suggest here a mechanism close to the usual klystron type. The energy modulation with period corresponding to the laser wavelength made with the help of the inverse free-electron laser mechanism. For the effective voltage amplitude after beam interacted with the co-directional wave in the wiggler we have an expression (1.11) what stands

$$eU_{eff} \cong (eE_{\perp}L_wK)/2\gamma \ ,$$

where L_w is the length of the wiggler and K is a wiggler parameter (Chapter 1). K/γ is an maximal angle of the trajectory to the direction of propagation, $eE_{\perp}L_w$ is a full voltage if electrical field applied on the distance of L_w. So it has clear physical meaning. For example, if the field strength $E_{\perp}$=100 *kV/cm*, γ = 4000, (E =2 *GeV*), K=40, then, first, the wiggler period will be $\lambda_u \cong 2\gamma^2/\left(1+K^2\right)\cdot\lambda_{acc}$=20$cm$ for obtaining the necessary spacing at 1 μm . If the length of the wiggler is equal to, L_u = 1000 cm, then the effective voltage will be $eU_{eff} \cong$ 2000keV.

So, in principle, the wigglers of such a type what are present in a Kayak-paddle damping ring* can provide a normal autophasing bunching. The system requires two mirrors for keeping the radiation inside optical cavity similar what is done say in free electron laser. We will call wiggler and mirrors an optical cavity. The wigglers could be installed practically in any racetrack with long straight sections, like it is done in Kayak-paddle dumpier, see above. In one section it can be installed a wiggler cavity, supplied with opposite-directional wave, and in the other - a short-period wiggler for obtaining the necessary damping time.

The field strength of a 100 *kV/cm* = 10^6 *V/m* can be obtained in case of co-directional movement, by the power flow $\vec{S} = \vec{E}\times\vec{H} = \vec{n}E^2/377 = \vec{n}10^{14}/377 = \vec{n}2.6\cdot 10^{11}$ W/m^2 . If we suppose, that the transverse size is of the order $\sigma \cong 3cm$, so the cross-section is of the order $10^{-3}m^2$. The power, flowing in this cross-section is about 260 *MW*. This is a reactive power; an active power from the laser generator could be lower, if the cavity is resonantly excited.

Let us estimate the power, radiated in the wiggler spontantenously. The simplest way is to calculate the number of the quants. One particle radiates the number of the photons

$$N_\gamma \cong \alpha\frac{L_w}{\lambda_u}\cdot\frac{K^2}{1+K^2} \cong \alpha\frac{L_w}{\lambda_u}\,, \tag{6.39}$$

where as usual, $\alpha = e^2/\hbar c = 1/137$ is a fine structure constant and λ_u is the wiggler period. As all of them radiates coherently, the total energy, carried by these photons will be

$$\Delta E \cong \hbar\omega N^2\alpha L_w/\lambda_u\,. \tag{6.40}$$

So the relative energy spread will be

$$\frac{\Delta E}{E} \cong \frac{\hbar\omega N^2\alpha L_w}{Nmc^2\gamma\lambda_u} = \pi\frac{Nr_0L_w\left(1+K^2\right)}{\lambda^2\gamma^3}\,, \tag{6.41}$$

where λ=10^{-4} cm. Estimations for $\gamma = 4000$, L=10m $N = 10^6$, $1+K^2 \cong 40$, yields $\frac{\Delta E}{E} \cong 5.510^{-5}$ only. A helical wiggler can be used as well as the plane one for this scheme.

Algorithm for the density modulation, Fig.6.6.

* The word “ring” used here for simplicity.

The algorithm for obtaining the energy modulation along the bunch is the same as for ordinary klystron. The frequency now is in μm level of wavelengths. Similar to the klystron cavities having different frequencies, the wavelength of spontantenous radiation the wigglers, or the undulatority factor K, could be chosen slightly ***different***. Here also the wiggler can be used on the second and so on harmonics. The focusing system such as FODO structure can be used here. Effective voltage of this “cavity” is $eU_{eff} \cong (eE_{\perp} L_w K)/2\gamma$ where L_w is the longitudinal length of the wiggler.

Arranging the series as a wiggler cavity, dispersion drift, the cavity again and so on, we came to the Wiggler Klystron Buncher (WKB). This is similar to the Optical Klystron (OK). The difference between the OK and the WKB is basically in that point, than in WKB their beam always gains energy from the laser beam. This is due to the tuning of the pass length. The main difference is that we use few wigglers and drifts in the process.

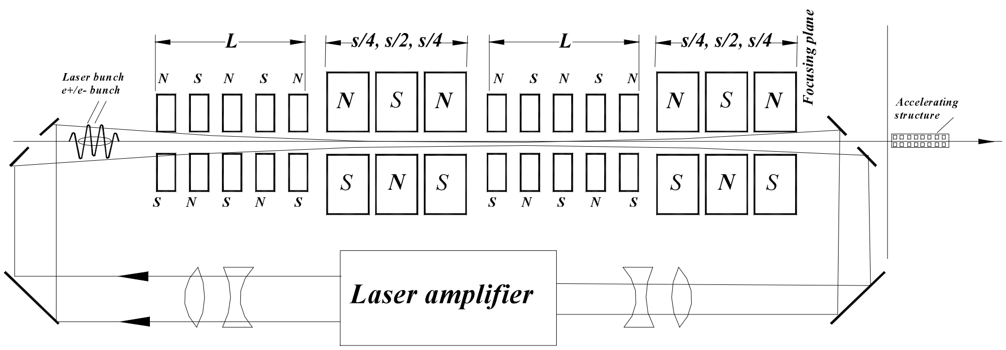

FIGURE 6.6: A cascade bunching scheme. K factor in second wiggler is other, than in the first one. This scheme is an analog of a Klystron with two cavities and two drifts

Thus with few wigglers the method can provide *much more deep* density modulation if compare with usual OK.

Let us consider this in more details. The density distribution could be characterized by the function of distribution $f(\Delta E, \vartheta)$, where ΔE and $\vartheta = \omega t$ are canonically conjugated variables. These variables are the characteristics of the equations of the longitudinal motion. During the motion the generating function, an action, cinematically transfers these variables from one point to another $(\Delta E, \vartheta)_1 \to (\Delta E, \vartheta)_2$. The distribution $f(\Delta E, \vartheta)$ as a function of these variables stills invariant. So the method used for definition of the modulation and the current in actual point is the kinematical consideration of the motion of the individual particle. We will consider for simplicity the function as factorized one $f(\Delta E, \vartheta) = f(\Delta E) \cdot f(\vartheta)$, where initially $f(\vartheta_1) = 1/2\pi$, and $f(\Delta E) = \frac{1}{\sqrt{2\pi}\sigma_E} \exp\left(-\frac{\Delta E^2}{2\sigma_E^2}\right)$, where σ_E is the energy spread in the beam, is a realistic assumption. So the Fourier component of the current at the second point can be defined as

$$i_m = \iint v f(\Delta E)\, f(\vartheta_2) e^{-im\vartheta_2} d\vartheta_2 d\Delta E\ , \qquad (6.42)$$

where $\vartheta_2 = \omega t_2$ is the actual phase at the second point. This integral can be easily transferred into

$$i_m = I_0 \int \left|\frac{\partial \vartheta_1}{\partial \vartheta_2}\right| e^{-im\vartheta_2} f(\Delta E) \frac{d\vartheta_2 d\Delta E}{2\pi} = I_0 \iint e^{-im\vartheta_2} \exp\left(-\frac{(\Delta E)^2}{2\sigma_E^2}\right) \frac{d\vartheta_1 d\Delta E}{2\pi\sqrt{2\pi}\sigma_E}\ , \quad (6.43)$$

where I_0 is the current at the input of the bunching

The phase on arrival of the particle to the second wiggler is defined by the formulas, which is similar to ones used in klystron theory

$$\vartheta_2 = \omega t_2 = \omega t_1 + \frac{\omega l}{v} = \omega t_1 + \frac{\omega}{v}\left(l + \frac{\partial l}{\partial E}\Delta E\right) = \omega t_1 + \vartheta_{12} + k\kappa\frac{\Delta E}{E}\ , \qquad (6.44)$$

where $k = \omega / v$, $\vartheta_{12} = \omega l / v = kl$ is a transit phase and the energy variation arises both from the modulation and the natural spread in the beam. For modulation with sinusoidal wave we obtain

$$\vartheta_2 = \omega t_1 + \vartheta_{12} + X_{12} \cdot Cos(\omega t_1) + k\kappa\left(\frac{\Delta E}{E}\right)_\sigma , \qquad (6.45)$$

where the energy spread shown as $\left(\frac{\Delta E}{E}\right)_\sigma$ and

$$X_{12} = k\kappa\left(\Delta E_{eff} / E\right) = k\kappa\left(eU_{eff} \ / \ E\right) = \left(\frac{1}{2} k\kappa e E_\perp LK / (E\gamma)\right) \qquad (6.46)$$

is a bunching parameter between the first and the second points. The physical sense of the bunching parameter is connected with amplitude of the phase modulation for an individual particle, while drifted from point of modulation to the actual one. Now one can obtain

$$i_{2m} = I_0 e^{i\vartheta_{12}} \int \exp\left(im\left(\vartheta_1 - X_{12} Cos\,\vartheta_1\right)\right) \frac{d\vartheta_1}{2\pi} \int \exp\left(ik\kappa\frac{\Delta E}{E} - \frac{(\Delta E)^2}{2\sigma_E^2}\right) \frac{d\Delta E}{\sqrt{2\pi}\sigma_E} \qquad (6.47)$$

$$\frac{i_m}{I_0} = J_m\left(X_m\right) \exp\left(-\frac{1}{2}\left(mk\kappa \cdot \frac{\sigma_E}{E}\right)^2\right), \qquad (6.48)$$

where $X_m = mX_{12}$, the term with exponent reflects the debunching due to the energy spread in the bunch. J_1 has a maximum at X_1 =1.82, J_1=0.57. If we suppose, that $\sigma_E / E \cong 0.001$, $\kappa = \gamma\frac{\partial l}{\partial \gamma} \approx \frac{(K^{bend})^2 s}{\gamma^2} \cong 0.01\ \ cm,\ E\ \approx 2\ \ GeV,\ \ k = 2\pi/\lambda_{ac} \cong 6\cdot 10^4$, this yields $\exp(...) \cong 1$, and the value for ratio $\frac{i_m}{I_0} \approx 0.26$, i.e. 25% variation of the (complex) density only. This estimation is well for FEL type of bunching. The particles approximately in half of periods will decrease the power, transferred to the wave.

If the beam comes to the second cavity at the phase ωt_2, then the modulation provided in the second wiggler cavity becomes

$$\left|\Delta E / E\right|_2 Cos\left(\omega t_1 + \vartheta_{12} + X_{12} \cdot Cos\left(\omega t_1\right)\right). \qquad (6.49)$$

It is clear from this relation that here many frequencies generated, due to appearance the cosine function as an argument of a cosine. For a $X_{12} \leq 0.4$ one can obtain

$$\vartheta_3 = \vartheta_1 + \vartheta_{12} + \vartheta_{23} - X_{13} Sin\vartheta_1 + X_{23} Cos(\vartheta_1 + \varphi) + X_{23} X_{12} Sin\vartheta_1 Sin(\vartheta_1 + \varphi) \quad (6.50)$$

where the bunching parameters are defined respectively, and the figures at phase subindexes shows the points, for which these phase shifts are calculated, φ reflects the phase shift of the first and the second cavities. The main output from this is appearance of the second harmonic in the phase modulation, which obtained due to *cascade* bunching. In fact, that the second harmonic can be obtained by directional installation the wiggler cavity with the second harmonic. As a result

$$i_{31} = 2I_0 \exp(-i(\vartheta_{12} + \vartheta_{23} - \vartheta')) J_1(X'), \quad (6.51)$$

where $X' e^{i\vartheta'} = X_{13} - iX_{23} e^{i\varphi}$. When $X' = 2$, $\vartheta' = \varphi - \pi/2$ and $\delta = \dfrac{X_{12} X_{23}}{2X'} = 0.4$, the level of the first harmonic is a 28% higher, than in case of a single stage bunching.

For estimation of the necessary value of the field strength for obtaining the bunching coefficient we can write

$$1 \cong X \cong k\kappa(eU_{eff}/E) \cong \frac{2\pi}{\lambda}\kappa\frac{eU_{eff}}{E} = 6\cdot 10^4 \frac{1}{cm}\cdot 0.01cm\cdot\frac{eU_{eff}keV}{2000\cdot 10^3 keV} \cong 1.$$

The last expression gives energy eU_{eff} ~3 *MeV*, so this corresponds to our estimations in the beginning of the bunching subsection.

The consideration of the amplification near the saturation one can find in [6.18].

The minimal energy defined by the limitation due to the space charge effects, characterized by the plasma frequency

$$\omega_p^2 \cong \frac{4\pi n r_0 c^2}{\gamma^3}, \quad (6.52)$$

where $r_0 = \dfrac{e^2}{4\pi\varepsilon_0 mc^2} = 2.8\cdot 10^{-15}$ meter is the classical electron radius, $n = \dfrac{N}{l_b \pi r_b^2}$, N is the number of the particles in the bunch with the length l_b ~10^{-4} *cm* and the transverse radius r_b. The space charge effects destroys the bunch when the plasma frequency is compared with the frequency of $\omega = 2\pi c/\lambda_{ac}$. Supposing that the plasma frequency is of the 0.1 of the last one, we came to estimation

$$\gamma^3 \geq 10^2 \frac{4Nr_0c^2}{l_b^3\omega^2}, \quad (6.53)$$

or $\gamma \geq 8.5$, which yields $E = mc^2\gamma \approx 4.5 MeV$ the total energy, of around 4 *MeV* accelerating voltage. This estimation is rather sensitive to the supposed partial value of the plasma frequency compared with the main frequency. Nevertheless this gives possible to estimate the energy spread in the beam.

Supposing that the factor

$$\exp\left(-\frac{1}{2}\left(mk\kappa\cdot\frac{\sigma_E}{E}\right)^2\right) \cong \frac{1}{2.718}, \quad (6.54)$$

one can evaluate $k\kappa\frac{\sigma_e}{E} \cong 2\pi\frac{\kappa}{\lambda}\frac{\sigma_E}{E} \cong 4$ and choose the necessary relations between them.

Dispersive drift space

Instead of a straight section, here, like in optical klystron [6.2], there used a dispersion section as drift one, which has a sufficient parameter $\kappa = E\frac{\partial l}{\partial E} = \gamma\frac{\partial l}{\partial \gamma} = \int_0^s \frac{D}{\rho}ds$, where $D(s)$ is the dispersion, ρ is the actual bending radius in the magnets used in the system. In the magnet the $D(\phi) = \rho(1 - Cos\phi)$, where $d\phi = ds/\rho$. Combining the bending magnets and the quads so that $D(0) = D(s) = 0$, one can arrange the device with sufficient dispersion lengthening. Well-known example with three-magnet scheme gives

$$\frac{\partial l}{\partial E} = \frac{e^2 H_0{}^2}{48}\left(\frac{s}{E}\right)^3, \tag{6.55}$$

or

$$\kappa = \gamma\frac{\partial l}{\partial \gamma} = \frac{(2\pi)^2}{48}\frac{(K^{bend})^2 s}{\gamma^2} \quad , \tag{6.56}$$

where H_0 is the bending field in the magnet, the s is a total length of the dispersion part, $K^{bend} \approx \frac{eH_0 s}{2\pi mc^2} >> 1$. The structure of the dispersion part has the first part is s/4 the second is s/2 and the last is again s/4. The fields in the side magnets are opposite to the field in the central one. For example, if s = 100cm, $H_\perp = 5kGs = 0.5T$, then $K^{bend} \cong 47$ $\gamma \cong 4000$, and $\kappa \cong 0.011$. The lengthening due to natural energy spread in the beam will be $\Delta l \cong 10^{-5}\,cm$ or $\Delta l \cong \lambda_{ac}/10$. For the controllable lengthening one need to substitute $\Delta\gamma \cong \frac{eE_\perp KL_w}{2mc^2\gamma}$ and for $\Delta\gamma/\gamma = \frac{eE_\perp KL_w}{2mc^2\gamma^2}$. The last gives $\Delta\gamma/\gamma = \frac{eE_\perp KL_w}{2mc^2\gamma^2}$.

For the straight-line section, the factor $\kappa = \gamma\frac{\partial l}{\partial \gamma} = \frac{s}{4\gamma^2}$, so the gain if compared with a straight line, will be of the order $(K^{bend})^2$. For example, if we estimate the beam lengthening on the distance 1 meter with $\Delta\gamma/\gamma \approx 10^{-3}$, $\gamma = 4000$, we obtain the $\kappa \cong 10^{-6}$ and *kinematical* lengthening in a straight section as $\Delta l = \kappa \cdot (\Delta\gamma/\gamma) \cong 6.25 \cdot 10^{-9}\,cm$ or much less, than $\lambda_{ac}/4$.

The lengthening due to finite emittance can be estimated from the general formula. In the first order one can obtain [6.12]

$$\Delta l = -\int_0^S \frac{1}{\rho}x d\sigma = -x_0\int\frac{C}{\rho}d\sigma - x_0'\int\frac{S}{\rho}d\sigma - \kappa\frac{\Delta\gamma}{\gamma} \ , \tag{6.57}$$

where $x = C(s)x_0 + S(s)x_0' + D\Delta\gamma/\gamma$, $C(s)$ and $S(s)$ are sin-like and cosine-like solutions of the equation of motion, x_0, x_0' are the initial coordinate and the angle. So as the dispersion

$$D(s) = -S(s)\int \frac{C}{\rho} d\sigma + C(s)\int \frac{S}{\rho} d\sigma \qquad (6.58)$$

is equal to zero at the input and the output points, it means that each of these integrals is equal to zero. This yields the absence of the lengthening in the first order due to initial conditions, or emittance.

7. TRANSVERSE FOCUSING DURING ACCELERATION

Other component influence to the beam size in a structure is a focusing system itself. A short wavelength of betatron oscillations helps against the wakefield influence and resistive wall instability. The focusing system includes the *quadrupole lenses* of appropriate dimensions and a *RF focusing* [7.1].

Quadrupole lenses could be placed between the accelerating sections, see Fig.2.2, 2.3, 5.1. The lens focusing parameter can be expressed as [6.12]

$$\frac{G}{(HR)} = k = \frac{\sqrt{2(1-Cos\mu)}}{2l(L+2l)} \qquad (7.1)$$

where G –is the lens gradient, $(HR) \cong pc/300$ –is the magnet rigidity of the particle, μ –is a betatron tune shift per one period, $2l$ –is the length of a quadrupole, L –is the distance between lenses, comparable with longitudinal size of accelerating structure L from Figs. 2.1, 2.2. The modulation factor M of the β-function between the lenses looks like

$$M^2 = \frac{\beta_{\max}}{\beta_{\min}} = \frac{1+\tanh\phi\cdot\left(\tan\phi + L\phi/l\right)}{1-\tan\phi\cdot\left(\tanh\phi + L\phi/l\right)} \qquad (7.2)$$

$\phi = l\sqrt{k}$ –is the half phase shift in the lens. For L=4*cm*, l=0.4*cm*, $\mu = \pi/6$ one can obtain $k \cong 5\cdot 10^3 1/m^2$, $\phi^2 = l^2\cdot k = 2\cdot 10^{-2}$, and $M^2 \cong 1.5$. For maximal value of the envelope function we have

$$\beta_{max} \cong M\frac{1}{|k|\cdot l}\sqrt{\frac{2+L/l}{2/3+L/l}} = \frac{2M\cdot(L+2l)}{\sqrt{2(1-Cos\mu)}}\sqrt{\frac{2+L/l}{2/3+L/l}}$$

which for previous values of L and l gives $\beta_{max} \cong 15cm$ and $\beta_{min} \cong 10cm$. These values we used above. One can see from (7.1) that to obtain certain value k [1/m^2] for the particles with momentum p [*GeV/c*], the gradient required is $G \cong 0.3pk$. For example, the particles with intermediate momentum p $\cong$ 10 *GeV/c* ($\gamma \cong 2\cdot 10^4$), $k \approx 5\cdot 10^3\ 1/m^2$, gradient required is $G \cong 1.5\cdot 10^4\ kG/cm$. As the beam has tiny cross section, the radius of aperture A of the quads can be also made small enough, providing high gradient G with small value of the pole field H as $G \cong H/A$. If we estimate H≅15 *kG*, A = 0.01 *mm* (20 μm in dia of aperture), then we come to the gradient required:

$G \cong 15kG/0.001cm = 1.5 \cdot 10^4 kG/cm$. At higher energy the actual emittance becomes adiabatically lower and the envelope function value allowed to be increased.
With $\beta_{max} \cong 15cm$ and emittances like (6.10a), (6.11a) the transverse size of the bunch at $\gamma \cong 2 \cdot 10^4$ goes to

$\sigma_x \cong \sqrt{2.5 \cdot 10^{-8} \cdot 15/2 \cdot 10^4/\pi} \cong 2.4 \cdot 10^{-6} cm$,

$\sigma_y \cong \sqrt{9.5 \cdot 10^{-10} \cdot 15/2 \cdot 10^4/\pi} \cong 4.7 \cdot 10^{-7} cm$.

The biggest size goes along the slit, y –direction in Fig.4.1. Once again if we suggest, that the safety margins must be ten times of this, we are coming to the slit narrow size as much as $10\sigma_y \cong 4.7 \cdot 10^{-6} cm$, what gives possibility to utilization $\lambda_{ac} \approx 5 \cdot 10\sigma_y \cong 2.35 \cdot 10^{-5} cm$, what is 4.25 times lower than $\lambda_{ac} \cong 1\mu m$. We suggested here again that the pass slits is 20%, $\delta \cong 0.2\lambda_{ac}$, Fig.4.1. So there is no problem with focusing *even for optical* accelerating wavelengths if the emittance like used in estimation available.
Example of a quadrupole design is represented in Fig. 7.1. The currents 3 at the left and right sides could be made slightly different, what give the possibility for a horizontal trimming of the quad's axis. An additional current 6 allow trimming vertical position of the quad.
Thus, the focusing with the quadrupole lenses only is *acceptable for all laser wavelengths* under consideration. This once again proves that the low emittance source of particles is the general task for laser driven accelerator.

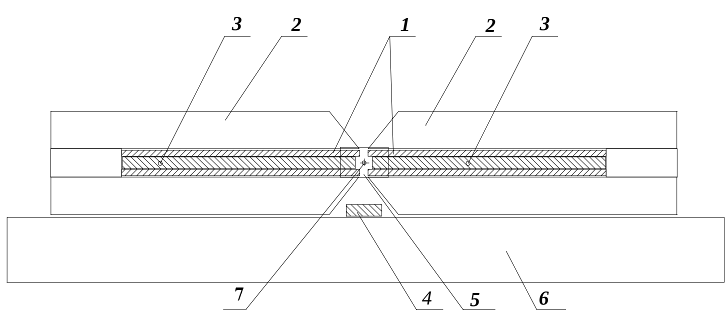

FIGURE 7.1: Example of a quadrupole design. Transverse cross-section is shown. Longitudinal dimension (perpendicular to the plane of drawing) is about 0.5 *cm*. Accelerating bunch is moving perpendicular to the plane of the drawing. 1–is an iron blades-like looking poles, 2–is a yoke, 3–is a current strips, 4–is a current strip for vertical axes trim, 5–is a profile of the accelerating structure, 6–is a base, 7–is a cross-section of the accelerating bunch.

RF focusing in the foxhole structure has some peculiarities if compared with usual travelling wave structure. Firs of all each cell could be considered as independent, so there is no energy flux from cell to cell. Due to this there is no cancellation between electric and magnetic forces acting to the particle as in a traveling wave structure. For example in round traveling wave structure transverse electric and magnetic fields could be expressed as derivatives of longitudinal component, see (1.4). In cylindrical coordinates this goes to

$$E_r(r,s,t) \cong -\frac{r}{2}\frac{\partial E_s(0,s,t)}{\partial s} \quad , \qquad B_\vartheta \cong \frac{r}{2c^2}\frac{\partial E_s(0,s,t)}{\partial t} .$$

So basically the power flux is $P \cong E_r \times B_\vartheta$ defines the power flow along the structure as $\int_0^a P \cdot rdr$ and so on. Resulting transverse force could be expressed as

$$\frac{dp_\perp}{ds} \cong -\frac{er}{2\lambda_{ac}}\{\lambda_{ac}[\frac{\partial E_s}{\partial s}+\frac{1}{v}\frac{\partial E_s}{\partial t}]+\frac{2\pi c}{\gamma^2 v_p}\frac{\partial E_s}{\partial \varphi}\} \tag{7.3}$$

$\varphi = \omega s / v_p - \omega t$ –is the RF phase of the particle (at the crest of RF $\varphi = 0$), v_p is the phase velocity of the wave. For the traveling wave structure far from the ends for the *main harmonic* first term is about zero and second is $\sim 1/\gamma^2$. So for round passing holes in *traveling* wave structure the transverse focusing/defocusing is absent with accuracy $\sim 1/\gamma^2$. First term in (7.3) could be important at the input/output ends of the structure where it can give a lens with focal distance $F \cong 2mc^2\gamma Cos\varphi / eE_s$ [7.7]. First term could be nonzero also if there are *reflections* from the end of structure, so some *standing* wave excited in structure. This could yield $\partial E_s / \partial s \neq 0$. In this case second term in (7.3) must be rewritten also as $\frac{dp_\perp}{ds} \cong +\frac{2\pi c}{v_p}(1 \mp \frac{v \cdot v_p}{c^2}\frac{\partial E_s}{\partial \varphi})$. For a standing wave, which is a separate cavity for example, the electric and magnetic fields are shifted in time so there is no longitudinal flux of power, and, hence, electric and magnetic fields may not be compensated. In cylindrical cavity without holes it could be clearly seen, as the transverse electric field is absent at all. The transverse force also occurs not to be a zero for a travelling wave, if the passing holes are not round, [7.2].

The net force on the particle can be obtained by integration the fields in the cell, see Chapter 4. This will bring an analog of transit-time factor. This brings for *x, y* ≈ 0 and for *s*=0 in the middle of the cell (see Fig.4.1),

$$< F_s >= e\int_{-g/2c}^{g/2c} E_m Cos(\omega t+\varphi)\cdot dt \Big/ \int_{-g/2c}^{g/2c} dt = eE_m \frac{Sin(\omega g/2c)}{\omega g/2c} Cos\varphi = eE_m \cdot I(g)\cdot Cos\varphi ,$$

(7.4)

where $I(g) = \frac{Sin(\omega g/2c)}{\omega g/2c}$ is a transit time factor, E_m –is the amplitude of the longitudinal (accelerating) field in the cell. Analogously

$$< F_y >= \frac{\int_{-g/2c}^{g/2c} ecH_x dt}{\int_{-g/2c}^{g/2c} dt} \cong \frac{\frac{eE_m\lambda}{2h}\cdot\frac{\pi y}{h}\int_{-g/2c}^{g/2c} Sin(\omega t+\varphi)dt}{\int_{-g/2c}^{g/2c} dt} \cdot = \frac{\pi e E_m \lambda y}{2h^2}\cdot\frac{Sin(\omega g/2c)}{\omega g/2c} Sin\varphi ,$$

(7.5a)

$$< F_x > = \frac{\int_{-g/2c}^{g/2c} ecH_y dt}{\int_{-g/2c}^{g/2c} dt} \cong \frac{\frac{eE_m\lambda}{2W} \cdot \frac{\pi x}{W} \int_{-g/2c}^{g/2c} Sin(\omega t + \varphi) dt}{\int_{-g/2c}^{g/2c} dt} \cdot = \frac{\pi e E_m \lambda x}{2W^2} \cdot \frac{Sin(\omega g/2c)}{\omega g/2c} Sin\varphi \tag{7.5b}$$

If $\omega g/2c = \pi g/\lambda = \pi/2$, what corresponds to $g = \lambda/2$, then $I(g) = 2/\pi$ and the forces (7.3)-(7.5) became

$$\langle F_x \rangle \cong \frac{e\lambda E_m}{W^2} Sin\varphi \cdot x, \quad \langle F_y \rangle \cong \frac{e\lambda E_m}{h^2} Sin\varphi \cdot y, \quad \langle F_s \rangle \cong \frac{2eE_m}{\pi} Cos\varphi. \tag{7.6}$$

These forces are quadrupole types for the particles out of the crest of RF. The effective focusing factor of the RF lens can be evaluated as

$$k_x = -\frac{1}{pc}\frac{\partial\langle F_x \rangle}{\partial x} \cong -\frac{e\lambda_{ac}E_m}{mc^2\gamma W^2} Sin\varphi, \quad k_y = -\frac{1}{pc}\frac{\partial\langle F_y \rangle}{\partial y} \cong -\frac{e\lambda_{ac}E_m}{mc^2\gamma h^2} Sin\varphi. \tag{7.7}$$

Substitute here $\lambda_{ac} = 10\mu m$, $\gamma = 2\cdot 10^4$ (*pc*=10 *GeV*), $W \approx 5\mu m$ (see Fig.4.1), $E_m \approx 10^{11} V/m$, we obtain $k_x \approx 4\cdot 10^5 \cdot Sin\varphi [m^{-2}]$. There are proposals to use this force for alternating phase focusing (APF), when the phase of the beam with respect to the RF crest is periodically changed, $\varphi = \pm\varphi_0$ [7.3]. The reason for this is in fact that for the foxhole structure or muffin-tin, [4.4], there is focusing in direction to the narrow side of passing slit, *x* in Fig.4.1 [7.2]. In our case this can be made by arranging periodical delay of the accelerating radiation arriving to the structure, for example, by modulation of the thickness of the lens 7 in Fig. 2.3 or by shifting the cell along the bunch trajectory, Fig 7.2.

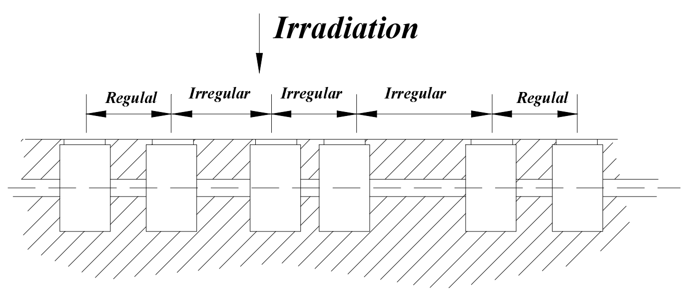

FIGURE 7.2: Arrangement of the phase shifts in the cells.

Anyway one can see that the RF focusing could be, in principle, two orders of magnitude more strong, than one uses a conventional quad, scaled to appropriate level.
Simplest Foxhole structure focuses the beam in direction across the narrowest size of passing holes, *x* in Fig. 4.1 [4.3] [2]. The focusing force is linearly dependent on the slot width. In other direction in first order over displacement there is no focusing. The

[2] The RF quadrupole focusing for both directions also may be arranged here as well. In this case the slits between the grooves has some variations in the channel cross section [7.2, 7.4].

possible scheme also is that the RF focusing arranged by the slots of the structure in horizontal direction and vertical focusing made by quadrupoles. This can reduce the betatron wavelength, in principle, two times, if the structures with horizontal and vertical focusing are periodically changed. Different dimensions of the beam according to variation of the envelope function make it possible to adjust the focusing slots sequence to this variation. In the ideal case each cell could be modified so that if focuses in appropriate direction. In this case the periodicity equates to the double period of the cells in structure, i.e. $2\lambda_{ac}$. In this case it is possible obtain the focusing two orders of magnitude stronger, than with ordinary magnetic quadrupoles. So the RF focusing in the structures with $\lambda_{ac} \cong 1\mu m$ and shorter is the only real possibility.

At the end of this chapter let us make a comparison of how RF focusing changes the focusing of the bunch in accelerating channel and how the focusing parameter changes due to the direct energy change as the accelerating phase is shifted from the crest. Or with other word how BNS de-tuning strong if compared with RF one. In BNS method suggested [7.5], the tail particles have lower energy and, hence, higher betatron tunes in the focusing system of accelerator if the wakes are ignored. As the interaction with the surroundings *reduces* the transverse frequency of the tail particles due to wakes, it is possible to adjust the *effective* transverse frequency so, that it is not dependent on the position along the bunch at all if both effects (wakes and energy difference) are taken into account. Thus there is no emittance dilution if this condition is satisfied. If the particle is shifted along the linac with phase φ with respect to RF, it will be a subject for additional RF focusing (7.7)

$$\Delta k_{RF} \cong -\frac{e\lambda_{ac}E_m}{mc^2\gamma h^2}\varphi \cong -\frac{4eE_m}{mc^2\gamma\lambda_{ac}}\varphi, \tag{7.8}$$

where we suggested that $h \approx \lambda_{ac}/2$. For round cavity this estimation is about the same. Now BNS variation in focusing for the particle with shifted phase goes after passing *n* cells to

$$\Delta k_{BNS} \cong \Delta\frac{eG}{pc} \cong -k\frac{\Delta p}{p} \cong -k\frac{eE_m gn}{mc^2\gamma}(1-Cos\varphi) \cong \frac{k\varphi^2}{2}. \tag{7.9}$$

Here we suggested that initial energy be much less than the current one, so $eE_m gn \cong pc$, $g \cong \lambda_{ac}/2$ –is the gap of a single cell. So the ratio of these shifts goes to

$$\frac{\Delta k_{RF}}{\Delta k_{BNS}} \cong \frac{8eE_m}{kmc^2\gamma\lambda_{ac}\varphi} \cong \frac{16}{k\lambda_{ac}^2\varphi n}, \tag{7.10}$$

as we put the phase $\varphi \to -\varphi$, what corresponds to the position behind the crest. In this case both effects increases the transverse focusing. This could be clearly seen from the statement, that this phase position gives rise to longitudinal RF *defocusing*, and, hence, transverse RF focusing. Let us estimate (7.10) for example at, say 10 *GeV*. This gives for $\varphi \cong 0.1rad$, for electrical field strength $E_m \cong 3GeV/m = 30MeV/cm$, $G \cong 1kG/cm$, $k = G/(HR) \cong 3\cdot 10^{-5}cm^{-2}$, where $(HR) \cong E/300 = 3\cdot 10^4 kG\cdot cm$ –is a magnet rigidity of the 10 *GeV* particle the ratio as

$$\frac{\Delta k_{RF}}{\Delta k_{BNS}} \cong \frac{8\cdot 30}{3\cdot 10^{-5}\cdot 10^4 10\cdot 0.1} \cong 8\cdot 10^2 .$$

This result shows that RF focusing is much stronger, than BNS effect.

8. ACCELERATING GRADIENT

Let us suggest that full energy carried by a laser bunch is Q. For a time duration τ (see Figs. 2.1, 2.2), we conclude, that the number n of periods in the bunch is about $n = \tau / T = c\tau / \lambda$, where $T = \lambda / c$ –is a period of radiation. So, the field energy stored in the volume corresponding to a half of period is $W_E \cong Q/2n$. From the other hand $W_E \cong (1/2)\varepsilon_0 E_m^2 V_{eff}$, where ε_0 –is the dielectric permeability of the vacuum, $V_{eff} \cong gWh \cong g\lambda^2/4$ (W from Fig.4.1) is the effective volume, where the energy is concentrated. We also could suggest that in conservative case only half of the energy of the half period i.e. one fourth is directly coming to the cell. This ratio could be improved by more complicated geometry of orifice input. From the expressions for W_E, one can obtain the maximal field strength

$$E_m \cong 2\sqrt{Q/(\varepsilon_0 c\tau\lambda g)} \tag{8.1}$$

For estimation let us take $Q = 0.01J$, $\tau \cong 0.1\ ns$, $\lambda \cong 1\mu m$, $g \cong \lambda/2 = 0.5\mu m$. This gives the field strength $E_m \cong 275 GeV/m$. This value must be reduced by the factor, taking into account the longitudinal length l_f instead of g, see Figs.2.1, 2.2. The longitudinal length could be estimated as a $l_f \approx L/N_R$, where L –is the length of the structure, N_R –is the number of resolved spots. For $\lambda \cong 1\mu m$ one can expect $N_R \approx 100$, so the length of our interest is $l_f \approx c\tau / N_R$, what is $l_f \approx 0.03cm \approx 300\lambda$. So the formula (8.1) must be rejected by factor $\sqrt{g/l_f} \approx 0.041$, what gives the field strength at the surface of the structure as high as $E_m \cdot \sqrt{g/l_f} \approx 11.2 GeV/m$. The value of electrical field *inside* the structure could be found by taking into account RF quality factor Q_{RF}, see section about accelerating structure. For $Q_{RF} \approx 9$ it could reach again $E_m\sqrt{Q_{RF}}\sqrt{g/l_f} \approx 33 GeV/m$ in conservative estimation. So despite of the radiation illuminates the orifice during $\sim l_f/\lambda_{ac} \approx c\tau / N_R / \lambda_{ac} \sim 300$ periods we suggest such low Q_{RF}. This gives guaranties that equilibrium in cell established well.

So the laser flash with $Q \cong 10\ mJ$ at $\lambda \cong 1\ \mu\ m$ is able to feed the accelerating structure with the length about $c\tau \approx 3cm$ with $\geq 33\ GeV/m$. A flash with $Q \approx 1J$ will feed the 3-m total accelerating length, providing the energy gain $\approx 100 GeV$. A pulse with $Q \approx 100 J$ could feed 10 TeV machine and so on.

Of cause *effective* length of accelerator will be longer, taking into account some filling factor reserved for focusing lenses, deflecting devices and so on.

For $\lambda \cong 10\mu m$ the numbers are the following. First of all E_m from (8.1) is ten times lower. Number of resolved spots for electro-optical device is also lower, $N_R \approx 10-20$. But the factor $\sqrt{g/l_f} \cong \sqrt{gN_R / c\tau}$ remains about the same. So for the same Q_{RF} factor accelerating gradient will be about 3.3*GeV/m* for laser flash 10*mJ* distributed along 3*cm* length. The damage level to the structure by a laser radiation is strongly correlated with the duration of illumination. In TLF method the energy about $Q \cong 10mJ$ effectively distributed on the area $S \cong W \cdot L$ in this time. So it gives density of energy falling on this area as high as $Q/S \cong Q/WL \approx Q/\lambda L \approx 3J/cm^2$ for $\lambda \cong 10\mu\ m$ and 30*J/cm*^{2} for $\lambda \cong 1\mu\ m$. Mostly of this energy reflected back. Widening the illumination area for $\lambda \cong 1\mu\ m$ by factor of two will lower the power density to 15*J/cm*^{2} on expense of the gradient reduction down to $33/\sqrt{2} \cong 23GeV/m$.
The illumination lasts for a time $t \cong l_t / c \cong l_f / c \cong 10^{-13} s$. Remind again, that this time is less than the time between electron-electron collisions, what is $\tau_{coll} \cong 10^{-12} s$, still however longer, than the time, corresponding to reaction of electron plasma in a metal, what is $\tau_p \approx 3 \cdot 10^{-16} s$.

Threshold to the Damage.

The latest measurements show a damage threshold increase while the illumination time is shortening. This breaks the $\tau^{1/2}$ low. This was explained by saturation of impact ionization rate per unit distance [8.1]. Measured threshold for 0.3 *ps* pulse was about 10 *J/cm*^{2}. For 1 *ps* the threshold measured was 6 *J/cm*^{2}. In our case we have 10*mJ* laser pulse distributed over area 3×10^{-3} *cm*^{2} what gives 3 *J/cm*^{2} and accelerating gradient 3 *GeV/m*. We believe that these figures could be improved after careful preparation the surface and optimizing the working temperature and proper chose of material.
The damaging level could depend on lot of factors, such as cleanness, vacuum, temperature of accelerating structure*, technology of fabrication, heat treating and so on. So, the threshold limit is not a singe number, it must reflect all conditions listed above.
As we mentioned, all these numbers allied with the number of resolved spots of deflecting device. In Table 8.1 we summarize the results on the power density. We would like to stress here again, that despite the time duration of laser flash is $\tau \approx 100\,ps$, the illumination time of every point on the surface of the structure is ~ 0.1 *ps* for $\lambda_{ac} \cong 1\mu m$, and ~ 0.3 *ps* for $\lambda_{ac} \cong 10\mu m$.

TABLE 8.1. Power required for excitation of the structure.

Wavelength	Energy/length	Gradient	Power density	Illumination Time
$\lambda \cong 1\mu\ m$	3 *mJ/cm*	30 *GeV/m*	30 *J/cm*^{2}	0.1*ps*
$\lambda \cong 10\mu\ m$	3 *mJ/cm*	3 *GeV/m*	3 *J/cm*^{2}	0.3*ps*

At the end of this section let us made estimation of possible limitation of electric field strength arising from the physical nature of metal. Recalling the Fig. 6.5 we can roughly

* One may suggest the working temperature of liquid Helium or Nitrogen to reduce electron-phonon interaction.

estimate the limit from the point of tunneling the electrons through the well, known in Quantum Mechanics [8.2]. The tunneling probability through the barrier like shown in Fig.8.1 could be expressed as the following

$$D \approx \exp\left[-\frac{4\sqrt{2m}}{3\hbar eE}\left(eU_F - e\sqrt{eE}\right)^{3/2}\right], \tag{8.2}$$

(CGSE units) where $eU_F \cong$ Fermi energy calculated from the free level and the second term defines the lowering of potential well due to Schottky effect, see Chapter 6. One can conclude that this probability is not sensitive to the exact view of potential well. The probability becomes of the order of unity when (SI units)

$$U_F \approx \sqrt{eE/(4\pi\varepsilon_0)} \ . \tag{8.3}$$

The last expression gives the estimation of the limiting field strength

$$E \approx \frac{4\pi\varepsilon_0 U_F^2}{e} \ . \tag{8.4}$$

Substitute here $U_F \approx 5V$, $\varepsilon_0 \cong \frac{1}{36\pi}10^{-9} F/m$, one can obtain $E \approx 17 GeV/m$. One can conclude from this estimation, that utilization of materials with low conductance level and high outs work, eU_F, is preferable. Ideally the low conductivity materials are the best from the point of the field strength. The losses in these materials could be low also, as at high frequencies the atomic electrons are responsible for the propagation of laser radiation. Extreme example gives the optical transparency.

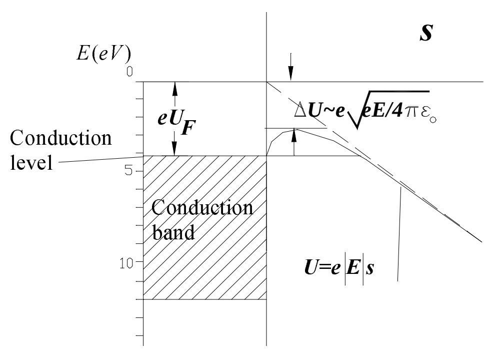

FIGURE 8.1: To the estimation of the limiting electrical field strength on the surface of metal.

In Chapter 6 we mentioned the diamond coating [6.10] of the tips used in solid state sources. The coating also proposed to reduce the heating of the surface [6.14]. Such type of coating could be done by a hot-filament chemical vapor deposition (HFCVD) technique [6.10]. Deposition was provided in CH_4 +H_2 gaseous mixtures at 10-20 *Torr* total pressure, with CH_4 concentration in the mixtures of 3%-5%, at substrate temperatures 700-800^{o}C, and at the temperatures of filament 1900-2100 ^{o}C.

This coating could help to increase the field strength. Really, in the presence of dielectric on the surface of the metal, the limiting field becomes ε times, where ε –is a relative dielectric permeability, the limiting electric field strength becomes higher, that for pure metal and could be estimated as

$$E \cong 4\pi\varepsilon_0\varepsilon U_F^2 / e \,. \tag{8.5}$$

As for Diamond, the $\varepsilon \cong 2.1$, and one can expect the same increase of electrical field strength what gives here $E \approx 36 GeV/m$. In addition we can say that only some particular places of the cell exposed to the high electric field strength. So the dielectric cover could be applied directly there. One possibility is to create a structure on Si with different types of conductivity. Now what is important is the proper arrangement of the input of the laser radiation into the cell so that for every point the angle of illumination of the material is lower than the angle of full reflection, if the coating was done.

One comment needs to be done here. Strictly speaking estimation (8.5) is valid for DC voltage applied to the surface. In RF, especially short lasting, *time dependence* of the quantum diffusion becomes important. So one can expect here significant increase of the damage threshold as the illumination time is small.

So the figures in Table 8.1 for $\lambda_{ac} \cong 1\mu m$ could be considered as the potential possibilities of the TLF method with the laser power indicated.

In any case final answer could be given as result of experiments with different materials.

Types of lasers for utilization in TLF method

TLF method promises up to 30 *TeV/km* or 300 *TeV* on 10 *km* with 0.3 *J/m* or with 3 *kJ* per pulse total for the 10 *km*. For lower energy the laser power is proportionally lower.

As it was mentioned the laser amplifier could be sectioned, Fig.5.6. So for 1 *km*, the total output power of the laser must be within 0.5 *MW* with repetition rate about 160 *Hz* for $\lambda_{ac} \cong 1\mu m$.

Nd-Glass lasers can be used here. For pumping the driving lasers the *diode laser arrays* could be used for the wavelengths indicated. This brings efficiency of the laser up to 10% level. This type of laser is probably the mostly powerful.

CO_2 laser based system gives lower final energy, but the total power required for 1 *km* is $P_i \cong Q/\tau \approx 3\cdot 10^{12} W$. within routinely obtained. With 10*m* sectioning the power required from one stage of the laser amplifier goes to $P_i \cong Q/\tau \approx 3\cdot 10^{10} W$ with total energy 3*J*. For pumping the laser on CO_2, the electron beam with ultraviolet flush is used. In [2.7] one can find the ways to enlarge the bandwidth by using isotopes mixture.

In *visible light the Nd:YAG* lasers working at doubled frequency are the best for application. The accelerating structure engineering and low emittance source adequate to this wavelength come to the edge of the present day technological possibilities however.

Lasers for the TLF method need to operate in intermediate time duration $\tau \approx 100 ps$. Equivalent time of illumination of any point on accelerating structure with TLF still however, very short – $0.1 \div 1 ps$ *only for* $\lambda_{ac} \cong 1 \div 10 \mu m$ *respectively*.

We would like to stress here, that the TLF method allows reaching the field limit with the lowest energy of laser source. TLF method allows a drastic reduction of illuminating time also.

9. BUNCH POPULATION

In Chapter 4 some energertics was considered from the language of wake potentials. Here we summarize these considerations. First let us make some simple physical estimations. The energy, accepted from the field by N particles is $W_a \cong eNE_m gI(g)$ where e is the charge of a particle, $I(g)$ is a function of the order of unity –an analog of the transit time factor, see (7.3). The share of the energy will be

$$\eta W \cong \eta \frac{Q\lambda}{2c\tau} \cong eNgI(g)\sqrt{\frac{Q}{\varepsilon_0 c\tau\lambda g}} \quad . \tag{9.1}$$

Last relation emerges

$$N \cong \frac{\eta}{2eI(g)}\sqrt{\frac{\varepsilon_0\lambda^3 Q}{c\tau\, g}} \, . \tag{9.2}$$

With $I(g)$= 0.5, $\eta \approx 0.05$ (i.e. only 5% of the energy stored in one cell carried out by the bunch), this yields $N \cong 1\cdot 10^6$ for $\lambda_{ac} \cong 1\mu m$. For $\lambda_{ac} \cong 10\mu m$ this number will be $N \cong 3\cdot 10^7$. One can compare the value $\eta \cong 5\%$ with what obtained from direct calculations of wake fields in Section 4 (7.5% for one particular structure). This means that our simple estimation is good enough.

Optimal length of the bunch.

Accelerating voltage in a cell near voltage crest can be expanded as the following

$$V(s) = V_0 Cos(2\pi s/\lambda) \cong V_0 \cdot (1 - \frac{1}{2}\frac{4\pi^2 s^2}{\lambda^2}) \, , \tag{9.3}$$

where the distance s is calculated from the crest, V_0- is unloaded voltage across the cell. The Wake Field, induced in the cell, changes the resulting accelerating voltage as it is shown in Fig. 4.4. We can use here analytical expression for the wake [9.1] and approximate the curve in Fig.4.4 analytically as

$$\Delta V(s) \cong \frac{eNZ_0 c}{(2\pi)^{3/2}\sigma_b}\ln\left(\frac{2g}{\delta}\right)\exp\left(-\frac{s^2}{2\sigma_b^2}\right) \approx \frac{eNZ_0 c}{(2\pi)^{3/2}\sigma_b}\ln\left(\frac{2g}{\delta}\right)\left(1-\frac{s^2}{2\sigma_b^2}\right)[Volt], \tag{9.4}$$

where N is the number of the particles in the bunch, g and δ indicated in Fig. 4.1, $Z_0 = 120\pi\Omega$, σ_b is the sigma of the bunch. This formula is valid in case, when $\sigma_b \approx \delta$. For other, than this ratio, additional factor of the order of unity could be introduced here. We define the equilibrium length σ_{b0} as a one, which gives the *flat* resulting top of the effective voltage [9.3]. Equating the terms ~s^2 in (9.4) and (9.3)

$$\frac{eNZ_0 c}{(2\pi)^{3/2}\sigma_{b0}}\ln\left(\frac{2g}{\delta}\right)\left(\frac{s^2}{2\sigma_{b0}^2}\right) \cong V_0\left(\frac{2\pi^2 s^2}{\lambda^2}\right) \tag{9.5}.$$

one can obtain

$$\sigma_{b0}^3 \approx \frac{eNZ_0 c\lambda^2}{(2\pi)^{3/2}4\pi^2 V_0}\ln\left(\frac{2g}{\delta}\right). \tag{9.6}$$

Substitute here $N \cong 10^7$, $g \cong 5\mu m$, $\delta \cong \sigma_b \cong 0.2\mu m$, $\lambda \equiv 10\mu m$, V_0~ 30 *kV* we obtain $\sigma_{b0}^3 \approx 23.5 \cdot 10^{-12} cm$, and $\sigma_{b0} \approx 2.86\mu m$. Namely this length gives flat resulting acceleration voltage along the bunch and could considered as optimal for acceleration with laser wavelength $\lambda = 10\mu m$. Smaller bunch population decreases the optimal bunch length, but dependence, as it could be seen from (4.4) is weak, $\sim \sqrt[3]{N/V_0}$.
For $\lambda \equiv 1\mu m$, the factor g/δ is the same, $N \cong 10^6$, V_0~ 300 *kV*, and formula (4.4) gives $\sigma_{b0} \approx 0.13\mu m$. These figures look reasonable. If the final energy of the beam is E_f, repetition rate *f Hz*, then the total energy, caring by these particles *per second* is $\dot{E}_t \cong eNE_f f$. Substitute here *f* =160 *Hz*, E_f =300 *GeV*, we obtain $\dot{E}_t \cong eNEf \approx 16 J/\sec$, or 16 *W*. As we suggested the efficiency about 10%, the power of the laser must be at least 160 *W* for 160 *Hz* repetition rate. The impulse power of the laser is $P_i \cong Q/\tau$ and we have $P_i \approx 10^8 W$ what is far below the limit achieved.

10. FINAL FOCUS

First let us consider some effects of synchrotron radiation in final focus lens, affecting the beam properties in interaction point (IP). Consideration of emittance growth in final lens was done in [10.1]. In [10.2] similar considerations done on fundamental basis for the bunch with arbitrary transverse dimensions. Some comments also done there about emittance growth in doublet of final lenses, as the beam needs to be focused in both directions. Calculations done in [10.1], [10.2] are valid for a single particle, or with other words, when radiated fields do not interfere. Here we made our consideration of the subject attracting simple physical meaning.
For realization the high luminosity the envelope function $\beta*$ in the interaction point must be of the bunch length value, what is about $0.1 \div 1\lambda_{ac}$, i.e. $\sigma_l \approx \beta^* \cong 0.5\mu m$. The envelope function value at the distance s from the interaction point will be, hence as big as

$$\beta \cong \beta^* + \frac{s^2}{\beta^*} \cong \frac{s^2}{\beta^*}, \tag{10.1}$$

where we neglected the focusing, arising from the incoming bunch, see Chapter 11. With such an envelope function, the transverse dimension $\sigma_{\perp max}$ will be of the order

$$\sigma_{\perp\max} \cong \sqrt{(\gamma\varepsilon)\beta/\gamma} \cong \sqrt{(\gamma\varepsilon)\frac{s^2}{\gamma\beta^*}} = \sqrt{\frac{(\gamma\varepsilon)}{\gamma\beta^*}} \cdot s\,. \tag{10.2}$$

The last is, simply, an angular divergence at IP multiplied by the distance.
For emittance we can take a value estimated on the basis of (6.10), $(\gamma\varepsilon_x) \cong 1 \cdot 10^{-8}\ cm \cdot rad$, what gives for energy $E \cong 1 TeV$ ($\gamma \cong 2 \cdot 10^6$) the transverse dimension $\sigma_{\perp\max} \cong 0.1\mu\ m$ for s= 1 *cm*. The angle, given to the particle by the field of the lens, must be of the order of the natural angular spread in the focal point,

$\sqrt{(\gamma\,\varepsilon)/\gamma\beta^*} \cong G\cdot\sigma_{\perp\max}L_F\,/\,(HR)$, where L_F and G are the length of the final lens and it's gradient, respectively, and $(HR) = pc/e$ is a magnet rigidity of the particle. Then one can obtain

$$H_\perp \cong G\sigma_{\perp\max} \cong \frac{(HR)}{FL_F}\sqrt{\frac{(\gamma\,\varepsilon)}{\gamma\,\beta^*}}s = \frac{(HR)}{L_F}\sqrt{\frac{(\gamma\,\varepsilon)}{\gamma\,\beta^*}}\,, \tag{10.3}$$

where we suggested, that the distance s is of the order of focal, $s \cong F$. The radiation formation length (length of coherence) for characteristic frequency is

$$l_F \cong \rho/\gamma = L_F \Bigg/ \left(\gamma\cdot\sqrt{\frac{(\gamma\varepsilon)}{\gamma\,\beta^*}}\right), \tag{10.4}$$

where $\rho \cong (HR)/H_\perp \cong L_F/\sqrt{\varepsilon/\beta^*}$ is the bending radius in the field of the lens. So the number of the radiated photons will be

$$N_\gamma \cong \frac{\alpha L_F}{l_F} = \alpha\cdot\gamma\cdot\sqrt{\frac{(\gamma\varepsilon)}{\gamma\beta^*}}\,, \tag{10.5}$$

where $\alpha = e^2/\hbar c$ –is the fine structure constant. As the critical photon energy is $\hbar\omega_{cr} \cong \frac{3}{2}\hbar\frac{c}{\rho}\gamma^3$, the total energy, radiated by single particle will be

$$\Delta E \cong \hbar\omega_{cr}\cdot N_\gamma = \frac{3}{2}\hbar\alpha\frac{c\cdot\sqrt{\varepsilon/\beta^*}}{L_F}\gamma\cdot\sqrt{\frac{\varepsilon}{\beta^*}}\cdot\gamma^3 = \frac{3}{2}\frac{e^2}{L_F}\gamma^4\frac{\varepsilon}{\beta^*} = \frac{3}{2}mc^2\gamma^3\frac{r_0}{L_F}\frac{(\gamma\varepsilon)}{\beta^*}\,, \tag{10.6}$$

and the energy difference between the central particle and the particle at the boundary of the bunch will be

$$\frac{\Delta E}{E} \cong \frac{3}{2}\gamma^2\frac{(\gamma\varepsilon)}{\beta^*}\frac{r_0}{L_F}\,. \tag{10.7}$$

From the other hand, variation of the focal distance due to the energy variation is

$$\Delta F \approx -F\frac{\Delta E}{E} \cong -\frac{(HR)}{GL_F}\frac{3}{2}\gamma^3\frac{\varepsilon}{\beta^*}\frac{r_0}{L_F}\,. \tag{10.8}$$

If we suggest that the focal distance is of the order of the length of the final lens, $F \approx L_F$, we came to final formula for the shift of focal point, what is basically the same as the *lengthening* of the bunch

$$\Delta F \approx -\tfrac{3}{2}\cdot r_0\gamma^2\frac{(\gamma\,\varepsilon)}{\beta^*}\,. \tag{10.9}$$

As it could be seen from here, the lengthening does not depend on the final length parameters ($\gamma \cong 2\cdot 10^6$). For the parameters under discussion, $|\Delta F| \approx 3.4\cdot 10^{-4}cm$, i.e. thirty five times the length of the bunch, which is $0.1\mu m$ for $\lambda_{ac} = 1\mu m$. For $\lambda_{ac} = 10\mu m$ this lengthening is comparable with the bunch length. So we came to conclusion [2.4], that the final focus for laser driven linac could not be arranged with help of single lens (or either a doublet) in case of focusing to the β^* required. This is due to lengthening of the bunch, not due to the emittance growth, although these values could be expressed one through other. The energy spread at IP arising from radiation could be estimated as the following

$$\delta(\Delta E) \cong \hbar\omega_{cr} \cdot \sqrt{N_\gamma} \approx \hbar \frac{c}{L_F} \gamma^3 \sqrt{\alpha\gamma} \cdot \left(\sqrt{\frac{\varepsilon}{\beta^*}} \right)^{3/2} \qquad (10.10).$$

In all consideration above we did not use any peculiarity, what the radiation might have in *quadrupole lens*. With other words, all estimations made above are valid for a single particle only. Let us consider if it isn't so. Formula (10.4) for the length of formation could be rewritten as the following

$$l_F \cong \rho/\gamma = L_F \Big/ \left(\gamma \cdot \sqrt{\frac{(\gamma\varepsilon)}{\gamma\beta^*}} \right) \cong \frac{L_F \beta^*}{\gamma\sigma_\perp^*}, \qquad (10.11)$$

where $\sigma_\perp^* \cong \sqrt{(\gamma\varepsilon)\beta^*/\gamma}$ –is the beam size at IP. The wavelength, corresponding to the critical frequency in magnetic field for the boundary particle is

$$\lambda_{cr} \cong 2\pi c/\omega_{cr} \cong \frac{4\pi\rho}{3\gamma^3} = \frac{4\pi L_F \beta^*}{3\gamma^3 \sigma_\perp^*}. \qquad (10.12)$$

Formula (10.12) yields the transverse size of coherence as

$$\sigma_\perp^{coh} \cong \sqrt{\lambda_{cr} l_F} \cong \frac{2 L_F \beta^*}{\sigma_\perp^* \gamma^2}. \qquad (10.13)$$

The ratio $\sigma_\perp^{coh}/\sigma_\perp^{lens}$ is a measure of involvement of neighboring particles in the formation of radiation. The transverse size of the bunch in the lens could be approximated as

$$\sigma_\perp^{lens} \cong \sqrt{\frac{\gamma\varepsilon}{\gamma}\beta^*(1+\frac{L_F^2}{\beta^{*2}})} \cong \sigma_\perp^* \frac{L_F}{\beta^*}, \qquad (10.14)$$

where we suggested again, that $F \cong L_F$. Substitute the last expression into (10.13) one can obtain

$$\sigma_\perp^{coh}/\sigma_\perp^{lens} \cong \frac{2L_F\beta^*}{\sigma_\perp^*\gamma^2}\frac{\beta^*}{\sigma_\perp^* L_F} = 2\frac{\beta^{*2}}{\sigma_\perp^{*2}\gamma^2} = 2\frac{\beta^*}{(\gamma\varepsilon)\gamma} = \frac{2}{< x'^{*2} > \gamma^2}, \qquad (10.15)$$

where $< x'^{*2} >$ is averaged square of angular spread at IP. For the parameters under discussion, $(\gamma\varepsilon_x) \cong 1\cdot 10^{-8} cm\cdot rad$, $\beta^* \cong 0.5\mu m$, estimation with (10.15) gives formally, $\sigma_\perp^{coh}/\sigma_\perp^{lens} \cong 2.5 10^{-3}$, what means that the radiation in transverse cross-section is not coherent for peripheral particles and estimations are valid.

We suggested an arrangement of the final focusing for our purposes as *a multiplet* of FODO structures. The number of the lenses in such a multiplet is around a few hundreds [2.4]. This is so called ***Adiabatic Final Focus***. The gradient in these lenses must vary from the very strong at the side closest to IP, to a weak one at opposite side. Focusing properties of the RF lens, discussed above can be used here. A laser radiation of general and multiple frequency can be used for such focusing.

The laser radiation, phased with the main driving one can excite the single groove directly from the side. The quadrupole parameter described by (7.4). Substitute here $\lambda = 10\mu m$, $\gamma = 2\cdot 10^6$ (pc=1TeV), $w \approx 5\mu m$, $E_m \approx 10^{11}V/m$, we obtain $k_x \approx 4\cdot 10^4 \cdot Sin\varphi\,[m^{-2}]$. For $\varphi = \pi/2$ this expression has a maximum, this means, that the lenses are phased for the focusing only. The variation of the focusing strength has a quadratic dependence with the deviation ψ from the angle $\varphi = \pi/2$, $k_x \approx Cos\psi$. For the longitudinal length of the grove about $g \cong 5\mu m$, the focal distance will be

$$F \cong 1/kg \cong 1/4\cdot 10^4 5\cdot 10^{-6} = 5\ [Meters/cell]. \qquad (10.16)$$

Equivalent gradient of the quadrupole lens is $G \cong 0.3pk \cong 1.2\cdot 10^7 kGs/cm$. So the lens with ≈ 500 cells having the length $L_F \cong 0.5cm$ reaches the focal length $F \approx 1\ cm$.

For flattering the longitudinal dependence of the gradient (elimination the quadratic term in $k_x \approx Cos\varphi$ as a function of φ, see (7.4)), one can use the *second and higher harmonics* of the laser radiation, excited an additional groove, placed on the beam trajectory close to the first groove. For phasing, the highest harmonics can be generated by *multiplying* the frequency in nonlinear crystal. As initial, the splitted radiation from the general source (see Fig.15.3) can be used both for driving the first harmonic grove and, after doubling, the second one. For arranging a doublet of the focusing lenses, one can use the phase shift between the RF crest and the beam $\varphi = -\pi/2$. Such a tiny lens, not sensitive to detector magnetic field can be easily installed inside the detector very close to the Interaction Point.

11. LUMINOSITY

Since the linear collider technique was proposed firstly in [11.1], the question about luminosity for single pass collisions (in contrast to circular machines with multi-pass collisions during particle's lifetime) is the general one. Usual formula for luminosity stands that $L = N^2 f/4\pi\sigma_x\sigma_y$ [11.2], where f –is a repetition rate, $\sigma_{x,y}$ are the Gaussian widths for x and y directions respectively. Expressed through emittances and envelope functions it comes to

$$L \cong \frac{N^2 fH_B\gamma\cdot N_B}{4\sqrt{(\gamma\varepsilon_x)(\gamma\varepsilon_y)\cdot\beta_x\beta_y}}\ , \qquad (11.1)$$

where H_B – is the enhancement parameter. N_B –is the number of bunches per train. For emittances from (6.10a), (6.11a) $\gamma\varepsilon_x \cong 2.5\cdot 10^{-8} cm\cdot rad$, $\gamma\varepsilon_x \cong 9.5\cdot 10^{-10} cm\cdot rad$ and for $\beta_x \approx \beta_y \approx 0.3\lambda_{ac}$, $\lambda_{ac} \cong 10\mu m$, $\gamma = 6\cdot 10^6$ (pc=3TeV), $N \cong 10^7$, $f \cong 160Hz$, H_B=1, N_B=*1*,

$$L \approx 1.7\cdot 10^{34} cm^{-2}s^{-1}.$$

It was suggested (see comments to the (6.10a), (611a)), that the emittances could be decreased even more than we used here by a factor 10 each by decreasing the envelope function in a cooler and decreasing the magnetic field in the wigglers. This could be considered as a safety reserve and could be used in future improvements.

For $\lambda_{ac} \cong 1\mu m$ result will be about the same as the number of the particles is lower here. The transverse Gaussian size will be

$$\sigma_x \cong \sqrt{(\gamma\varepsilon_x)\beta_x{}^*/\pi\gamma} \cong \sqrt{2.5\cdot 10^{-8}\cdot 3\cdot 10^{-4}/2\cdot 10^6/\pi} \cong 1.1\cdot 10^{-9}cm\ (\equiv 0.11\overset{o}{A}) \qquad (11.2a)$$

$$\sigma_y \cong \sqrt{(\gamma\varepsilon_y)\beta^*/\pi\gamma} \cong \sqrt{9.5\cdot 10^{-10}\cdot 3\cdot 10^{-4}/2\cdot 10^6/\pi} \cong 2.2\cdot 10^{-10}cm\ (\equiv 0.022\overset{o}{A}). \qquad (11.2b)$$

So the aspect ratio in this case is about $\sigma_x/\sigma_y \cong 5$, what looks reasonable.

Effective longitudinal distance between the particles has the order $l_b/N \approx \lambda/N$. The last number in our case is formally $\leq 10^{-11}cm$. As the distance $\approx \lambda\!\!\!{}^{-}_C \cong 3.8\cdot 10^{-11}cm$ is absolute limit for such spacing, we conclude that in each transverse slice $\approx \lambda\!\!\!{}^{-}_C$ the number of the particles $\approx 1-2$. The dimension (11.2) formally corresponds to ≈ 2 particles per slice in cross section.

In (10.14) we suggested that the envelope function enlarge like in free space. This suggestion was acceptable there. More exactly, however, the incoming bunch looks like extremely powerful lens, as the effective focusing parameter $K_F \equiv eG/pc$ could be estimated from the gradient

$$G_y = \frac{\partial H_x}{\partial y} \cong \frac{eNc}{2(\sigma_x^* + \sigma_y^*)\sigma_x^*\sigma_b}, \qquad (11.3)$$

as the following

$$K_F \cong \frac{eG}{pc} \cong \frac{e^2N}{2mc^2\gamma\sigma_\perp^{*2}\sigma_b} \approx \frac{r_0N}{2\gamma\sigma_\perp^{*2}\sigma_b}\ . \qquad (11.4)$$

We would like to mention here, that in a presence of the charge, the gradients of *x* and *y* components of magnetic field does not have an opposite sign, like it is in a vacuum ($\partial H_y/\partial x = -\partial H_x/\partial y$ as a sequence of $\vec{\nabla}\times\vec{H} = 0$). Indeed in the presence of a charge, $\partial H_y/\partial x = \partial H_x/\partial y$. Or with other words, the oppositely moving and oppositely charged bunch *focuses* in both directions.

The last formula gives formally $K_F \cong 6\cdot 10^8 1/cm^2$. So in formula for envelope function [13.2]

$$2\beta\beta''(s) - \beta'^2 + 4\beta^2K_F = 4, \qquad (11.5)$$

the last term could not be simply eliminated. Let us estimate the order of the terms. First of all the derivative in longitudinal direction could be estimated as $\beta' = \partial\beta/\partial s \approx \beta/\sigma_b \approx 1$ at the entrance into collision region, $\beta\beta'' = \beta\partial^2\beta/\partial s^2 \approx \beta^2/\sigma_b^2 \approx 1$ and $4\beta^2K_F \approx 4\sigma_b^2\cdot 6\cdot 10^8 \cong 4\cdot 10^{-10}\cdot 6\cdot 10^8 = 0.24$. So the input of the focusing term is noticeable.

First of all the envelope function could be not a symmetric function as it is in circular machines. Moreover it is direction dependent as the incoming beam focusing properties

are taken into account. Some optimization is possible. On Fig.11.1 there is represented some qualitative behavior of the envelope function, obtained with computer modeling.
By number 1 there is marked an envelope function behavior with K_F =0 in (11.5). This is a parabola, described by (10.1). The curve 2 describes the same initial conditions far from IP. Additional lowering behind the IP associated with additional focusing by the incoming bunch. The curve 3 describes the envelope function for incoming from the left bunch with slightly shifted crossover point to the left.

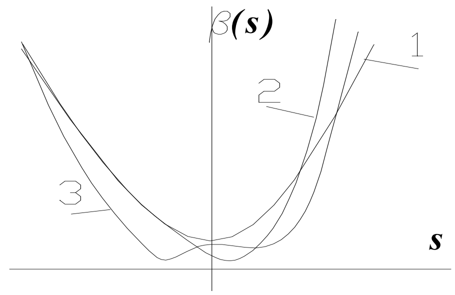

FIGURE 11.1: The envelope function behavior. 1 – corresponds to $K_F \cong 0$ or weak incoming bunch, 2 – corresponds to the same initial conditions as 1 but K_F is big, 3 –corresponds to the changed initial conditions, so the crossover shifted to the left. All envelope functions shown for the bunch moving from the left to the right.

It yields a flattering of envelope function at IP, so some enlargement of the bunch length compared to optimum $\beta^* \approx \sigma_b$ is possible here. One can suggest using a controllable variation of the focal pint for head and tail particles to use the field of incoming bunch for flattering the effective envelope function at IP. Simplest possibility to do this in arrangement a phase shift in the focusing RF lenses so that the head and tail particles are focused in slightly different places. Tails particles are focused before idealized IP (corresponding to zero charge effects), head particles are focused beyond IP. Fig. 7.2 gives an example of such phase shift arrangements. As the bunch position is strictly linked to the accelerating phase, is easy to arrange controllable variation of the focusing along the bunch. Other possibility proposed for *cm* wavelength colliders, consist on utilization of the chromaticity of final lens and controllable difference in energy of head and tail particle [11.5]. Tail particles must have lower energy in this method and IP must have nonzero dispersion, what makes this method less attractive. Indeed, our method does not require this and could be recommended for *cm* –wavelength colliders also. For this an accelerating structure with standing wave or with travelling wave structure with non-round passing holes should be properly phased and installed around final lenses of IP.
The conditions for coherency in radiation in the field of incoming bunch will be checked in the next Chapter.
Using a *train* of bunches (up to 10, see below) one can decrease the number of the particles in each bunch and/or to increase the cross section of the beam, thereby allow some reasonable losses.

A small *crossing angle* [11.1] required for prevention of irradiation of the final lenses by used beams. This angle is absolutely necessary for multi- bunch operational mode. Tiny dimensions of the beam can help to push the beams through.
Notice here that total length for acceleration up to 300 *GeV* could be about twenty meters, taking into account that a fraction of the accelerating sections is of the order 50%. As the total energy of the full energy accelerator will be around *1 J*, what gives the average power of the order 160 *W*.
The beams of electrons and positrons could be polarized what gives the effective gain in luminosity and reduces the background [11.3, 11.4]. The possibility of operation with high repetition rate, up to *few kHz* is favorable, see papers represented at Conference mentioned in [8.1].

12. INTERACTION POINT

Let us begin with formal estimations valid for the radiation in the field of incoming bunch. The conditions, considered in Chapter 6 for diluted beam (6.26), must be satisfied here, so the field could be considered as a coherent one. Formally, for dimension (11.2) one can expect significant energy losses by synchrotron radiation in the interaction point. The Y_0 parameter which characterizes the radiation is

$$Y_0 \equiv \frac{2}{3}\frac{\hbar\omega_c}{E} = \gamma\frac{H}{H_c}, \tag{12.1}$$

where H is the magnetic field, $H_c = m^2c^3/e\hbar \cong 4.4\cdot10^{13}\ G$ is the Schwinger critical field strength, ω_c is the critical frequency of classical synchrotron radiation. This parameter is a function of position inside the bunch. In our case magnetic field value H_0 in the longitudinal center of the bunch at its boundary can be estimated

$$H_0 \cong \frac{4\pi}{c}\frac{eNc}{2\pi\sigma_x\sigma_b} \approx 2.8\cdot10^{10}\ G, \tag{12.2}$$

so even for E =300 GeV , $\gamma \cong 6\cdot10^5$, $Y_0 \cong 760$. It was taken into account, that the electrical field of incoming beam doubles the Y_0 value. Thus the radiation is in a strong quantum regime. Energy losses for *Gaussian* bunch estimated in [12.1]. For uniform transverse and Gaussian longitudinal distributions the Y parameter was represented as $Y = Y_0\rho_\perp exp(-\varsigma^2/2)$, where Y_0 calculated for the maximal field in the center of the bunch,
$\rho_\perp = r/\sigma_\perp$, $\varsigma = z/\sigma_b$ are normalized coordinates. The normalized to the bunch length formation length defined

$$l_F \cong l_{0F}\cdot\rho^{2/3}e^{\zeta^{2/3}} \cong \left(\frac{3}{2}\right)^{1/3}\frac{\lambda\!\!\!^{-}_C\gamma}{Y_0^{2/3}\cdot\sigma_b}\cdot\rho^{2/3}e^{-\zeta^{2/3}} = \left(\frac{3}{2}\right)^{1/3}\frac{\Gamma_0}{Y_0^{2/3}}\cdot\rho^{-2/3}e^{\zeta^{2/3}}, \tag{12.3}$$

where $\Gamma_0 = \lambda\!\!\!^{-}_C\gamma/\sigma_l$.
The average fractional energy losses for strong quantum regime $Y_0 \gg 1$, described by Sokolov-Ternov formula, see [12.2]

$$\varepsilon_E = \frac{\Delta E}{E} = \frac{16\cdot\Gamma(2/3)\cdot 3^{2/3}}{243}\cdot\alpha\cdot\frac{Y_0^{\;2/3}}{\Gamma_0}\langle\rho_\perp\rangle^{2/3}\int_{-\infty}^{+\infty}\exp(-\varsigma^2/3)d\varsigma \approx \alpha/<l_F>, \quad (12.4)$$

what has clear physical sense, that at the length of formation $\approx\alpha$ photons are radiated. For $Y_0 << 1$, the critical energy is, as usual, $\hbar c\gamma^3/\rho \cong \hbar eH\gamma^3/pc$. For $Y_0 >> 1$, the critical energy goes to $\sim mc^2H_c/H \cong mc^2\gamma/Y_0$ [12.2]. The number of radiated photons goes to $N_\gamma \cong \alpha/l_F$. As each photon carries energy about critical one, the energy lost by one electron goes to $\Delta E \cong E_c N_\gamma = \alpha mc^2\gamma\sigma_b/Y_0$. The last expression yields (12.4). For the parameters discussed above, $\Gamma_0 \cong 2.3$. Substitute the figures in (12.3) one can obtain that $l_{0F} \approx 0.0044$ so on the length of the bunch, a few photons with characteristic energy are radiated. The last one for *E* =300 *GeV*, $Y_0 \cong 760$, goes to ~390 *MeV*.

In [12.3] the interaction of the beams with the parameters $\sigma_l \cong 0.4\mu m$, $\sigma_\perp \cong 2.5\overset{\circ}{A}$, $N \cong 1.2\cdot 10^8$ was considered. In their case Y_0 =5094. The quantum beamstrahlung average fractional energy loss was found around 10% for the beam with energy 5 *TeV*. The calculations made for non-coherent radiation of single particle in the field of incoming bunch (validity of such approximation discussed lower). In out case the number of the particles is 10^{-2} of considered there, but the cross section is 10^2 times smaller. So the peak magnetic field is about the same. The radiation processes required more detailed considerations, however.

So formally the radiation is going in very strong quantum regime and models with coherent field might not be applicable here as the bunch is diluted. Strong reduction of radiation one can expect due to Landau-Pomeranchuk effect, see in [12.4]. The radiation processes required more detailed considerations, however.

As the number of the particles in the bunch is about ~10^6 only, the background effects are much lower here, than for any linear collider under consideration [6.1].

In addition to background arising from synchrotron radiation on incoming bunch, the other sources are – radiation from scattering on the residual atoms due to vacuum conditions, scattering on thermal photons, a halo due to limited aperture, direct scattering on residual atoms.

At room temperature the density of photons is $n_\gamma \cong 5.3\cdot 10^{14} 1/m^3$. Taking into account that the cross section of interaction is $\sigma_\gamma \cong \frac{8}{3}\pi r_0^2 \cong 0.665\cdot 10^{-24} cm^2$, the scattering length goes to $l_\gamma \cong 1/n_\gamma\sigma_\gamma \cong 2.86\cdot 10^{15} cm$. So this effect is not important here. For estimation of radiation losses on residual atoms, one can estimate the scattering length for the residual pressure 10^{-9} *Torr* as $l_s \cong N_A X_0/N_r A \cong 5\cdot 10^{15} cm$, where X_0 –is a radiation length, N_A–is the Avohadro number. This effect is also negligible.

The emittance growth due to multiple scattering could be estimated as $\Delta\varepsilon \cong \beta < \vartheta^2 > \cong \beta\cdot 13.6^2[MeV]L_c/X_0/(pc)^2$, where L_c is a characteristic distance, which is under interest. We can estimate it as a fraction of the accelerator. Taking into account, that the X_0 for air at atmospheric pressure is about 300*m*, and hence, at 10^{-9} *Torr* it will be about $X_0^{Torr} \sim 3 \cdot 10^8 m$, for $pc = 1TeV \equiv 10^6 MeV$, $\beta \cong 1cm$, L_c~100m, the emittance perturbation goes to $\Delta\varepsilon \cong \beta < \vartheta^2 > \cong 5.6 \cdot 10^{-15} cm$. Even for beginning of accelerator the effect is negligible also.

Radiation from interaction region.

Let us examine the conditions for radiation from IP. The formation length for the boundary particles goes to $l_F \cong \dfrac{\lambda\!\!\!^{-}_C \gamma}{Y_0^{2/3} \sigma_b}$. As the critical frequency of radiated photons goes to $\omega_c \cong mc^2\gamma / Y_0\hbar$, the corresponding wavelength goes to $\lambda\!\!\!^{-}_{cr} \cong c/\omega_c = cY_0\hbar / mc^2\gamma$. So the transverse size of coherence goes to $\sigma_\perp^{coh} \cong \sqrt{\lambda\!\!\!^{-}_{cr} l_F \sigma_b} = \sqrt{\dfrac{cY_0\hbar}{mc^2\gamma} \dfrac{\lambda\!\!\!^{-}_C \gamma}{Y_0^{2/3}}} = Y_0^{1/6} \lambda\!\!\!^{-}_C \sim$ $3\lambda\!\!\!^{-}_C \cong 1.15 \cdot 10^{-10} cm$. The transverse dimensions of the bunch at IP, according to estimations (12.2a,b) are $\sigma_x \cong 1.1 \cdot 10^{-9} cm$, $\sigma_y \cong 1.4 \cdot 10^{-10} cm$, what is about the size of coherence. So the radiation from the incoming bunch formally *could not* be described as a dipole radiation of a single particle in coherent field of oncoming bunch. . For the central zone of the bunch it is definitely so. In this case the particles on opposite vertical sides of the bunch have opposite accelerations. This yield opposite polarizations of electromagnetic fields, radiated by these oppositely located particles. In it's turn this yields a destructive interference of radiation in forward direction. So the resulting radiation looks like a quadrupole one, what is $\approx \frac{1}{120} \dddot{Q}^2 / \ddot{d}^2 / c^2$ times, where $\dddot{Q}$ is a third order derivative of quadrupole moment, lower is the rest frame. This type of radiation has zero intensity in forward direction. A remaining dipole part could be estimated as the following. Instead of magnetic field at the periphery, defined by the transverse size $\sigma_\perp \equiv \sigma_{x,y}$ the size $\sigma_\perp \equiv \sigma_{x,y} / \sqrt{N}$, where N –is a bunch population, needs to be taken for these estimations. The factor $\sqrt{N}$ reflects fluctuations of relative positions of the bunch's centroid. So the radiation is strongly suppressed here $\sim 1/N$. This is a peculiarity of a laser driven accelerator. More detailed analyses required however.

13. MULTI-BUNCH OPERATION MODE (UPGRADES)

In [13.1] was attracted attention, that the energy acquired by the bunch from electric field could be not more, that contains in a cylinder with the height equal to the size of field region along the bunch path and having the radius equal to the bunch length. This is a direct sequence of a causality principle. So to get more energy from the accelerating cell one need to increase the length of the bunch. To compensate the energy variation along the bunch in this case one need to increase the bunch population, so that wake fields flatten the effective energy gain. This is always a feature. This way we can call as acquiring the energy from the cavity by spontantenous radiation, including this in higher modes. Thus as the energy acquired from the field is high (high wakes), this regime is good for a single bunch acceleration. Other way is the energy acquisition from general mode by many weak bunches. The TLF method allows this regime also. This might be useful for reduction of the collision effects at IP.

As the length of the laser spot on the structure is $l_f \cong L / N_R$, what means that in principle, that the number of the bunches could reach

$$N_B \cong l_f / \lambda \cong L / N_R \lambda . \qquad (13.1)$$

Substitute here the numbers one can obtain $N_B \leq 300$ for $\lambda \cong 1\mu\ m$, and $N_B \leq 100$ for $\lambda \cong 10\mu\ m$. Of cause the real number of the bunches is less due to the raise/decrease finite time.

Using a train of bunches (up to 100, see above) one can decrease the number of the particles in each bunch and/or to increase the cross section of the beam, thereby allow some reasonable losses. The length of the laser spot at the structure is about $l_f \cong L / N_R$, what we estimated in section 9 as $l_f \approx 0.03 cm$ what is $\approx 30\lambda$ for $\lambda \cong 10\mu\, m$ and $\approx 300\lambda$ for $\lambda \cong 1\mu\, m$. As the $Q_{RF} \cong 9$ required, the bunch number could be up to 30. If collision arranged for few bunch per train, N_B, then the luminosity will get a gain factor up to 30 also. These factors will allow increasing the transverse cross section and reducing the problems with radiation at IP. The H_B value required detailed considerations.

Multi-bunch structure could be arranged in a damping ring, in principle, with FEL methods. Using a laser with the same wavelength as required by acceleration structure and a dipole wiggler with period $\lambda_W \cong \lambda \cdot 2\gamma^2 / (1+K^2)$, one could arrange an effective voltage $V \cong EKL_W / \gamma$, where E –is laser field strength. Then the bunching could go with usual autophasing regime. For example if $E \cong 1MV / cm$, $\gamma \approx 10^3$ (500 *MeV*), $L_W \approx 20m$, then effective voltage could reach $V \cong 2MV$. Harmonics number (see Chapter 7) could reach $q \approx \Pi / \lambda \approx 10^5 \div 10^6$, where Π –is perimeter of the cooler. This is equivalent to 2*GeV* of fundamental accelerating RF (q=*1*).

14. ALIGNMENT

If the accelerating section is tilted on angle $\Delta\vartheta$ then the particles obtain the transverse momenta $\sim \Delta p_\perp \cong \Delta p_\| \cdot \Delta\vartheta$, where $\Delta p_\|$ –is an energy gain per section. Let us find the highest allowable value for the angle $\Delta\vartheta$. Ratio of the random component of transverse momentum per stage $\Delta p_\perp$ to the *full* momenta $p_\|$ must be less if compared with angular spread in the beam

$$\frac{\Delta p_\perp}{p_\|} << \sqrt{\frac{(\gamma\varepsilon)}{\beta\gamma}} . \qquad (14.1)$$

Basically this is the same as a requirement that an increase of emittance must be small compared with the emittance itself. The increase of emittance could be represented as the following

$$\Delta\varepsilon \cong \beta(\Delta x')^2 \cong \beta(\frac{\Delta p_\perp}{p_\|})^2 << \beta\frac{\gamma\varepsilon}{\beta\gamma} = \varepsilon\,. \tag{14.2}$$

Substitute in (14.2) $\Delta p_\perp \cong \Delta p_\| \cdot \Delta\vartheta$, one can obtain

$$\beta(\Delta p_\| \;/\; p_\|)^2(\Delta\vartheta)^2 << \varepsilon \tag{14.3}$$

The last yields

$$(\Delta\vartheta)^2 \equiv (\frac{\Delta p_\perp}{\Delta p_\|})^2 << \frac{\varepsilon}{\beta}(\frac{p_\|}{\Delta p_\|})^2 \equiv \frac{\varepsilon}{\beta}(\frac{\gamma}{\Delta\gamma})^2 \equiv \frac{\gamma\varepsilon}{\gamma\beta}(\frac{\gamma}{\Delta\gamma})^2 \equiv (\Delta\vartheta)^2_{beam}(\frac{\gamma}{\Delta\gamma})^2, \tag{14.4}$$

where $(\Delta\vartheta)^2_{beam} \cong \gamma\varepsilon/\gamma\beta$ is a squared angular spread in the bunch. This estimation of angular tilt allowable is different from one represented in [14.1].

Substitute here extreme $\gamma\varepsilon_y \cong 2\cdot 10^{-9}\, cm\ rad$, $\gamma\varepsilon_x \cong 2.5\cdot 10^{-8}\, cm\ rad$, $\beta \cong 1\ cm$, $\gamma \cong 4000$ ($E \cong 2GeV$, at the beginning of acceleration), $\Delta\gamma \equiv 200$ for $\lambda_{ac} \cong 10\mu m$, $\Delta\gamma \equiv 2000$ for $\lambda_{ac} \cong 1\mu m$, and for the accelerating structure of 3 *cm* long one can obtain for $\lambda_{ac} \cong 10\mu m$ the allowable tilt of the order of

$$(\Delta\vartheta)^2_y << \frac{\gamma\varepsilon}{\gamma\beta}(\frac{\gamma}{\Delta\gamma})^2 = \frac{2\cdot 10^{-9}}{2\cdot 10^3}(\frac{4\cdot 10^3}{200})^2 = 4\cdot 10^{-10}, \text{ or } \quad \Delta\vartheta_y \cong 2\cdot 10^{-5}$$

$$(\Delta\vartheta)^2_x << \frac{\gamma\varepsilon}{\gamma\beta}(\frac{\gamma}{\Delta\gamma})^2 = \frac{2.5\cdot 10^{-8}}{2\cdot 10^3}(\frac{4\cdot 10^3}{200})^2 = 5\cdot 10^{-9}, \text{ or } \quad \Delta\vartheta_x \cong 7\cdot 10^{-4}$$

For $\lambda_{ac} \cong 1\mu m$ these numbers is ten times less. These numbers yield that the ends of 3*cm* Long structure must be aligned better that 0.6 micrometers for vertical and 21 micrometers for radial directions.

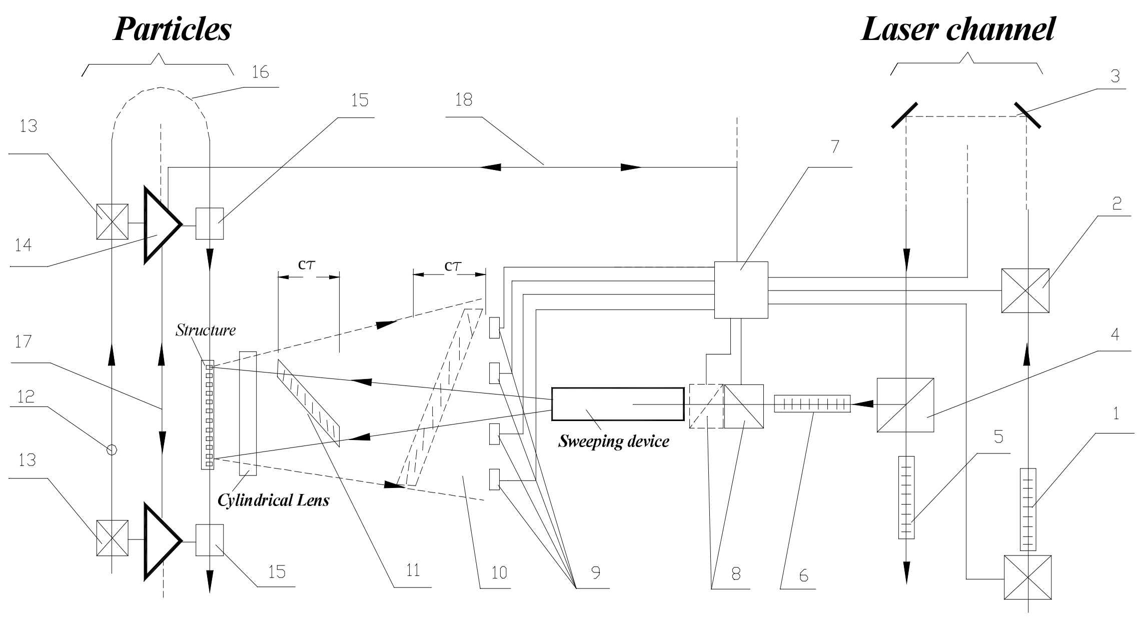

FIGURE 14.1: Schematic view on the feedback system fragment. On the right the optical part and on the

left the beam part represented respectively. 1–is a driving laser bunch, 2–is transverse position sensor for a laser bunch, 3–is a laser back reflector loop, 4 –is a power splitter, 5–is a driving bunch on the way to next module, 6–is a splitted part of driving laser bunch, 7–is a processor, 8–are the beam deflectors for two transverse directions, 9–is an array of optical sensors, 10–is a reflected laser bunch, 11–is a sweeped laser bunch. 12–is an electron/positron bunch on the way to the beginning of accelerator. 13–are the pick up electrodes, 14–is a functional amplifier, 15–is a transverse kickers, 16–is a beam back returning loop, 17,18 –are the lines of the signal processed. Lines across the laser bunch indicate the wavefronts. The back loop 3 located at the beginning of accelerator (acceleration process).

Alignment *in situ* is going with the help of radiation reflected from the structure. The $\Delta\vartheta$ can be expressed in terms of phase registered

$$\Delta\vartheta \cong \Delta\phi\lambda / L \cong \Delta\phi\lambda / L \cong \Delta\phi \cdot 10^{-3} / 3 = 3 \cdot 10^{-4} \Delta\phi \,, \qquad (14.3)$$

where $\Delta\phi$ –is the phase resolution in diffraction method. Compare the last expression with (14.1) one can conclude, that $\Delta\phi \cdot \lambda / L \leq \sqrt{(\gamma\varepsilon) / \beta\gamma}$ and required resolution is expected to be $\Delta\phi \cong 10^{-3}$, what is big enough to be registered.

The structure could be installed on the tables, moved by piezoelectric, see Fig.5.5. Adaptive optics principles could be used here as well. Basically, the radiation reflected from the structure will go back to the sweeping device, where it could be collected and processed. The feedback fragment is represented in Fig. 14.1. The principle of operation is rather clear. Basically the system has two loops for the accelerated particles and for the laser beam. For correction fluctuations of different nature the laser and particle are going along the accelerator back and forward. On one way the signals corresponding to the misalignments (optical and particle's) processed and applied to the laser and particle's bunch on the way back, when the laser bunch is going through the splitters and the particle's bunch through the accelerating structures. The necessary interchange of signals arranged between the optical and particle's feedback systems locally and along the accelerator to diminish the result of fluctuations.

Angle $\Delta\phi$ (14.3) could be resolved with the help of array 9. Using a holographic method with a dedicated laser beam it is possible to achieve angular resolution of the order 10^{-9} *rad*.

In [14.2] one can find a description of the sensors, transparent for infrared radiation. The equipment was used for alignment of chambers. A resolution better than $1\,\mu m$ at the distance ~20*m* is easily achievable with the semi-transparent silicon sensors at 30 points along one laser line. The resolution could be improved by adding special readout electronics. These sensors are available from industry [14.2]. These types of sensors could be used for preliminary alignment. These silicon strip sensors could be implemented into accelerating structure easily. The same ideas could be used for obtaining a feed back signal from the main laser beams during propagation to the end of accelerator. Further the signals after processing with necessary algorithms, could be used to drive a correctors, operated with electro optical elements, similar to what used in the sweeping devices. This is only one example of possibilities now open with micro technology.

15. GENERAL PICTURE

As the system deals with the extreme bunch's parameters, a lot of feedback elements pursuit the beam's fluctuations. So that is why we suggested that both beams, the laser and particle's bunch go first to the end of all linac apart from the central station. On the way forward the bunch's (both, optical and particle's) parameters picked up, processed with appropriate algorithms locally and applied to correcting elements (see previous Chapter).

Simplified view of such an assembly is represented in Fig. 15.1. All elements are placed in vacuumed volume, not shown in this Figure.

Primary laser beam 1 goes to the end of accelerator. Mirrors 2 redirect it back, pos.3, trough the sequence of splitters. In the similar way the particle's beam 5, goes trough bending system 6 and further trough structures to next modules, 4. 7 and 8 –are the focusing elements for the laser and particle's beam respectively. Optical platform 9 is standing on legs 10 with active damping system to minimize vibrations. 13–cylindrical lenses, 14–are the accelerating structures. All elements on the table are located in a vacuumed volume, not shown here.

The direction of the accelerating structures as indicated in Fig. 15.1 helps to run the elecron/positron bunch through the structures, as in horizontal plane the corresponding emittance is bigger. For ion/meson beams this advantage is not used.

Cross-section of a tunnel with accelerating system is shown in Fig. 15.2. All elements have a clear functional meaning, described in figure's capture. We supposed that the tunnel has a thermal stabilization of internal atmosphere. The duct 11 is a part of this system. A rack for control electronics and deflecting devices is shown as 8. Other elements, not marked in the capture are the water, vacuum and possible cryogenics ducts. Vacuumed tube 9 holds the Fresnel lenses for preliminary alignment (similar what used in SLAC [15.1]). The tunnel diameter shown is 3 *m*. For energy around 0.5×0.5 *GeV* the LLC could be preferably located on the surface, so any other shape is acceptable.

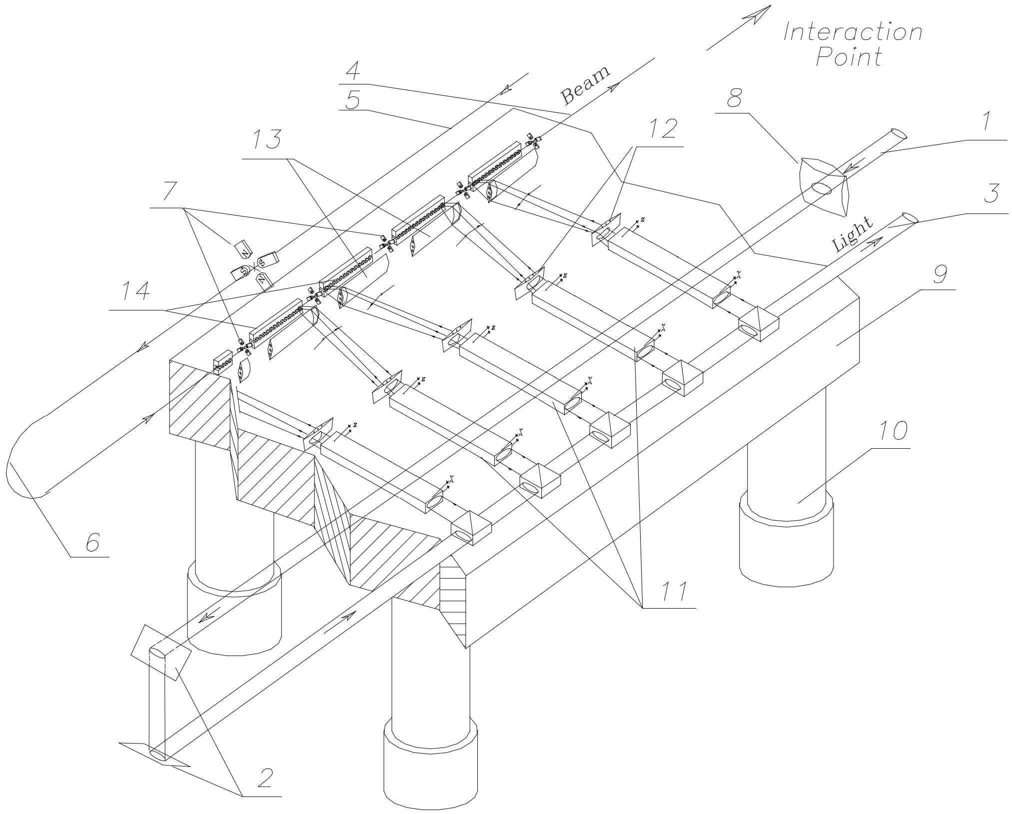

FIGURE 15.1: All elements from Fig.5.1 installed on a platform (9). The direction of largest emittance in damping ring (horizontal, if wigglers have vertical magnetic field) is now going along the passing slots in structure. This helps to keep emittance low during acceleration. Light means laser beam. Other comments are in the text.

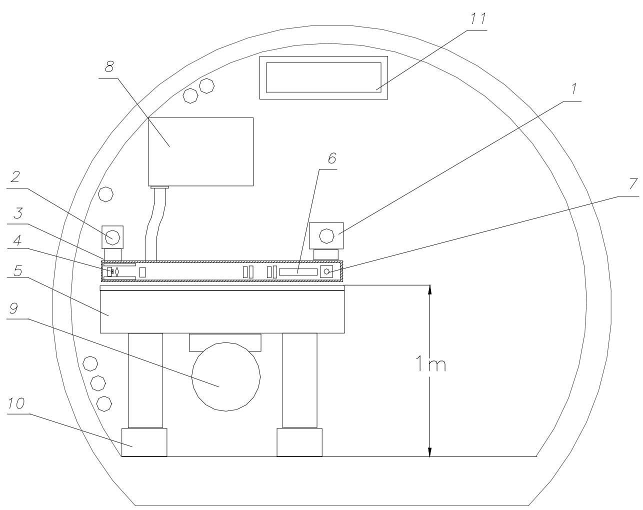

FIGURE 15.2 (color**):** Cross section of a tunnel with accelerating system for underground location. 1– is a primary optical beam line. 2–is a primary particle's beam line. 3–is a vacuumed container with all equipment. 4–is an accelerating structure with sub systems. 5–is an optical table. 6–is the deflecting device, 7 –is the line for driving optical beam, 8–is a box with equipment for deflecting device and control. 9–is a tube with optical elements for active alignment of all optical tables. 10–is an anti-vibration active system. 11–is a duct for air-conditioning.

General view of Linear Laser Collider (LLC) complex is represented in Fig.15.3. In figure's capture all sufficient elements are mentioned. What is important here –to keep all final elements at both sides on the same stabilized platform to avoid affectation by vibration. Positioning the final stage of laser amplifier on the same platform is desirable for the same reason.

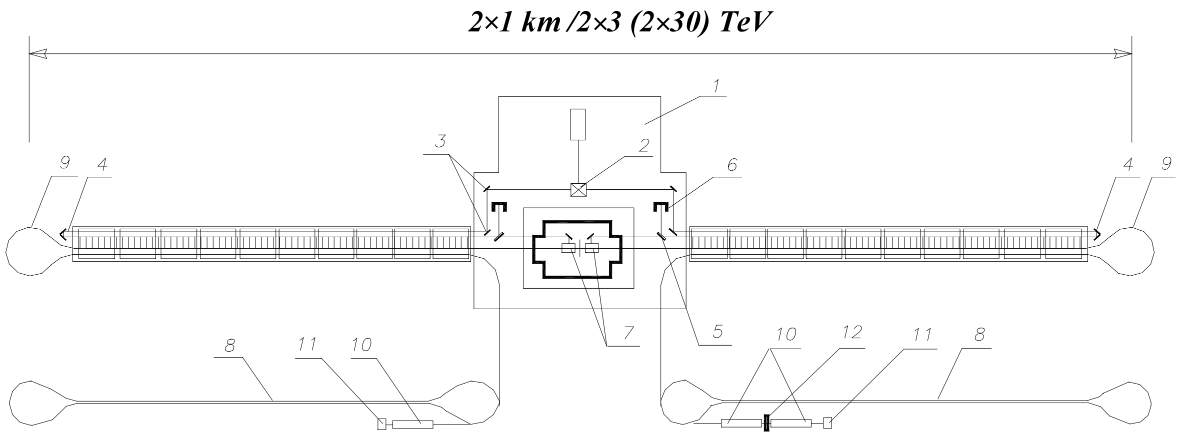

FIGURE 15.3: Laser Linear Collider (LLC) complex. 1–is a laser master oscillator platform, 2 –is an optical splitter, 3,4–are the mirrors, 5–is a semi-transparent mirror, 6–is an absorber of laser radiation. 7–are the Final Focus Systems. 8–are the damping systems for preparing particle's beams with small emittances, 9–are the bends for particle's beam. 10–are the accelerating X-band structures, 11–is an electron gun, 12–is a positron converter. The scheme with the damping rings as sources are shown here.

TABLE 15.1. Parameters of the Laser Linear Collider.

Parameter	$\lambda_{ac} \cong 10\mu m$	$\lambda_{ac} \cong 1\mu m$
Energy of $e^{\pm}$ beam	3×3 *TeV*	30×30 *TeV*
Total two-linac length	2×1 *km*	2×1 *km*
Main linac gradient	3 *GeV/m*	30 *GeV/m*
Luminosity/bunch	$10^{34} cm^{-2} s^{-1}$	$10^{34} cm^{2} s^{-1}$
No. of bunches/pulse	10 (≤ 100)*	30 (≤ 300)*
Laser flash energy/Linac	300*J*	300*J*
Repetition rate	160 *Hz*	160 *Hz*
Beam power/Linac	2.3 *kW*	760*W*
Bunch population	10^7	10^6
Bunch length	$1\mu m$	$0.1\mu m$
$\gamma\, \varepsilon_x \;/\; \gamma\, \varepsilon_y$	$\approx 10^{-8}/10^{-9}\, cm\cdot rad$	$5\cdot 10^{-9}/1\cdot 10^{-10}\, cm\cdot rad$
Damping ring energy	2 *GeV*	2 *GeV*
Length of section/Module	3*cm*	3*cm*
Wall plug power**	2×0.5 *MW*	2×0.5 *MW*

*–Maximal possible number. **–Laser efficiency$\approx 10\%$. The power for supplemental electronics is not included.

In Table 15.1 we summarized the parameters of LLC. The parameters are represented for two different laser wavelengths. One can imagine, however, that LLC has *two stages* with these two wavelengths. Two types of lasers required for this obviously. In this Table the power for supplemental electronics is not included.

A small *crossing angle* required for preventing illumination of the final lenses by used beam. This angle is absolutely necessary for multi-bunch operation mode. Tiny dimensions of the beam can help to push the beams through with ordinary optics. Relatively low repetition rate, even few *kHz*, allows easily manipulate with the beams. Full energy in the laser flash distributed in the volume $\approx L_{ACC} \cdot \lambda^2$, so $Q \cong E_m^2 \cdot L_{ACC} \cdot \lambda^2$, where L_{ACC} –is a
total length of accelerator. As we keep energy of the flash constant, $E_m \cdot L_{ACC} \approx \frac{1}{\lambda}\sqrt{Q \cdot L_{ACC}}$. That is why the final energy for $\lambda \cong 10\mu m$ is ten times lower.

As far as total laser flash energy (300 *J* in the Table 15.1), it could be generated either by a single amplifier unit or by *many amplifiers* distributed along the Linac, Fig.5.6. All the linac length is sectioned by modules having the length *L*~3 *cm*. Within each of these sections the laser flash having duration $\tau \cong 100$ *ps* becomes distributed along the length of accelerating structure. Energy required for excitation the field in the structure up to 3*GeV/m* is about 10 *mJ* for the laser wavelength $\lambda \cong 10\mu m$. For $\lambda \cong 1\mu m$ this pulse will give 30*GeV/m*. Interaction of beams at IP is going in deep quantum regime.

The beams of electrons and positrons can be polarized what gives the effective gain in luminosity and reduces the background [15.1, 15.2].

16. PERSPECTIVES

TLF method promises up to 30 *TeV/km* or 300 *TeV* on 10 *km* with 0.3 *J/m* or with 3 *kJ* per pulse total. So the total output power of the laser must be within 5 *MW/10km* with repetition rate about 160 *Hz* for $\lambda \cong 1\mu m$. Nd-Glass laser can be used here. CO_2 laser based system gives lower final energy, but the power required is within routinely obtained. The gradients still far below the *absolute* limit of the acceleration gradient, what is defined by Schwinger field (1.2), $E^{\infty} \cong 2.6 \cdot 10^9$ *GeV/m*, or 2.610^{10} *TeV* on 10*km*.

Feasibility of $\mu^+\mu^-$***,*** $\pi^+\pi^-$, $\pi p, \mu p$ ***and ion-ion collisions.***

In this brief remark we are not pretending for final consideration. The goal of it –to show that new approach associated with TLF allows also new look to the subject. The accelerating gradients of the order 30 *GeV/m* allows to reach 150 *GeV* at a ten-meter distance, suggesting 50% filling with accelerating structures. This could delivery the gamma factors $\gamma_\mu \cong 150/0.105 \cong 1430$ and $\gamma_\pi \cong 150/0.139 \cong 1079$ for μ –mesons and π –mesons respectively. So the decay distance for these particles at this energy will be $c\tau_\mu\gamma_\mu \cong 658 \cdot \gamma_\mu[m] \cong 9.4 \cdot 10^5 m$ for μ –mesons and $c\tau_\pi\gamma_\pi \cong 7.8 \cdot \gamma_\mu[m] \cong 8.4 \cdot 10^3 m$ for π –mesons respectively. So these figures make $\mu^+\mu^-$ and $\pi^+\pi^-$ *direct* collisions feasible. Let us discuss in brief the possible source of these particles, taking into account, that despite emittances required are tremendously small, the number of the particles is extremely small. Luminosity, required for $\mu^+\mu^-$ collider, is about 10^{30} cm^{-2} sec^{-1} as a minimum. So the number of the particles required is 10^4 only, if the cross-section of colliding beams is the same as we suggested for electrons in (11.1)[♣]. The general idea here to get this amount with emittance required from ordinary $p \to \pi \to \mu$ conversion at the sacrifice of the number of the particles by trivial scratching the extra mesons. If we take the primary proton beam with population 10^{14}, which is under discussion for traditional $\mu^+\mu^-$ collider [16.1], we can conclude that the resulting efficiency 10^{-9} required. Let us make some estimation with a 3*TeV* proton beam as a primary one. Effective spectrum of the secondary pions accelerated to final energy E_f, could be represented as the following [16.2]

$$\frac{dN_\pi}{dy} \cong \frac{< n_\pi^\pm >}{\sqrt{2\pi L}} \left(\frac{m_\pi c^2}{E_{fin}} \gamma^{1+\mu/2} \right)^\mu \exp[-\frac{(y-(y_0+\mu L_n))^2}{2L}], \tag{16.1}$$

where $< n_\pi^\pm >$ –is an average multiplicity of pions per collision, $L_n = \ln\gamma$, y, y_0 –are rapidity of the secondary particles and the center of mass respectively, $\mu = \frac{m_\pi c^2}{c\tau_\pi dE/ds}$, $\frac{dE}{ds}$ –is an average accelerating gradient. Value *dy* is the same as relative energy interval, practically. A term in brackets in power μ describes the reduction of the number of pions due to decay. For the $\frac{dE}{ds} \cong 3GeV/m$, $\mu \cong \frac{0.139}{7.8 \cdot 3} = 6 \cdot 10^{-3}$ and these losses are absent practically. Also the shift of maximum $\Delta y_0 = \mu L$ is absent here. For the target made on Copper, and primary 3*TeV* proton beam, the maximum of dN_π / dy is around ~2.8 *GeV/c*, shifted from the maximum of *pp* collisions on $\Delta y \cong -1/6 \ln A$, where *A* is the atomic number of the target material. Transverse momentum distribution of the secondary beam defined by [16.2]

$$\rho(p_\perp)d^2 p_\perp \cong m_\perp \sum_{k=1}^{\infty} K_1 \left(\frac{km_\perp}{T} \right) d^2 p_\perp, \tag{16.2}$$

where $m_\perp = \sqrt{m_\pi^2 + p_\perp^2}$, K_1 is a Macdonald's function, $T \cong m_\pi$ is effective temperature. The distribution (16.2) gives $< p_\perp^2 > \cong 0.15\,(GeV/c)^2$. So the angular spread of the secondary particles is about $< \vartheta^2 > \cong < p_\perp^2 > / p^2$. At the maximum of the spectra, the last gives $\sqrt{< \vartheta^2 >} \cong 0.14\,rad$. Of cause, if the secondary particles selected at higher that maximal energy, this angle drops proportionally. Transverse emittance could be estimated as $\varepsilon_\perp \cong \lambda < \vartheta^2 >$, where $\lambda = 1/n\sigma_{pA}$ is an effective nuclear length of absorption. For $p \cong 2.8\,GeV/c$, i.e. $\sim 10^{-3}$ of primary beam one, $\varepsilon_\perp \cong 0.15$ $cm \cdot rad$ and

[♣] The number of the particles is not a limiting factor for accelerating structure, as the radiation for heavy particles is practically absent.

$\frac{1}{N_0}\frac{dN_\pi}{dy} \cong 1/\,proton$. The dependence of the last expression on emittance is weak, however, as the pions yield drops weakly from the maximum beyond the maximum. Invariant emittance will be

$$\gamma\varepsilon_\perp \cong \lambda\gamma < \vartheta^2 > \cong \frac{\gamma < p_\perp^2 >}{n\sigma_{pA}p^2} \propto \frac{1}{\gamma}. \tag{16.3}$$

The last one is $\gamma\varepsilon_\perp \cong 0.15\cdot 20 = 3cm\cdot rad$ and $N_\pi \sim 10^{14}\Delta y$ per pulse. Let us suggest that we can collect the pions with energy in 10^{-3} of absolute interval. This yields for the number of pions $N_\pi \sim 10^{11}/\,pulse$. As we need 10^4 only we allowed having efficiency of the order of $N_\pi / N_p \approx 10^{-7}$. To obtain the - $\gamma\varepsilon \cong 10^{-8}cm\cdot rad$ required, we suggest first to shift the center of collected particles to the higher energy so, that corresponding emittance (16.3) will drop respectively. Suggesting new collecting energy as high as 28*GeV* i.e. about 1% of initial (3*TeV*), we are coming to $\varepsilon \approx 0.3cm\cdot rad$ and about $N_\pi \sim 10^{11}/\,pulse$ (as practically $\frac{1}{N_0}\frac{dN_\pi}{dy} \cong 1/\,proton$ does not change). In this case we could collect only 10^{-7} of all pions. Now the center of the problem shifted to the longitudinal phase space acceptance.

The bunching of proton beam could be described by the same formulas, see Chapter 6. Suggesting the energy spread in the primary bunch as 10^{-4} we are coming to necessity to have the energy modulation required overcoming the energy spread about $300MeV$. A few stages system could easily provide the energy modulation of few times of this value. So we are about optimistic on the possibility to prepare the number of particles required distributed along the distance of the laser-accelerating wavelength.

Even if the primary proton bunch has infinitely small length, the length when the secondary pion bunch will be generated is of the order of $\lambda = 1/n\sigma_{pA}$, an effective nuclear length of absorption. The last one is ~10 *cm* long. But as the proton bunch and secondary particles having about the same speed, the length of the secondary bunch will increase not drastically. Secondary bunch will have the same length as a primary proton bunch, enlarged as a result of energy spread in secondary bunch. According to Chapter 6, lengthening in space free of bending fields associated with energy spread could be expressed as

$$\Delta l \cong \gamma\frac{\partial l}{\partial\gamma}\frac{\Delta p_\parallel}{p} \cong \frac{s}{4\gamma^2}\frac{\Delta p_\parallel}{p}, \tag{16.4}$$

where s –is a distance. Estimating $\Delta p_\parallel \cong p - \sqrt{p^2 - p_\perp^2} \cong p\frac{< p_\perp^2 >}{2p^2} \cong \frac{p < \vartheta^2 >}{2}$, so $\Delta p_\parallel / p \cong \frac{1}{2} < \vartheta^2 >$, one can find the lengthening as

$$\Delta l \cong \gamma\frac{\partial l}{\partial\gamma}\frac{\Delta p_\parallel}{p} \cong \frac{s}{\gamma^2}\frac{< \vartheta^2 >}{8}. \tag{16.5}$$

Estimating $\gamma \cong 2800/139 \cong 20$, $s \cong 10cm$, $<\vartheta^2> \cong 0.02$, one can find the lengthening on the distance inside the target as $\Delta l \cong 6.3 \cdot 10^{-5} cm$ or ~$0.63\,\mu m$. On the distance ~1.5 meters the lengthening will be of the order of the $10\,\mu m$. The last figure gives the reference for positioning accelerating structure after the target. From the point of energy deposition in the material of the target, the shorter bunch is better, as there is no mass depletion in the tube of material exposed by primary beam, as this time is extremely short. It is much shorter, than the time associated with the speed of sound in material of the target. The last one needs to be made on heavy liquid metal, as Gold for example.

Let us consider some possible applications of formula (16.3). In we shift the collecting energy to say 1*TeV*, the emittance will be $\gamma\varepsilon_{\perp} \cong 3 \cdot 10^{-3} cm \cdot rad$ and the number of particles again around 10^{11} per pulse. Now one needs to select only 10^{-5} of this amount to come to emittance $\gamma\varepsilon_{\perp} \cong 3 \cdot 10^{-8} cm \cdot rad$. Rest 100 particles are distributed in longitudinal phase space. So one needs to collect only one of these. So direct collision at high energy without any acceleration at all could be a possibility. Of cause some of the figures could be treated as extremely optimistic, but there is no *fundamental* restrictions on them.

For direct $\mu^+\mu^-$ collisions the luminosity will be lower, but here the method with dedicated ring could be used as well. Tiny emittance of the bunch allow a compact size magnetic system. Few lines of laser driven linacs could be considered here as injectors.

Proton-proton collisions and ***ion-ion*** ones are straightforward here as the low emittance sources of these particles available here, Chapter 6.

17. CONCLUSION

Combination of words –"Laser Acceleration" – probably expels interest, rather than attracts it because of extremely heavy history. Since it was understood, that electric field strength in a focused laser spot has tremendous values, numerous proposals were generated in attempt to utilize this high field strength. Laser people suddenly, swamped this new field open. That was the first wave. Acceleration far from surface seemed mostly attractive for these investigators, as it was understood that the surface failure might be a limiting factor. It was spend a lot of time (and publications) for explanations from accelerator physicists, that there is no long-term acceleration in free space and that the field what accelerates the particles, reaches it's maximum on the surface. There is no either any *stable* acceleration if the distance between trajectory and closest point on the surface is more than an accelerating wavelength. Stable means here –not sensitive to fluctuations in a laser beam intensity and its transverse distribution and, of cause, *a long terms* acceleration. This first wave undermined the subject significantly in the minds. Second disastrous wave arrived from the plasma physics. People worked there for decades could not reach the goal of their activity–controlled thermonuclear reaction♣.

♣ A lot of useful applications of plasma technologies emerged for the utilization in other than thermonuclear fusion and acceleration of particles. Generally speaking any big technological effort has some positive results.

Probably they understood now, that the really working prototype would require enormous scale and they are not able to convince anyone to pay for this exercise♣♣. Some of them began to look for escape subjects. These people have rather high formal qualification. However, only recently they realized that the small parameter in accelerator physics is $\Delta p / p$, surprisingly not $\Delta v / v$. Even now not all of them realized that in accelerator physics small value is something about 10^{-7} (say in terms of emittance) but not with respect to unity. Seems, that nobody of these people till now have clear understanding that any scheme for a long-term acceleration must be stable under fluctuations of parameters. This stability and the only *it* –is important for any possible scheme. It is easy to met publications made with use of tens of hours of supercomputer processor time for modeling the plasma waves for acceleration and numerous sophisticated theoretical investigations on this subject. But only one look onto results of these publications– and it is clear that they do not contain any indications that fluctuations included. Same surprisingly look some experimental results from the plasma people. They are showing the transverse cross-section of the laser driving beam or electron driving beam even without mentioning that these cross-sections must be *round* with the accuracy satisfying the emittance preservation $\text{-}10^{-8}$. Even then they must prove that *statistical* fluctuation in diluted plasma can not destroy the emittance. The accuracy of *numerical* calculations must correspond to the accuracy required. These people, probably, will come to understanding of importance of fluctuations at least, and will ask for more powerful computers and resources. But result will be likely negative, as these people lost the spirit of finished work, as they did this in a plasma activity. A lot of other factors not taken into account and important for linear collider operation [6.1], will destroy any scheme proposed by plasma people.

From the other hand, the accelerator physicists fell this new emerging technology out of their hands. They feel also, that the size of accelerator facilities came to saturation now (LEP, SSC)♣. Naturally they are trying to suggest something different from what was before. They are more easily going into complicated large–scale projects (such as a $\mu\mu$ collider for example). Despite of evident difficulties–any part of such project looks familiar to accelerator physicists. A little bit more effort, scale, financing and… As this looks as an attempt to escape for overloading infrastructures, which the big laboratories are, the result could be the same as for plasma people, if they will not convince to pay for the large–scale prototype.

Probably it is time to accept for accelerator physicists, that the new ***micro–technology*** available, opens new possibilities for accelerator physicists themselves. This new technology opens new approaches to accelerator physics at all. Accelerator physicists and engineers need to study this new subject from the beginning. Now there is no necessity for huge infrastructure to make a high-energy accelerator, as it could be located in average room now practically at any University. Moreover, the financing of a laser

---

♣♣ I am not sure however, that the project of *really working large-scale prototype* is existing at al. If such estimation existed, it will be much easier to consider a financing, I think.

♣ It is interesting, that plasma people never suggested a device, comparable in scale with what accelerator people operate easily.

driven accelerator project is now available for private companies. These compact, brief case-size accelerators generating high-energy beams could be used not for the linear collider purposes, but for moderate industrial applications also. As the number of the particles is low, the hazardous radiation could be reduced too. We hope that a compact size high-energy accelerator giving 10^7 particles per pulse, tremendously bright with repetition rate of few *kHz* could easily find industrial applications.

What only matters in view of this new technology –is how to use it for accelerator design in this new 3D scale emerged. Namely here the power source exists for a long time–a laser. So we think it is time to circle the investigation with utilization of laser to a really nice and clear approach as making scaled accelerating structures and feed them with laser radiation. It is mostly engineering now. And when the new method will bring success, it will be easy to arrange collisions with μ, π, p, *ion-ion* (and what ever) naturally and cheaper.

In this publication an attempt was made to summarize our understanding of the problem, brining it to a practical plane. Of cause a lot of things are far from accomplishment, but the whole picture is illuminated clearly and some details could be unclosed later on. Similar to the mosaic picture production: some parts are missed for the moment, but the picture exists.

Now one, who makes an attempt to propose something effective, must clearly realize what the basic principles are. First is a simple fact, that greater accelerating gradient requires higher power density of radiation at the structure. Higher gradients required not only as a desire to make accelerator more compacted but as a vital necessity to accelerate amount of particles, necessary to obtain a reasonable luminosity. As the scale goes down, the wakes grow even faster and the only way to keep the proper ratio of wakes to accelerating field –to make the last one as big as possible. Second is that any point of accelerating structure must be illuminated for the minimal time in order to avoid the damage associated with the overheating. This requirement is obvious. Other important moment for acceleration in laser wavelength scaled structures arises from necessary to obtain the envelope function at Interaction Point (IP) region below $1\,\mu m$, what defined by laser wavelength. This requires very strong focusing, what yields a strong radiation. Electromagnetic collisions at IP are going in deep quantum regime and always require careful considerations. The collision theory of diluted beams need to be developed.

Traveling Laser Focus, TLF- method solves most of the problems in acceleration. Illuminating time and total laser power reduction both defined by the number of resolved spots (pixels) associated with deflecting device. Number of resolved spots $\approx 20-100$ achievable for mostly of their types. Lasers for the TLF method need to operate in intermediate time duration $\tau \approx 100 ps$ in contrast with the other proposals. Equivalent time of illumination of any point on accelerating structure with TLF still however, very short – $0.1 \div 1 ps$ only.

For a $0.5\times 0.5\,TeV$ Collider the total length becomes 2×170 *m* for $\lambda_{ac} \cong 10 \mu m$ and 2×17 *m* for $\lambda_{ac} \cong 1 \mu m$ respectively with 0.3*J/m* feeding power. One can compare these numbers with that from Linear Collider projects, which are under consideration in few Laboratories around the World (2×10 *km* gives the same 2×0.5 *TeV*). With TLF approach, main investments are going into *new technology*, what in any case will serve in a future.

It is possible to begin with moderate luminosity ~10^{33}. There are few possibilities to increase the luminosity in future. First –is a *repetition rate*, which is extensive parameter, far from saturation in our estimations. Next is a *multi bunch* operation mode. *Polarization* of colliding beams could be a crucial issue in reduction of electromagnetic background at IP. *Parallel wo*rking of few accelerator structures for one experimental detector is another of this kind. The last is evident and even not discussed here.

We deliberately did not made any final choice for the accelerating wavelength λ_{ac}. This choice depends on the availability of appropriate laser, what is different for different laboratories. Nevertheless, we suggest that new job must begin with $\lambda_{ac} \cong 1\mu m$. This looks as more fundamental investment. We believe that even optical wavelengths will be acceptable in future. The basis of this is in low emittance sources. As this is not prohibited by quantum mechanics, the emittances could reach its lowest values $\gamma\varepsilon_x\gamma\varepsilon_y\gamma\varepsilon_s \geq \lambda\!\!\!^{-}{}_C^3 N$.

Collisions of μ, π, p in any combinations and *ion-ion* collisions are the natural possibilities in a future. The laser accelerator could be a small laboratory in the staff of a proton accelerator. Also, in a future, laboratories using electron/positron rings could use them after upgrade as injectors to the laser linear collider[♣].

The TLF method could be staged very well with clear results after each stage completed. One stage may include fabrication and cold testing of accelerating structures. Small power lasers could be used for these purposes. This will include exercises on alignment, tuning and fabrication experience. Other stage includes development and test of the sweeping device. The low emittance solid-state electron or ion source might be another stage for this job.

Existing *synchrotron-light laboratories* could serve as a basis. These laboratories, located around storage rings, have an experience in work with newest technologies required. They have knowledge about basic beam properties also and they can easily get help from neighboring accelerator physicists. Thus this is a natural way to go.

At the end we can conclude, that the problem of acceleration in a laser-driven linac could be reduced with TLF method to a present day technology.

[♣] See example for CESR in [2.3].

18. REFERENCES

Chapter 1. Introduction

[1.1] G. Fowles, *Introduction to Modern Optics*, Dover Publications, INC New York, 1975.

[1.2] Jakson, *Classical Electrodynamics,* third edition, 1998.

[1.3] M.V. Fedorov, *Electron in Strong Light Field*, Moscow, Science Publishing Co., ISBN 5-02-014373-1, 1991 (in Russian).

[1.4] A.M. Kondratenko, E.L.Saldin, *Acceleration of Electrons by Electromagnetic Wave in an Undulator*, Preprint INP 82-58, Novosibirsk, 1982 (in Russian).

[1.5] Ya.S. Derbenev, N.S. Dikansky, *Damping of Coherent Beam Oscillations in a Storage Ring. 1. Betatron excitations*, (Novosibirsk, IYF). SLAC-TRANS-0106, 1969. 38pp. Translated from a Novosibirsk preprint, IYF-69-315 (1969)(translation).

Chapter 2. The TLF method.

[2.1] A.A. Mikhailichenko, *The Method of Acceleration of Charged Particles*, Author's certificate USSR N 1609423, Priority May 1989, Bulletin of Inventions (in Russian), N6, p.220, 1994.

[2.2] A.A. Mikhailichenko, *Excitation of the Grating by Moving Focus of the Laser Beam*, EPAC 94, London, Proceedings, p. 802.

[2.3] A.A. Mikhailichenko, *A concept of a Linac Driven by a Traveling Laser Focus*, 7th Advanced Accelerator Concepts Workshop, 12-18 October 1996, Granlibakken, Lake Tahoe, CA, AIP 398 Proceedings, p.547.

[2.4] A.A. Mikhailichenko, *Laser Acceleration: a Practical Approach*, CLNS 97/1529, Cornell, 1997; also a Talk on LASERS'97, Fairmont Hotel, New Orleans LA, December 15-19, 1997.

[2.5] A.A. Mikhailichenko, *A Laser Linear Collider Design*, CLNS 98/1562, Cornell LNS, 1998.

[2.6] I.V. Pogorelsky *et al.*, in *CO_2 Laser Technology for Advanced Particle Accelerators*, Advanced Accelerator Concepts Workshop, 12-18 October 1996, Granlibakken, Lake Tahoe, CA, AIP 398 Proceedings, p.930.

[2.7] I.N. Cobransky, *Antennas*, “Energy” Publishing, Moscow, 1973, in Russian.

[2.8] I.S. Gradshteyn, I.M. Ryzhik, *Table of integrals, Series and Products*, AP, 1965,(8.25).

Chapter 3. Sweeping device.

[3.1] C.L. Ireland, J.M. Ley, *Electrooptical Scanners,* in *Optical scanning*, Edited by G. Marshall, Marcel Dekker, Inc., 1991. See also further references there..

[3.2] Selected *Papers on Laser Scanning and Recording*, *SPIE* Vol. 378, Editor Leo Beiser, 1985.

[3.3] V.J.Fowler, J.Schlafer, *A Survey of Laser Beam Deflection Techniques,* Applied Optics, Vol.5, N10, 1657(1966).

[3.4] F.S.Chen et. al., Journ. *Applied Physics*, Vol.37, N1, p.388 (1966).

[3.5] J.F. Lotspeich, *IEEE Spectrum*, 45 (Feb. 1968), see also [5].

[3.6] L. Bademain, *Acousto-Optical Laser Recording*, in [3.1], p.255.

[3.7] Ch. C. Davis, *Lasers and Electro-Optics. Fundamentals and Engineering*, Cambridge, 1996.

[3.8] C.L. Olson, C.A. Frost, E.L. Patterson, J.W. Pokey, IEEE *Trans. of Nucl. Sci.*, vol. NS-30, N4, 1983, p.3189.

[3.9] P. Das, *Lasers and Optical Engineering*, Springer-Verlag.

[3.10] S. Reich, *The use of Electro-mechanical Mirror Scanning Devices*, [3.2], p. 229.

[3.11] F.S.Chen et. al., *Light Modulation and Beam Deflection with Potassium Tantalate-Niobate Crystals*, Journ. Applied Physics, Vol.37, N1, p.388 (1966).

[3.12] J.F. Lotspeich, *IEEE Spectrum*, 45 (Feb. 1968), see also [5].

[3.13] M. Gottlieb, *Acoustooptic Scanners and Modulators*, in [3.1], p.615.

[3.14] L. Bademain, *Acousto-Optical Laser Recording*, in [3.2], p.255.

Chapter 4. Accelerating structure.

[4.1] E.M. Lifshitz, L.P. Pitaevsky, *Physical Kinetics*, In series of L.D. Landau and E.M. Lifshitz Theoretical Physics, vol.X, 1979, Moscow, in Russian.

[4.2] J. Rosenzweig, A. Murokh, C. Pellegrini, *A proposed Dielectric-Loaded Resonant Laser Accelerator*, Phys. Rev. Let. **74**, 2467(1995).

[4.3] R.C.Fernow, J.Claus, *Properties of the Foxhole Accelerating Structure*, AIP Conference Proceedings, 279, 1992, p.212.
R.C.Fernow, J.Claus, *The Foxhole Accelerating Structure*, BNL 52336, UC-414 1992.

[4.4] H.Henke, *mm Wave Linac and Wiggler structure*, EPAC 94, London.

[4.5] J. Kirchgessner et al., *Superconducting RF Activities at Cornell University*, SRF 950908-13, Cornell, 1995, see also SRF 950714-05 and references.

[4.6] W. Bruns, **GdfidL,** TU Berlin, 1997.

Chapter 5. Some technical details of the scheme.

[5.1] R. Palmer, *A Laser Driven Grating Linac*, Particle Accelerators, Vol. 11, pp.81-90(1980).

[5.2] C.Kittel, *Introduction to Solid State Physics*, Wiley, NY, 1976.

Chapter 6. The Injection source.

[6.1] *International Linear Collider Technical Review Committee Report*, Editor G. Loew, SLAC-R-95-471, 1995.
[6.2] N.A. Vinokurov, A.N. Skrinsky, *The Generator-Klystron on the Optical Band with Ultrarelativistic Electron* , Preprint BINP 77-59, Novosibirsk 1977.
[6.3] A. Mikhailichenko, V.V. Parkhomchuk, *Damping Ring for a Linear Collider*, BINP 91-79, Novosibirsk, 1991.
[6.4] A.A. Mikhailichenko, *On the physical limitations to the Lowest Emittance (Toward Colliding Electron-Positron Crystalline Beams)*, 7th–Advanced Accelerator Concepts Workshop, 12-18 October 1996, Lake Tahoe, CA, AIP 398 Proceedings, p.294. See also CLNS 96/1436, Cornell, 1996, and in *To the Quantum Limitations in Beam Physics*, CLNS 99/1608**,** PAC99, New York, March 29- April 2 1999, Proceedings, p.2814.
[6.5] N.S. Dikansky, A.A. Mikhailichenko, *A Linear Damping System for Obtaining High Energy $e^{\pm}$ with Extremely Low Emittance*, EPAC 92, Berlin, 1992, Proc., p.898; BINP 88-9, Novosibirsk, 1988.
[6.6] A.A. Mikhailichenko, *Injector for a Laser Linear Collider*, AAC98.
[6.7] Ya.S. Derbenev, *Collision Relaxation of the Heavy Particles in a Damping Ring*, All Union Conference, Dubna, 1979, vol.1, p.119-121.
[6.8] A.A. Mikhailichenko, M.S. Zolotorev, *Optical Stochastic Cooling*, Phys. Rev. Let. **71**, 4146(1993).
[6.9] S. Kablizer, A. Knoblauch, *High Brightness Source for Ion and Electron Beams*, Rev. Sci. Instr., Vol 69, N2, 1026(1998).
S. Kablizer, *Bright Ion Source for the Nuclear microprobe*, NIM B, 158 (1999) 53-60.
[6.10] E.I. Givargizov et al., *Cold Emission from the Single-Crystalline Microparticle of Diamond on a Si Tip*, J. Vac. Sci. Technol. B 14(3) May/Jun 1996.
E.I. Givargizov et al., *Mater. Lett.* **18**,61 (1993).
[6.11] L.Reimer, *Scanning Electron Microscopy*, Springer-Verlag, ISBN 3-540-63976-4.
[6.12] K. Steffen, *High Energy beam Optics*, Interscience Publishing, 1965.
[6.13] L.D. Landau, E.M. Lifshitz, *Statistical Mechanics*.
[6.14] X.E. Lin, *Diamond coating in Accelerating structures*, AAC Baltimore, MA,AIP Conference proceedings 472, p.676.
[6.15] V.G. Dudnikov, A.L. Shabalin, *Electro- Hydrodynamical Emitters of Ion Beams*, BINP 90-31, Novosibirsk, 1990.
Applied Mechanics and Technical Physics, **2**(1990), pp.3-30.
[6.16] G. Taylor, *Disintegration of Water Drops in an Electric Field*, Proc. Royal Soc. Ser. A, 1964,v.280 N 1382, pp. 383-397.
[6.17] L.W. Swanson, A.E. Bell, *Liquid Metal Ion Sources; The Physics and Technology of Ion Source*, Edited by I.G. Brown, John Wiley&Sons, Inc., pp.313-330.
[6.18] R.Bonifacio, R.Corsini, P.Pierini, *Theory of the High Gain Optical Klystron*, Phys. Rev. A, vol.45, N6, p.4091, 1992.
[6.19] U. Amaldi, *A Possible Scheme to Obtain e^-e^- and e^+e^- Collisions at Energies of Hundreds of GeV*, Physics Letters, vol.**61B**, n.3 (1976), p.313.

Chapter 7. Transverse focusing during acceleration.

[7.1] A.A. Mikhailichenko, *A Beam Focusing System for a Linac Driven by a Traveling Laser Focus*, PAC95, Dallas, TX, Proceedings, p. 784.

[7.2] W. Schnell, *Microwave Quadrupoles for Linear Colliders*, CLIC Note 34, 1987.

[7.3]F.E.Mills, A. Nassiri, *Alternating Phase Focusing in mm-wave Linear Accelerators*, Argonne National Laboratory, internal report ANL/APS/MMW-9, 1994.

[7.4] R.C. Ffernow, J. Claus, *The Foxhole Accelerating Structure*. BNL –52336, UC-414, 1992.

[7.5] V.P. Smirnov, private communication.

[7.6] M. Filtz, *Analytical Calculation of Waves in Muffin-Tin Structure*, Proc. Of EPAC, London 1994, pp.1333-1335.

[7.7] A.N. Lebedev, A.V. Shal'nov, *Foundations of Physics and Techniques of Particle Accelerators*, Moscow, ISBN 5-283-03971-4, 1991, in Russian.

Chapter 8. Accelerating gradient.

[8.1] D. Du, X. Lu, G. Korn, J. Squuier, G. Mourou, *Optical Breakdown with Femtosecond Laser Pulses*, CLEO94, May 8-13, 1994, Anaheim, California, Vol.8, p.407.

[8.2] L.D. Landau and E.M. Lifshitz, *Quantum Mechanics*, Theoretical Physics Series, vol. III, 1979, Pergamon Press.

Chapter 9. Bunch population.

[9.1] K. Bane, A. Chao, T.Weiland, CERN/ISR-TU/81-02.

[9.2] V.E.Balakin, O.N.Breznev, A.A. Mikhailichenko, A.V. Novohatsky, V.P.Smirnov, N.A.Soliak, *Physical Foundation for Linear Colliders***,** ICFA Seminar on Future Perspectives in High Energy Physics, Upton, 5-10 October 1987, Proc., pp.244-266.

[9.3] V.V. Anashin, *et.al. Prototypes of the Damping Ring and the Buncher for the VLEPP Project*, XIII international conference on high-energy accelerators, Novosibirsk, USSR, Aug 7-11, 1986, pp. 159-163. Published in Novosibirsk Accel.1986 v.1: 159 (QCD183: I5: 1986). See also SLAC-TRANS-0224, Oct 1986. 14pp.

Chapter 10. Final Focus.

[10.1] K.Oide, *Synchrotron-Radiation Limit on the Focusing of Electron Beams*, Phys. Rev. Lett., Vol. 61, n.15, p.1713 (1988).

[10.2] T.A. Vselolojskaya, *An Emittance Growth in the Final Lens of Linear Collider*, Preprint BINP 90-41, Novosibirsk 1990.

Chapter 11. Luminosity.

[11.1] M. Tigner, *A Possible Apparatus for Electron Clashing-Beam Experiments*, Il Nuovo Chimento, **37**(1965), p.1228.

[11.2] H. Wiedemann, *Particle Accelerator Physics*, Springer-Verlag, ISBN 3-540-56550-7, 1998.

[11.3] A.A. Mikhailichenko, *Use of Undulators at High energy to Produce Polarized Positrons and Electrons*, Workshop on new Kinds of Positron sources for Linear Colliders, SLAC, March 4-7, 1997, Proceedings, SLAC-R-502, p.229.

[11.4]V.E. Balakin, A.A. Mikhailichenko, *Conversion System for Obtaining Highly Polarized Electrons and Positrons*, Preprint Budker INP 79-85, see also XII

international conference on high-energy accelerators, Batavia, August 11-16, USA, 1983, Proceedings, pp. 127.
[11.5] V.E. Balakin, *Travelling Final Focus*, SLAC Workshop on LC95.

Chapter 12. Interaction point.

[12.1] P. Chen, *Quantum Beamstrahlung from Gaussian Bunches*, in *New Developments in Particle Acceleration Techniques*, Proceedings, CERN 87-11, ECFA 87/110, vol.2, p.593, (1987).

[12.2] V.B. Berestetsky, E.M. Lifshits, L.P. Pitaevsky, *Quantum electrodynamics*, Pergamon Press, 1982.

[12.2] T. Himel, J. Siegrest in *Laser Acceleration of Particles*, editors C. Joshi and T. Katsouleas, AIP Conference Proceedings No. 130 (1985).

[12.3] V.N. Baier, V.M. Katkov, *The Theory of Landau, Pomeranchuk, Migdal Effect*, Preprint Budker INP 97-70, Novosibirsk 1997.

Chapter 13. Multibunch operation mode (upgrades).

[13.1] A.A. Mikhailichenko, *Some Qualitative Analyses of the Nature of the Impedance and Limitations for the Bunch Length Following from there*, DESY M 92-05, Aug. 1992, 8 pp.

[13.2] M. Sands, *The Physics of Electron Storage Rings, An Introduction*, SLAC-121, UC-28, 1970.

Chapter 14. Alignment.

[14.1] B. Richter, *The SLAC Electron-Positron Colliders: Present and Future*, XIII International Conference on High-Energy Accelerators, Novosibirsk, Aug. 7-11, 1986, Proceedings, p. 33.

[14.2] W. Blum, H. Kroha, P Widman, *A Novel Laser Alignment System for Tracking Detectors Using Transparent Silicon Strip Sensors*, Contribution to the 1995 Wire Chamber Conf., Vienna, 13-17 February 1995, MPI-PhE/95-05.

Chapter 15. General picture.

[15.1] SLAC 2 mile Accelerator.

Chapter 16. Perspectives.

[16.1] C.M. Ankenbrandt et al., *Status of Muon Collider Research and Development and Future Plans*, Phys. Rev. Special Topics-Accelerators and Beams, Vol. 2, 081001 (1999).

[16.2] T.A. Vsevolojskaya, G.I. Silvestrov, A.N.Skrinsky, *Acceleration of Pions and Muons in the UNK-VLEPP complex*, Preprint BINP 91-36, Novosibirsk, 1991.